THE UNIVERSITY *of* EDINBURGH

A Cat and Mouth Game: Genetic influences on initiation and progression of feline tooth resorption

Brandon Shek

Thesis presented for degree of Master of Science

The University of Edinburgh

2021

Abstract

Feline tooth resorption (TR) is a painful and progressive disease characterised by the destruction of mineralised tissue. This is caused by the dysregulation of odontoclasts; specialised cells which resorb teeth and responsible for tooth shedding, sharing many similarities with osteoclast, bone resorbing cells. TR is one of the most common dental problems found in cats; affecting 29%-70% of the domestic cat population. Currently, there are no effective treatments for TR; tooth extraction or coronal amputation are the only solutions. This is due to the aetiology of TR remaining unknown. Various factors such as genetic, inflammatory, and mechanical factors have been implicated in the development of TR but is still being investigated. The highest prevalence of TR is observed in pure bred cats, implying genetic cause of odontoclast dysregulation.

The aim of this MSc project was to investigate the expression of genes by odontoclast within TR affected and unaffected samples and their function in resorption activity. Using data from transcriptome analysis by RNA sequencing, many differentially genes were identified between TR affected and unaffected cats. To localise this differential expression, feline dental samples were collected to localise the expression of specific differentially expressed genes within affected samples. Immunohistochemistry was performed to stain for targets MMP9, CTSK, and P2XR4 which co-localised with tartrate resistant acid phosphatase activity found in osteoclasts/odontoclasts in resorptive lesions on TR affected teeth. To elucidate the role of MMP9, CTSK, and P2XR4 in osteoclast/odontoclast differentiation and resorption, osteoclasts were transfected with siRNA via electroporation to target these three genes using an established protocol for deriving osteoclasts from feline bone marrow in vitro. Cells were seeded onto hydroxyapatite covered wells plates to assess osteoclast differentiation and resorptive activity. RNA extraction and quantitative PCR was performed on transfected cells to investigate the effect of siRNA on MMP9, CTSK, and P2XR4 expression. Through further bioinformatics analysis of RNAseq data, a large number of single nucleotide polymorphisms (SNPs) were found and impact on gene function was predicted.

The results from this study indicate key components of odontoclast formation in TR positive teeth and their associated pathways. Further testing of candidate genes and assessing their downstream products may provide potential therapeutic targets for feline TR using the methods and results indicated in this study.

Lay summary

Tooth resorption is a disease that causes tooth loss in cats. This is caused by odontoclasts, which are specialised cells which normally resorb the milk teeth for tooth shedding in the young. This is a normal process, but in this disease these cells begin to attack the adult dentition in later life. This abnormal activity leads to the loss of the tooth and causes pain. This is one of the most common dental problems found in cats, where 29% to 70% of domestic cats suffer from the disease. There are no effective treatments other than removal of the affected tooth. The reason why and how this disease starts is not yet known. However, the disease is quite common in pure bred cats, which points to a genetic reason. The aim of this research project was to see the difference in gene activity between cats with and cats without tooth resorption and to see if they take part in starting tooth resorption. Three genes were found to have a difference between affected and unaffected cats. To find exactly where this expression is found and what cells expressing these genes, thin teeth slices with tooth resorption were microscopically examined. Odontoclasts were seen in tooth resorption areas expressing these genes. To see what these genes do in tooth resorption, odontoclasts were taken from cat samples and grown on a mineralised surface, to imitate the surface of teeth. Under normal conditions, the cells would grow and eat away at the mineralised surface. Each gene was silenced individually and examined to see if this affects the cell's ability to absorb the mineralised surface. Lastly, by looking into past data, differences between different cats of the same genes were checked and their effect on the gene's function was predicted.

The results from this study show important parts responsible for odontoclast formation in tooth resorption and what other elements are involved. By looking into other genes also thought to be involved in tooth resorption and investigating how they work, this might give possible ways to treat tooth resorption in cats.

Declaration

I, Brandon Shek, hereby declare that the work presented in this thesis has been composed, was carried out by myself or with due acknowledgement, and has not been presented for a degree at any other university.

Brandon Chi Fung Shek

31st January 2021

Acknowledgments

I would like to first give my thanks to my supervisor Dr Gurå Therese Bergkvist who has provided great support and guidance through my project. I would also like to extend my appreciation and gratitude to my assistant supervisor Prof. Colin Farquharson who first introduced me to the opportunity. I would especially like to thank assistant supervisor Dr Seungmee Lee for her continual patience and kindness in guiding and teaching me throughout this project for which I am extremely grateful.

I owe many thanks to all the people that have helped me in countless ways. I would like to thank Dr Stephen Bush for his invaluable knowledge in bioinformatics and assistance in the bioinformatics portion of this project. From the Farquharson group, I would also like to thank Dr Louise Stephen, Shun-Neng Shu (Lewis) and Masahiro Horita who has always been kind and helpful with whatever problem I had. I will miss our little lab and office chats. I would also like to extend my thanks to Kanchan of the Macrae group who has always been welcoming since my arrival. There are many others that I would like to mention by name if I had more space but thank you to you all.

I would like to give special thanks to my parents for their love and support, who have always taking care of me and helping wherever they can.

Most importantly I would like to give thanks to Lord Jesus Christ. By His grace and mercy, He has granted me the opportunity to study in this project, sustaining and guiding me throughout.

This work was supported by the Waltham’s Foundation.

List of abbreviations

AGO2	Argonaute 2
AP-1	Activator protein-1
aPCK	Atypical protein kinase C
AVDC	American Veterinary Dental College
BLNK	B-cell linker protein
BMP	Bone morphogenic protein
BMP-2	Bone morphogenetic protein-2
BP	Bisphosphonates
Btk	Bruton's tyrosine kinase
CEJ	Cementoenamel junction
CFU-GM	Colony forming unit for granulocytes
COQ4	Coenzyme Q4
CSF-1	Colony stimulating factor 1
CTSK	Cathepsin K
DAP12	DNAX-activation protein 12
dbSNP	Single nucleotide polymorphism database
DNA	Deoxyribonucleic acid
dNTP	Deoxynucleoside triphosphate
EDTA	Ethylenediaminetetraacetic acid
EEIG1	Early estrogen-induced gene 1
EGFR	Epidermal growth factor receptor
EMP	Edinburgh Memorial Programme
ENA	European Nucleotide Archive
ERK	Extracellular signal-regulated kinase
FAM8A1	Family with Sequence Similarity 8 Member A1
FBS	Foetal bovine serum
FcRγ	Fc receptor common γ subunit
FGF	Fibroblast Growth Factor
FOS	Proto-oncogene c-Fos
Gab2	Growth factor receptor-bound protein 2 (Grb2)-associated binder-2

GAPDH	Glyceraldehyde 3-phosphate dehydrogenase
GATK	Genomic analysis toolkit
Gsk-3β	Glycogen synthase kinase-3β
gVCF	Genomic variant call format
HERS	Hertwig Epithelial Root Sheath
HPRT	Hypoxanthine-guanine phosphoribosyltransferase
IEE	Inner enamel epithelia
IFNγ	Interferon gamma
IHC	Immunohistochemistry
IKK	IκB kinase
IL10RB	Interleukin-10 receptor subunit beta
IL12RB2	Interleukin 12 receptor subunit beta 2
IL1R1	Interleukin-1 receptor type 1
IL1β	Interleukin 1β
IL4R	Interleukin-4 receptor
IL6	Interleukin 6
ITAM	Immunoreceptor tyrosine-based activation motif
JNK	c-Jun N-terminal kinase
KRT76	Keratin 76
MAPK	Mitogen-activated protein kinases
MCP-1	Monocyte chemotactic protein-1
MMP13	Matrix metallopeptidase 13
MMP9	Matrix metalloproteinase 9
mRNA	Messenger RNA
MT-CYB	Mitochondrially encoded cytochrome B
MYH13	Myosin heavy hain 13
NFATc1	NF-κβ induces nuclear factor of activated T-cells cytoplasmic 1
NFKB2	Nuclear factor kappa b subunit 2
NGS	Next generation sequencing
NOX1	NADPH oxidase 1
OEE	Outer enamel epithelia
OPG	Osteoprotegerin

OSCAR	Osteoclast-associated receptor
P2XR4	P2X purinoceptor 4
PCR	Polymerase chain reaction
PDL	Periodontal ligament
PI3K	phosphoinositide 3-kinase
PIRR	Peripheral Inflammatory Root Resorption
PIRR	Peripheral inflammatory root resorption
PKCβ	Protein kinase Cβ
PLAUR	Urokinase plasminogen activator surface receptor
PLCγ2	Phospholipase Cγ2
qPCR	Quantitative polymerase chain reaction
RACK1	receptor for activated C kinase 1
RANK	Receptor activator of NFκB
RANKL	RANK ligand
RISC	RNA-induced silencing complex
RNA	Ribonucleic acid
RNAi	RNA interference
RNA-seq	RNA sequencing
ROS	reactive oxygen species
RT	Room temperature
SEM	Standard error of mean
SHH	Sonic Hedgehog protein
siRNA	Small interfering RNA
SLP-76	Src homology 2 domain-containing leukocyte protein of 76 kD
SNAPC4	Small nuclear RNA activating complex polypetide 4
SNP	Single nucleotide polymorphism
SR	Stellate reticulum
SRC	proto-oncogene tyrosine-protein kinase Src
SYK	Spleen associated tyrosine kinase
TAB	TGF-Beta Activated Kinase 1 (MAP3K7) Binding Protein
TAK1	TGFβ-activated kinase 1
TGFB1	Transforming growth factor beta 1

TNF	Tumour Necrosis factor
TNFRSF1A	TNF receptor superfamily member 1A
TR	Tooth resorption
TRAcP	Tartrate-resistant acid phosphatase
TRAF	TNF receptor-associated factors
TRAF6	TNF receptor-associated factors 6
TREM-2	Triggering receptor expressed in myeloid cells-2
TTN	Titin
VCF	Variant calling format
VDR	Vitamin D receptor
ZMYM6	Zinc finger MYM-Type containing 6

Table of Contents

Table of figures

Table of Tables

1 Introduction

1.1 Tooth biology

Teeth are hard, calcified structures located in the jaws of many vertebrates. Their primary use involves mastication, important in speech for humans and used by some animals for attack and defence (Nanci and TenCate, 2017). In order to fulfil these functions, teeth must be hard and firmly attached to the bones of the jaw.

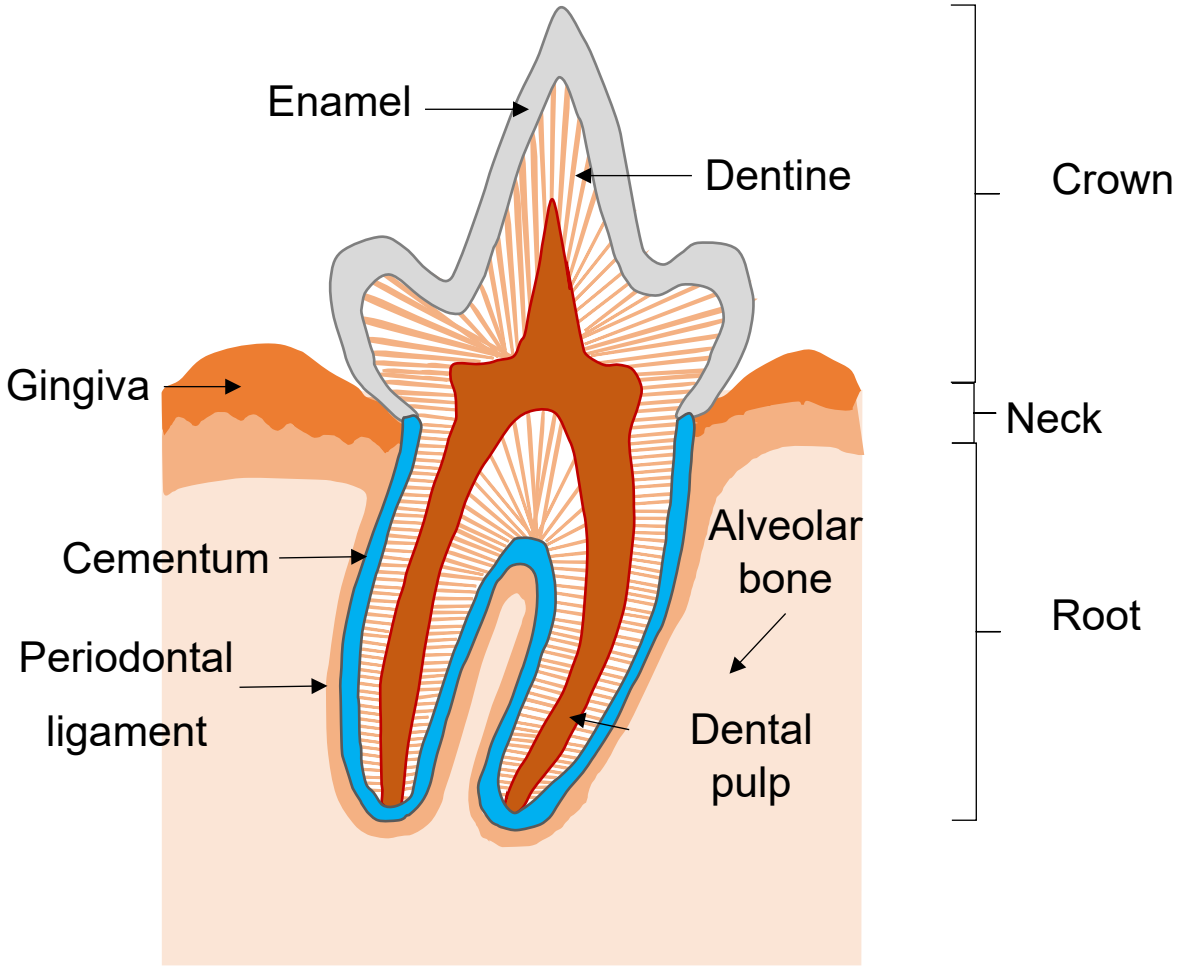

Figure 1.1 A diagram of showing the structure of the mammalian (feline) brachydont tooth and periodontal tissue. The tooth can be divided into sections, the visible external part (crown) over the gingiva, the extending portion into the bone of the jaw (root), and the junction between the crown and root (neck). The crown is covered by enamel, the hardest tissue in the body. Dentine is located beneath the enamel and a larger proportion of the tooth is made up of cementum. Dentine is lined with over 40,000/mm^2 dentinal tubules and forms a dental-pulp complex which lines the pulp cavity. Pulp is a soft connective tissue with blood vessels, nerves, and lymphatics. Fibres of the periodontal ligament tightly anchor the tooth to the alveolar bone (Figure modified from Lee, 2019).

The general structure of teeth is similar among vertebrates, though there is considerable variation in both their form and distribution. The most common type of tooth is the brachydont tooth, also described as low-crowned tooth, that possesses a short crown and root ratio which is observed in humans, dogs, and cats (Figure 1.1).

The tooth can be split into individual anatomical regions (Figure 1.1). The visible exposed portion of the tooth in the oral cavity above the gingiva (gums) is referred to as the dental crown. The section between the crown and root of the tooth is referred to as the cementoenamel junction (CEJ) or commonly referred to as the neck of the tooth. The anatomical root extends below the CEJ into the tooth socket where the tooth is then attached to the bone of the jaw through periodontal tissues.

The typical mammalian tooth primarily consists of four major tissues: Enamel, dentine, cementum, and dental pulp (Nanci and TenCate, 2017). Enamel forms the outer portion of the crown, covering the dentine and extends to the CEJ, just below the soft gingival tissue. This is the most mineralised tissue of the body, formed by ameloblasts, enamel-forming cells, and are composed of 96% inorganic matter as apatite crystals and traces of organic material (Bartlett, 2013; Nanci and TenCate, 2017). Unlike other calcified tissues, enamel lacks the capacity for repair due to shedding of the ameloblast layer upon eruption of the tooth into the oral cavity (Nanci and TenCate, 2017).

Two other tissues of the crown are dentine and dental pulp, which extend apically as the root of the tooth into the alveolar bone. Dentine is an avascular tissue that encloses the central pulp chamber consisting of 70% inorganic matter and an organic component primarily composed of collagen fibres, making it less mineralised than enamel but slightly harder than bone (Nanci and TenCate, 2017). This provides the bulk of the tooth and is vital in supporting the enamel against forces of mastication due to enamel’s brittle nature. Dentine forms dentinal tubules which are tightly packed together and span the entirety of the dentine to form a peripheral boundary of the dental pulp cavity. Nerve fibres run along these tubules which allow the transmission of various stimuli to the pulp cavity including pain, pressure, heat, and cold. These contain odontoblasts which align along the inner edge of the dentine,

providing deposition of dentine for further growth and repair (Goldberg et al., 2011; Nanci and TenCate, 2017).

The dental pulp is situated in the central portion of the tooth including the pulp chamber of the crown and pulp canals of the roots, enclosed by dentine. The pulp is composed of blood vessels, nerves, lymphatics, and various cells including odontoblasts. These are closely associated with dentine as they produce the dentine surrounding it, providing nutrients to the avascular dentin and is capable of producing new dentine as required after damage (Nanci and TenCate, 2017; Yu and Abbott, 2007). Overall, the combination of these tissues provides teeth both hardness and resilience.

Surrounding and supporting the teeth to attach the teeth to the jaw is the periodontium, specialised tissues consisting of cementum, periodontal ligament (PDL), and the alveolar bone which are all protected by the gingiva.

Cementum is an avascular mineralised connective tissue which covers the surface of the tooth root, consisting of 45-50% inorganic material and produced by cementoblasts (Nanci and TenCate, 2017). Cementum attached to the root dentine and covers the upper (cervical) portion of the root is acellular and the lower (apical) portion of the cementum is covered by cellular cementum. This is formed when cementoblasts become embedded in their own matrix, similar to osteocytes occupying lacunae in bone, to become cementocytes. This allows self-repair to a limited degree (Nanci and TenCate, 2017; Yamamoto et al., 2016).

The PDL is an important structure of periodontal tissue which generates connective collagen fibre bundles which spans the gap between the cementum and alveolar bone proper to suspend the tooth (Lekic and Mcculloch, 1996; Nanci and TenCate, 2017). This is a complex structure, comprised of several different cell populations at various stages of differentiation and lineage responsibility, primarily PDL cells which predominantly form fibroblasts and are crucial in the maintenance and regeneration of periodontal tissue (Choi et al., 2011).

The alveolar bone or process is the thickened ridge of bone that contains the tooth sockets. This is comprised of fibres, a variety of cells, intercellular substances,

nerves, lymphatics, and blood vessels (Jiang et al., 2015; Nanci and TenCate, 2017). The gingiva (gums) is the soft mucosal tissue lining which surrounds the cervical neck of teeth and are mostly tightly bound to the underlying bone.

Typically, mammalian teeth are heterodont which may come in various tooth shapes: incisors, canines, premolars, and molars. The number of tooth types across species can vary considerably. In veterinary dentistry, conventional anatomical tooth types as well as the tooth numbering system, the modified Triadan system, is widely used (Floyd, 1991). The modified Triadan system allocates a three-digit number to each tooth. The oral cavity is divided into four quadrants (1-4) which is indicated in the first digit, the next two digits indicate the tooth in each quadrant; 01-03 for incisors, 04 for canine, 05-08 for premolars, and 09-11 for molars. In cats, the carnassials are used as landmarks. The upper carnassials, the last premolars are 108 and 208. The lower carnassials, the first molars, are 309 and 409. Gaps in the numbering sequence indicate where there are missing teeth, such as the first premolar in the feline left maxilla is 206, not 205. The two lower right premolars are 407 and 408, not 405 and 406 (Figure 1.2).

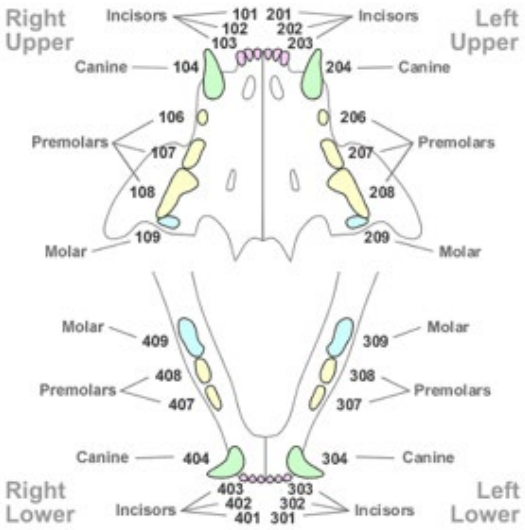

Figure 1.2: Modified Triadan System for feline dental nomenclature. The Triadan system is a three-digit numbering system for numbering teeth across different animal species. The first digit denotes the quadrant: 1-Right upper permanent, 2-Left upper permanent, 3-Right lower permanent, 4-Left lower permanent. The second and third digits denote the tooth position within the quadrant, always starting from the midline. In domestic cats, 01-03: incisors, 04: canine, 06-08: premolars, 09 molars. Images available at: https://www.rvc.ac.uk/review/Dentistry/Basics/triadan/other.html

1.2 Embryonic tooth development

In mammals, the development of these structures of the tooth begins by odontogenic epithelial-mesenchymal interactions and integration of the root with the jawbone, blood supply, and nerve innervations. Tooth formation starts with the ectodermal epithelium, forming the dental lamina as two U-shaped structures. The position of these correspond to the position of the future dental arcades in the upper and lower jaws.

A key stage in eliciting tooth formation is neural crest cells interacting with the mandibular epithelium (Lumsden, 1988). Neural crest cells migrate to a position beneath the oral epithelium and form the ectomesenchyme. The thickened band of epithelium is responsible for producing two subdivisions of cells, the vestibular lamina and the dental lamina. The vestibular lamina forms the vestibule, the space between the cheeks and the gingiva. The dental lamina forms the sites for future deciduous teeth.

Tooth germ proceeds in three stages: Bud stage, cap stage, and bell stage (Nanci and TenCate, 2017)(Figure 1.3). In the bud stage, epithelial cells proliferate which forms invaginations into the underlying ectomesenchymal tissues where ectomesenchymal cells gather deep in the bud and cluster, initiating the condensation of the ectomesenchyme. These form a characteristic bud at the distal aspect of the dental lamina of each arch. The arrangement of these cells is unclear until the first signs are shown in the cap stage.

In the cap stage, the epithelial bud enlarges by cell division to form a convex, cap-like surface. The epithelial cells differentiate into several cell layers to form the enamel organ which includes the outer enamel epithelium, the inner epithelium which lines the concavity, and the stellate formed with the cap. At the centre of the inner enamel epithelium are enamel knots, localised non-dividing epithelial cells which are responsible for communicating with signalling molecules to proliferate surrounding cells. As the ectomesenchyme becomes more condensed, below the enamel organ the dental papilla is formed as a ball and is surrounded by the condensed dental follicle. Together, these three entities the enamel organ, dental papilla, and dental follicle form the tooth germ.

The dental papilla contains cells which develop into odontoblasts, which are responsible for dentine formation, and mesenchymal cells, which develop into pulpal cells. The dental follicle is a loose connective tissue responsible for three key cells: cementoblasts, osteoblasts, and fibroblasts which form the future periodontium, the cementum, periodontal ligament, and some alveolar bone. The dental organ establishes a bell shape through folding of the inner enamel epithelium. During this stage, terminally differentiated dental secretory cells secrete dentine and enamel begin to form at the crest of the inner enamel epithelium, beginning to form the tooth crown shape (Thesleff, 2003).

Once crown formation is completed, root formation starts. This begins with the cervical loop, where the outer enamel epithelium and inner enamel epithelium join at the edge of the enamel organ. Proliferation of this cell bilayer forms the Hertwig's Epithelial Root Sheath (HERS). The classic theory of root formation states that these cells migrate through the underlying dental ectomesenchymal tissues as these cells divide. Though it is widely accepted that HERS is important in root development (Huang et al., 2009; Zeichner-David et al., 2003). This sheath of epithelial cells extends and encloses the dental pulp and the dental follicle, enclosing all but the basal portion of the pulp and the rim of this root sheath encloses the primary apical foramen. During this process where the inner epithelial cells of the HERS enclose more of the expanding dental pulp; they initiate the differentiation of ectomesenchymal cells to form odontoblasts at the periphery of the pulp to lay down the dentine of the root. The root sheath does not grow at the same rate as the crown of the tooth, which grows rapidly away from the bony socket of the jaw, and instead stretches. The root sheath disintegrates as root formation progresses and only remains intact where cells are dividing at the advancing root edge. As the root sheath fragments, discrete clusters of epithelial cells are produced known as epithelial cell rests of Malassez (Huang et al., 2009). The epithelial cell rests persist in adults by the root surface within the periodontal ligament and are thought to contribute to periodontal repair and regeneration. Some cells in the outer layer of HERS in the coronal root region induce the formation of cementoblasts from dental follicle cells, leading to cementum formation. During cementogenesis, fibroblast precursors from the dental follicle interact with the predentine matrix where bundles of collagen fibres

are deposited to form extrinsic Sharpey's fibres (Nanci and TenCate, 2017). Cementoblasts and cementocytes in the late stage of cementogenesis are involved in intrinsic fibres. Collagen and non-collagenous proteins are secreted to maintain the space of the periodontal ligament. The developmental biology of the tooth root and formation of the periodontium is the least known aspect of tooth development and requires further investigations (Nanci and TenCate, 2017).

The formation of the tooth requires consideration of gene and molecular signals which control cell proliferation, migration, and differentiation, as like other organ developments (e.g. limbs, kidney, bone), gene expression and molecular signalling for the developing tooth are unique and very complex. A large number of genes have been identified for each development stage with different temporal and spatial expression patterns. The most conserved signalling pathways observed are bone morphogenic protein (BMP), Fibroblast Growth Factor (FGF), Sonic Hedgehog protein (SHH), and WNT ligands and their receptors. These are all involved in tooth development and in the epithelial-mesenchymal interactions (Bei, 2009; Nanci and TenCate, 2017; Thesleff, 2015) After the tooth has been formed, the tooth erupts into the oral cavity, where the enamel depositing cells, ameloblasts, are shed. This also results in the inability to restore damage or loss of enamel, particular in the crown section exposed to the oral cavity.

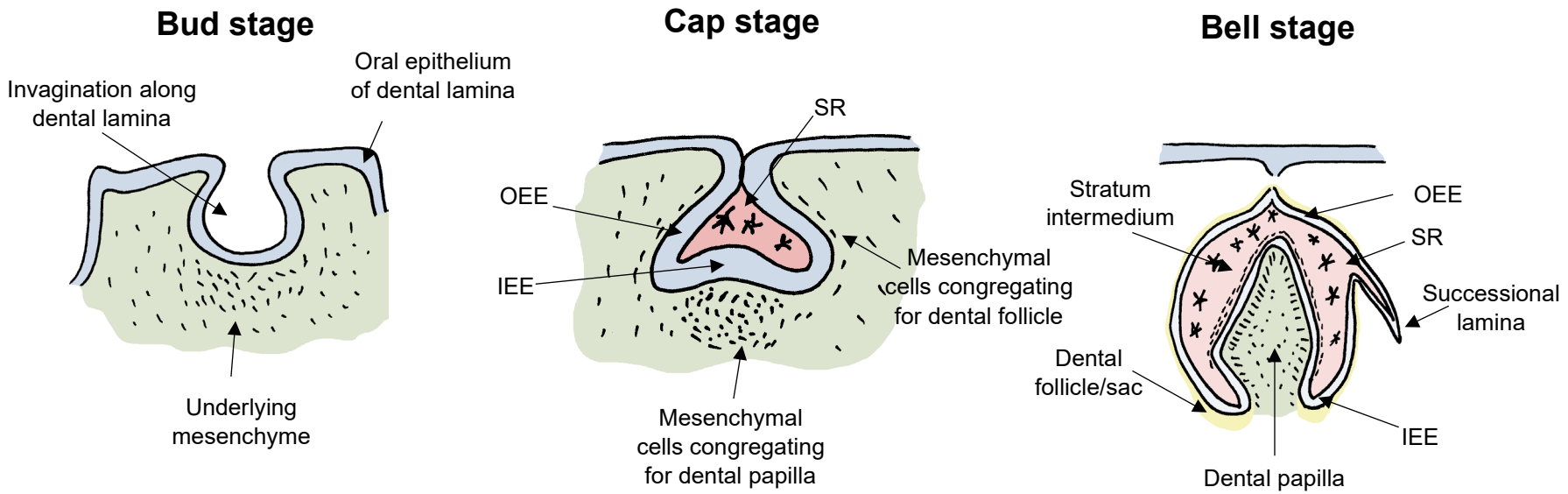

Figure 1.3: Tooth development stages. Tooth development beings with ectodermal oral epithelium thickening to form 2 U-shaped structures: the dental lamina, which outlines the upper and lower dental arcades. Tooth formation begins in three stages: bud stage, cap stage, bell stage. In the bud stage, invaginations along the dental lamina correspond with each deciduous tooth. In the underlying mesenchyme, mesenchymal cells condense for early bone formation. In the cap stage, the deepest potion and three parts can be identified: Outer enamel epithelia (OEE), inner enamel epithelia (IEE), stellate reticulum (SR). Bell stage: Stratum intermedium (SI) layer formed between IEE and SR provides nourishment for the IEE. Successional lamina forms the enamel organ for the permanent tooth (Images courtesy of Dr Gurå Therese Bergkvist, R(D)SVS & The University of Edinburgh).

1.3 Tooth eruption and deciduous tooth shedding (physiological tooth resorption and RANK/RANKL/OPG pathway)

Tooth eruption is the sequence of events where the tooth is moved from the alveolus into the mouth. After appearing in the mouth cavity, the tooth is then brought into occlusion with opposing deciduous teeth. The process of eruption has not been fully elucidated but there are four theories: root growth, bone growth, pulpal proliferation, and periodontal ligament fibres creating traction (Cahill and Marks, 1980; Marks and Schroeder, 1996; Nanci and TenCate, 2017). However, it is most probable that a combination of all four causes tooth eruption (Wise and King, 2008). This would involve several correlated processes including pulpal growth, root formation, periodontal ligament formation, and bone deposition and resorption.

Upon completion of crown development, root formation initiates and tooth eruption also commences. Root formation continues throughout eruption and is three-quarters completed at the point of tooth emergence into the oral cavity. For deciduous teeth, the erupting crown moves through the dental follicle and into the overlying gingival tissue. As the tooth moves into the mouth, root formation continues to proceed. At this stage, the dental follicle is believed to give rise to supporting tissues of the tooth such as the periodontal ligament. The follicle area surrounding the growing tooth root develops into the PDL. The alveolar bone proper is also redirected to surround and support the developing root, involving bone formation on the opposite sides of the erupting tooth (Marks and Schroeder, 1996).

The deciduous dentition is shed when each member is replaced by a permanent tooth. This loss of deciduous teeth is mainly due to the resorption of the bones and roots associated with the permanent teeth. The permanent teeth are lodged in bony crypts with their developing crowns in close proximity with the roots of the deciduous teeth. Pressure of the erupting permanent dentition on the overlying tissues leads to activation of osteoclasts that carry out resorption of the bone, to separate the teeth from surrounding bone before root resorption (Nanci and TenCate, 2017). Osteoclasts are vital in removing the overlying alveolar bone by performing bone resorption as inhibition of osteoclast activity and osteoclastogenesis delays or stops tooth eruption (Grier IV and Wise, 1998; Kong et al., 1999). An adequate number of

osteoclasts is needed for resorption, which arises from an influx of mononuclear cells, osteoclast precursors, into the dental follicle at a time specifically prior to eruption which then fuse to form osteoclasts (Wise and King, 2008).

Another key feature of tooth shedding is the resorption of the deciduous tooth roots. This is performed by odontoclasts, cells which resorb dental hard tissue and are similar to osteoclasts. These are derived from the myeloid (monocyte) lineage and migrate from blood vessels to the resorption site. Though active resorption takes place on the root, the coronal pulp appears normal with odontoblasts still lining the surface of the predentin. As root resorption is almost complete, the odontoblast lining degenerates, and mononuclear cells emerge from the pulpal vessels to migrate to the predentin surface. These fuse with other mononuclear cells to form odontoclasts which actively engage in dentine removal (Nanci and TenCate, 2017). Resorption stops before exfoliation of the tooth, where odontoclast migrate away from the dentine surface and remaining pulp cells deposit a cement-like tissue on it. The tooth then sheds with some pulpal tissue intact.

Signalling pathways during tooth eruption and shedding are not clearly defined. However, these events are recognised to be localised, where the patterns of differential gene expression involved in physiological tooth resorption are both temporal and spatial (Nanci and TenCate, 2017; Wise and King, 2008). As mentioned previously, the dental follicle is involved in alveolar bone resorption but is also involved in promoting alveolar bone formation (Harokopakis-Hajishengallis, 2007; Nanci and TenCate, 2017; Wang and McCauley, 2011). How this is achieved is by the distinct temporal and spatial manner of the molecular pathways.

At the coronal region of the dental follicle, osteoclasts are induced to resorb the alveolar bone whereas in the basal dental follicle, alveolar bone formation is promoted at the base of the crypt for tooth eruption (Wise et al., 2002). The generation of spatial effects are due to regional differences in gene expression (Wise et al., 2002). In the coronal portion, RANKL expression is greater than the basal portion whereas bone morphogenetic protein-2 (BMP-2), a bone formation marker is much greater in the basal region than the coronal region (Wise et al., 2002; Wise and Yao, 2006). The dental follicle is also involved, attracting osteoclast precursors

through secretion of chemokines such as colony stimulating factor-1 (CSF-1) and monocyte chemotactic protein-1 (MCP-1)(Que and Wise, 1997; Wise et al., 2002). Endothelial monocyte-activating polypeptide (EMAP-II) is also secreted in the dental follicle, directly recruiting mononuclear cells but also indirectly through enhancing expression of CSF-1 and MCP-1 (Liu and Wise, 2008).

The activation of the recruited osteoclasts in the follicle is tightly controlled at both a spatial and temporal scale by the Receptor Activator of Nuclear factor Kappa-β (RANKL)/ RANK ligand (RANKL)/osteoprotegerin (OPG) system (Burgess et al., 1999; Kong et al., 1999; Sasaki, 2003a; Wise et al., 2000). RANKL is a Tumour Necrosis factor (TNF)-related cytokine which stimulates the fusion of osteoclast precursors by interacting with RANK located on haematopoietic precursors (Boyle et al., 2003; Burgess et al., 1999; Hsu et al., 1999). Both CSF-1 and RANKL are required to differentiate the precursor into the osteoclast lineage. This cell-to-cell signalling results in a signalling cascade and the recruitment of various members of TNF receptor-associated factors (TRAFs) within the osteoclast precursor (Figure 1.4A). In early stages of osteoclastogenesis, TRAF6 recruiting is a key factor which leads to the activation of mitogen-activated protein kinases (MAPKs) along with transcription factor nuclear factor-κB (NF- κβ)and activator protein-1 (AP-1) (Park et al., 2017; Wise and King, 2008). Once active NF-κβ induces nuclear factor of activated T-cells cytoplasmic 1 (NFATc1), a key osteoclastogenesis regulator. During intermediate stages of signalling, co-stimulatory signals (Figure 1.4B) induces Ca^{2+} oscillation by activated phospholipase Cγ2 (PLCγ2) and c-Fos/AP-1. Ca^{2+} signalling facilitates the production of NFATc1. NFATc1, in late stages of osteoclastogenesis, translocates into the nucleus of the cell to induce numerous osteoclast-specific target genes responsible for cell fusion and function. Other specific subsets of genes induced by RANKL and CSF-1 include cathepsin K (CTSK), tartrate-resistant acid phosphatase (TRAP), and calcitonin receptor and β3-intergrin (Lacey et al., 1998). This regulation by RANKL is vital in osteoclastogenesis throughout several steps including, progenitor survival, differentiation to mono-nuclear pre-osteoclasts, fusion to multi-nuclear mature osteoclasts, and their activation in mineralised tissue resorption. Many cell types express RANKL and include osteoblasts, osteocytes, chondrocytes, stromal cells, T and B lymphocytes in bone and dental follicle cells in

developing teeth and by periodontal ligament cells in adult teeth (Fukushima et al., 2003; O'Brien, 2010).

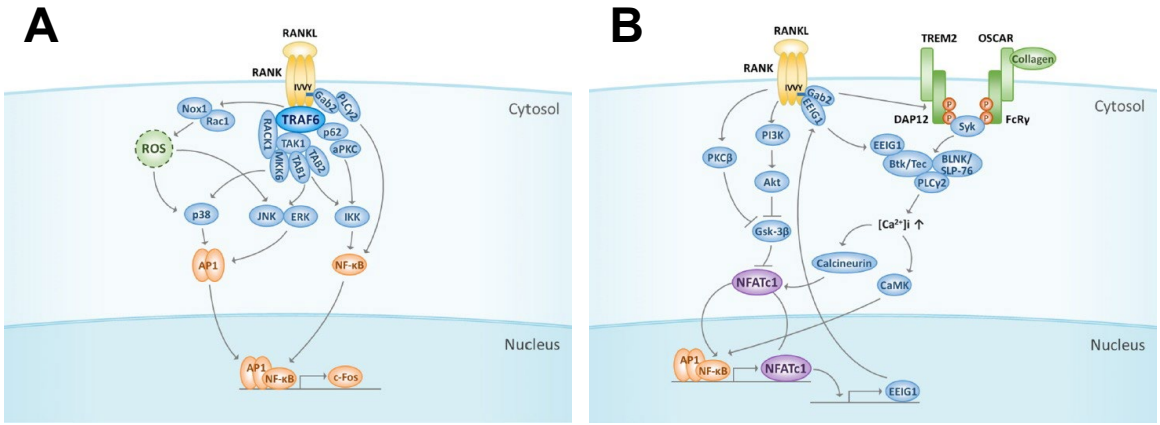

Figure 1.4:A) Initiation of RANK signalling mediated by TRAF6. RANK, receptor activator of nuclear factor-κB; RANKL, receptor activator of nuclear factor-κB ligand; TRAF6, TNF receptor-associated factors 6; NF-κB, nuclear factor-κB; aPCK, atypical protein kinase C; IKK, IκB kinase; TAK1, TGFβ-activated kinase 1; Gab2, growth factor receptor-bound protein 2 (Grb2)-associated binder-2; PLCγ2, phospholipase Cγ2; TAB, TAK1-binding protein; RACK1, receptor for activated C kinase 1; MAPKs, mitogen-activated protein kinases; JNK, c-Jun N-terminal kinase; ERK, extracellular signal-regulated kinase; ROS, reactive oxygen species; NOX1, NADPH oxidase 1; AP-1, activator protein-1; NFATc1, nuclear factor of activated T-cells cytoplasmic 1.

B) Cooperation of RANK signalling with co-stimulatory receptors. ITAM, immunoreceptor tyrosine-based activation motif; TREM-2, triggering receptor expressed in myeloid cells-2; DAP12, DNAX-activation protein 12; OSCAR, osteoclast-associated receptor; FcRγ, Fc receptor common γ subunit; Btk, Bruton's tyrosine kinase; BLNK, B cell linker protein; SLP-76, Src homology 2 domain-containing leukocyte protein of 76 kD; EEIG1, early estrogen-induced gene 1; Gsk-3β, Glycogen synthase kinase-3β; PI3K, phosphoinositide 3-kinase; PKCβ, protein kinase Cβ. (Figures adapted from (Park et al., 2017)

Control of this stimulation for osteoclastogenesis is required and is regulated by OPG, a soluble decoy for RANKL which prevents RANK-RANKL interaction and thus preventing osteoclast formation and activation (Nanci and TenCate, 2017; Sasaki, 2003a; Wise and King, 2008). During a period of major osteoclast formation, it is not the upregulation of RANKL that predominates but the down-regulation of OPG in the dental follicle (Wise et al., 2002). RANKL is expressed but the gene expression is not upregulated (Liu et al., 2005). Osteoclast formation is therefore regulated by the bone and tooth microenvironment. This is a finely tuned system and is particularly important due to the immediate proximity of the permanent tooth crown to the root of the deciduous tooth, where odontoclasts are required to target only the roots of the

deciduous dentition instead of the permanent dentition. This is a chronological and spatial process thought to be a programmed events and has been applied to primary tooth shedding (Harokopakis-Hajishengallis, 2007). In short, physiological tooth resorption during tooth eruption which includes the resorption of alveolar bone and the deciduous teeth are regulated by the local microenvironment of the tooth through the RANK/RANKL/OPG regulatory system with various co-stimulating factors.

1.4 Distinctions between osteoclast and odontoclast

Within physiological tooth resorption two types of cells are responsible for the resorption of mineralised tissue, osteoclasts and odontoclasts. Osteoclasts, as previously mentioned, are responsible for the physiologically regulated resorption of bone of both mineralised and organic material. These are large cells, typically 100 μm in size which require attachment to the bone substratum for activation. The size of the osteoclast is linked to the degree of multinucleation via fusion of osteoclast progenitors. The number of nuclei vary between species such as a normal human osteoclast possessing a range of 4-10 nuclei (Seibel et al., 2006). The number of nuclei appear to reflect osteoclast activity, where *in vitro*, osteoclasts show a positive correlation of nuclei number with the volume of the resorption pit, however as the number of nuclei increases, the volume per nucleus decreases (Piper et al., 1992). A small number of studies have shown these nuclei are all transcriptionally active (Boissy et al., 2002; Saltman et al., 2005). However, it remains unknown if these nuclei work equivalently or specific nuclei express subsets of genes to carry out different functional activities. Osteoclast attachment is mediated by classical integrin receptors, vitronectin receptor αvβ3 and collagen receptor α2β1 (Seibel et al., 2006). This interaction leads to cell spreading and polarisation of the nuclei, where the podosome, a specialised cell-extracellular matrix adhesion structure allow the formation of a tight seal against the bone surface (Väänänen and Horton, 1995). The lower part of an osteoclast forms finger-like processes by deep infoldings of the cell membrane, forming the ruffled border, which lies in contact with the mineralised surface, devoid of cell organoids and is rich in actin filaments (Seibel et al., 2006). This tightly sealed area is where the osteoclast carries our resorption, forming pits referred to as Howship's lacunae (Nanci and TenCate, 2017). In this tightly sealed area, a proton impermeable acidic environment is generated within the Howship's

lacunae by carbonic anhydrase II and vacuolar H^+ ATPase in the ruffled border (Toyosawa et al., 1991). This low pH is responsible for the removal of the bone mineral. Additionally, matrix-degrading enzymes are commonly produced by osteoclasts, particularly cathepsins and collagenases (Delaissé et al., 1993; Ek-Rylander et al., 1997; Goto et al., 1994; Sasaki and Ueno-Matsuda, 1992) such as cathepsin K and matrix metalloproteinase 1. A characteristic marker of osteoclasts is TRAP isoenzyme and its presence is routinely used to identify osteoclasts in tissue sections (Ek-Rylander et al., 1997).

Odontoclasts are involved in the physiological resorption of the roots of deciduous teeth. Though these are smaller in size and have fewer nuclei, odontoclasts appear highly similar to osteoclasts in their ability to resorb mineralised tissue but also in their differentiation pathway (Hammarström and Lindskog, 1985; Kamat et al., 2013; Sasaki, 2003a). Results have suggested that there is a common regulatory mechanism of cellular resorption of mineralised tissues of bones and teeth (Oshiro et al., 2001; Sasaki, 2003a). Though the substrate differs, there appears to be no observable difference in both structural and cytochemical properties between odontoclasts and osteoclasts and there appears to be a common regulatory mechanism of cellular resorption of mineralised tissues (Sasaki, 2003a). Overall, osteoclasts and odontoclasts are similar both in appearance and functionally and differ primarily by their substrate. From this point, the use of osteoclast and odontoclast will be used in relation to the respective substrate.

1.5 Feline tooth resorption (feline odontoclastic resorptive lesions or neck lesions)

Physiological tooth resorption is a normal process which is responsible for tooth eruption and tooth shedding. This is aided by osteoclasts and odontoclasts and the dental follicle as previously described. However, in the permanent dentition this is largely pathological (Darcey and Qualtrough, 2013) and the dental follicle has no involvement due to shedding of the entire follicle during tooth eruption. This is referred to as tooth resorption (TR) and is commonly observed in domestic cats. The factors in physiological resorption may not be the same as those responsible for TR. An important aspect of TR is that this often initiates anywhere on the root surface and

is not confined to the cementoenamel junction (Harvey et al., 2004). Though there have been reports of TR initiating within the pulp space (Bellows, 1993; Reiter and Mendoza, 2002), TR usually occurs externally in cats (Farcas et al., 2014; Lommer and Verstraete, 2000). Internal resorption lesions which include the apical and coronal dentine and pulp are usually resultant of external TR progressing inwards.

TR can be classified into different stages. Currently, classification follows the criteria suggested by the American Veterinary Dental College (AVDC). This classification is based on the severity of resorption (Stages 1-5), on the location of the resorption

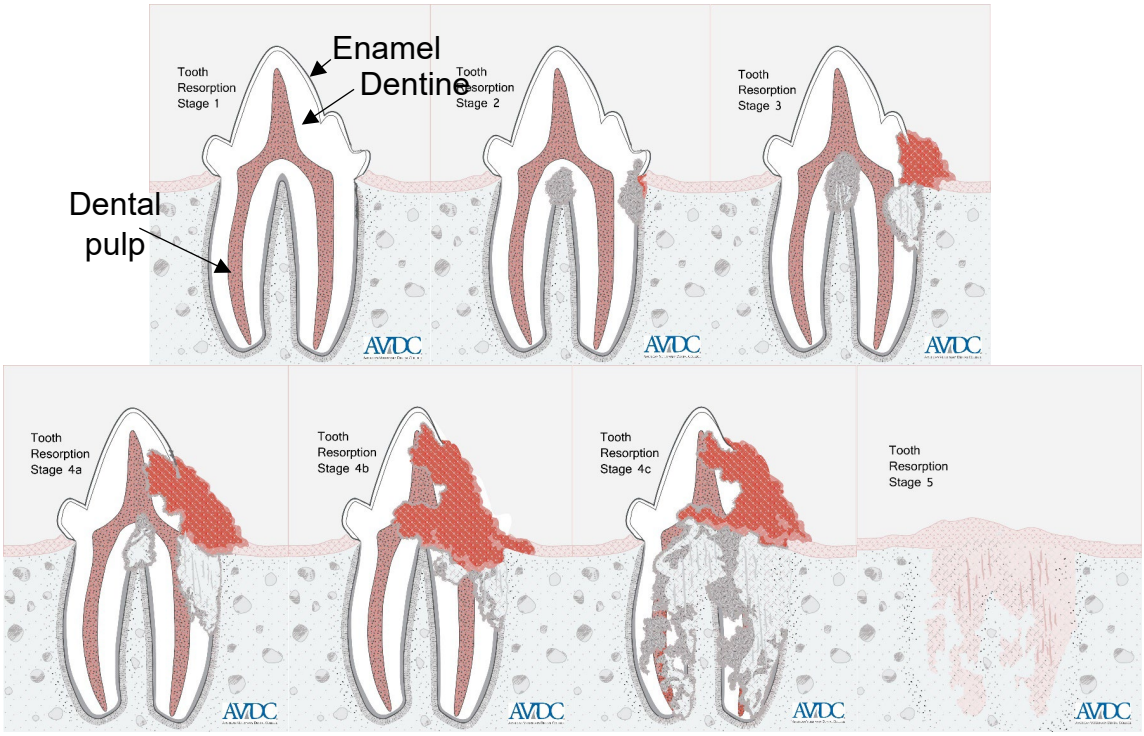

Figure 1.5: Stages of tooth resorption. Stage 1 – early TR development, mild dental hard tissue loss (cementum or cementum & enamel); Stage 2 – Moderate dental hard tissue loss (Cementum or cementum & enamel with loss of dentin, but loss does not extend to the pulp cavity); Stage 3 – Deep dental hard tissue loss (cementum or cementum & enamel with loss of dentin, loss extending into the pulp cavity). Most of the tooth still retains integrity. Stage 4 – Extensive dental hard tissue loss (cementum or cementum & enamel with loss of dentin, loss extends to the pulp cavity); most of the tooth has lost its integrity. Stage 4 is subdivided into three further stages based on the extent of damage to the crown or root. Stage 4A – crown and root are equally affected; 4B - crown is more severely affected than the crown; 4C - Root is more severely affected than the crown. Stage 5 – Remnants of dental hard tissue are only visible as irregular radiopacities, and the gingival covering is formed (Figure adapted from ("AVDC Nomenclature | AVDC.org," n.d.)).

(Types 1-3) based on radiographic appearance, and the assumption that TR is a progressive condition (Figure 1.5)(“AVDC Nomenclature | AVDC.org,” n.d.).

The types of resorption are based on radiographic appearance. In type 1, a radiograph with a focal or multifocal radiolucency is present in the tooth with otherwise normal radiopacity and normal PDL space. In this lesion, the lost root structure is not replaced with bone. In type 2, a radiograph would show the narrowing or disappearance of the PDL space in at least some areas and decreased radiopacity of part of the tooth. This may be observed histologically where there is marked replacement of the lost tooth structure with bone. Type 3 appearance features both type 1 and type 2 in the same tooth. In some areas of this tooth there are areas of normal and narrow or lost PDL space, and there is focal or multifocal radiolucency in the tooth and decreased radiopacity in other areas of the tooth.

In early stages, stage 1, lesions are barely detected both clinically and radiographically due to their small size and is confined to the cementum and enamel which is too thin to reflect resorptive activity to be observed radiographically (Heaton et al., 2004; Lommer and Verstraete, 2000). However, TR unaffected teeth have been shown to possess offstage 1 TR, where histological features include the degeneration of the PDL, a narrow PDL space, and a localised resorption lesion which may be surface root resorption with cementum resorption or replacement resorption, ankylosis fusion of tooth and alveolar bone (Gorrel and Larsson, 2002). It is also important to note that there is no inflammation reported adjacent to these early TR lesions.

In stage 2 TR, which can be radiographically detected, however clinical signs are not apparent, and the histological features are similar to stage 1 TR, with moderate loss of cementum and enamel with a loss of dentine that does not extend into the pulp cavity.

In stages 3 to 5, this involves extensive dental hard tissue loss and dentine loss that extends into the pulp cavity. Clinically, advanced stages of TR are often observed in the neck region as red granulation tissues hence their initial reference as neck lesions or feline odontoclastic resorptive lesions (FORLs). In these stages, clinical signs detected by oral examination are represented by histological features of active

and advanced TR described in two phases: a resorptive phase and reparative phase. Odontoclasts rapidly resorb mineralised tissue and have a limited life time which makes obtaining histological sections of each stage difficult (Booij-Vrieling et al., 2010; Okuda and Harvey, 1992; Reiter et al., 2005a). The morphology of the resorptive phase consists of multiple lacunae similar to resorptive activity observed in deciduous teeth shedding, where multinucleated odontoclasts were sitting in the lacunae of intact dentin or cementum (Okuda and Harvey, 1992). Surrounding tissues are involved in inflammatory lesions that often accompany TR, however there is currently no conclusive evidence that determines if this is the consequence of TR lesions or if they contribute to the aetiology of TR (Gorrel, 2015; Okuda and Harvey, 1992). In the resorption lesions, these are filled with hyperplastic gingiva and vascular granulation tissue. Various inflammatory cells such as macrophages, neutrophils, and plasma cells along with fibroblasts are recruited to the TR lesions.

The reparative phase follows, this is a coordinated process where rounded osteoblasts and cementoblasts produce hard tissues such as cementum and osteodentine in order to replace the damaged tissue. It should also be noted that these two phases are not exclusive and can occur simultaneously. In late and prolonged stages of TR, the odontoclasts may reach a quiescent stage, where most of the dental tissues undergo dental-alveolar ankylosis, replacement with bone-like tissue. During these phases, not only the mineralised tissue is lost, but the morphology of the PDL is also affected where it is either altered or destroyed. The assumption is that the damaged PDL is repopulated by progenitor cells from adjacent bone marrow onto the resorbed root surface allowing the formation of bone directly on the dental tissue (Andreasen, 1985). Overall, these histological findings indicate the importance of the periodontium's dynamic properties in TR development (Booij-Vrieling et al., 2010; Okuda and Harvey, 1992; Reiter et al., 2005a; Reiter and Mendoza, 2002; Roux et al., 2005).

Along with the advanced TR where the two phases of resorption and repair are described, another type of tooth resorption is also observed, namely peripheral inflammatory root resorption (PIRR). PIRR is where the resorptive process is propagated by osteoclast-activating factors provided by inflammatory lesions in adjacent PDL tissues (Andreasen, 1985). These two types of tooth resorption are

most commonly observed in cats and may be defined as either inflammatory or non-inflammatory, however there is no distinction made between tooth resorptions from inflammatory causes from those which are truly idiopathic (Gorrel, 2015). Overall, the loss of dental tissue and replacement with bone-like tissue results in compromised structural integrity. The loss of the PDL removes dampening of the occlusal forces and mechanical stress on the tooth which instead directly transmits to the alveolar bone. This causes pain for the cat and possible loss of tooth upon sudden forces which may cause the tooth to shatter.

1.6 Prevalence of TR

TR is not a new disease. Reports of TR lesions have been observed in cat skulls from the 13th century (Berger et al., 2004). It was only in the 1980's onwards where feline tooth surveys became commonplace where increasing incidence and high prevalence are reported. This sudden rise of TR in cats is most likely due to a variety of factors including the improved lifespan and rising population of ageing cats, the development of small animal practice, and an increased awareness and detection of this condition through systematic clinical examination and improvements in accessibility of dental radiology for diagnosis. Many reports have reported on the prevalence of TR among the domestic cat population. These range from 29 – 58% (average 43%) in the general population of cats (Coles, 1990; Girard et al., 2008; Ingham et al., 2001; Lund et al., 1998; Mestrinho et al., 2013). The prevalence appears to show a difference between breeds as mixed breed cats showed a prevalence of 38% while in pure bred cats a prevalence as high as 70% is observed (Ingham et al., 2001; Lommer and Verstraete, 2000). TR also appears to most commonly affect the mandibular third premolars (Okuda and Harvey, 1992; van Wessum et al., 1992) and these are commonly used as a marker in rapid screening. TR is not confined to premolars and can affect any tooth (Harvey et al., 2004; Ingham et al., 2001). The prevalence and number of affected teeth is also associated with increased age (Farcas et al., 2014; Ingham et al., 2001). Neutering, gender, age at neutering or mean whole mouth gingivitis index does not affect the prevalence of TR (Gorrel, 2015; Ingham et al., 2001; Lommer and Verstraete, 2000). In summary, TR affects a large proportion of the domestic cat population, with increased risk with age and a higher prevalence in pure bred cats.

1.7 Treatment of tooth resorption

There are currently no effective treatments that prevent the development of TR due to its progressive nature and the lack of knowledge of the aetiology (Gorrel, 2015). Current TR treatment is palliative and aimed to relieve pain and prevent TR related infection through conservative management. This includes clinical and radiographic examination of the lesions which is particularly useful in monitoring early lesions confined to the tooth root. Under specific clinical symptoms and progression of TR, coronal amputation or total tooth extraction is performed. Total tooth extraction ensures the removal of all resorbed and potentially infected substances occurring through TR. However, this is notoriously difficult due to extensive resorption of the roots and their replacement by bone tissue through ankylosis, leading to the fusion between the tooth and alveolar bone. This leads to loss of structural integrity and therefore becomes prone to shattering either due to occlusal stress or during tooth extraction. Coronal amputation is better suited in this circumstance, where the crown and upper part of the root are removed while the remaining resorbed root is closed through suturing the surrounding gingival tissue.

There have been previous attempts to prevent TR, such as a pilot study in which osteoclasts were targeted due to their primary role. A class of bisphosphonates (BPs), Alendronate, was used in the study, which is used in humans for treating osteoporosis. This acts by high affinity binding of hydroxyapatite in the bone to inhibit osteoclast recruitment and resorptive activity, ultimately leading to induction to osteoclast apoptosis (Drake et al., 2008). Alendronate accumulates on subgingival tooth and alveolar bone surfaces next to vascularised tissue, concentrating the deposition around the tooth roots and effectively suppressing TR progression in cat (Mohn et al., 2009). This appeared promising as a potential anti-resorptive drug for future treatment, however BPs have been linked with bisphosphonate-related osteonecrosis of the jaws suspected to be resulting from off target complications as a result of long-term use of these medications (Barba-Recreo et al., 2014).

From these studies, the treatment may not have been effective and appropriate for future use. However, the high deposition of BPs in calcified tissues demonstrated

prevention of odontoclast formation and their resorptive activity in TR. This ultimately indicates dysregulated osteoclasts are responsible for TR (Mohn et al., 2009).

1.8 Aetiology of tooth resorption

Though feline TR is one of the most common dental problems observed in cats and it is understood that odontoclasts are responsible for resorption, the aetiology of TR remains unknown. This is an ongoing discussion where many studies have attempted to elucidate the aetiology, but the precise causes are still unknown.

Various studies have been performed to identify local and systemic factors involved such as diet, gender, biomechanical stress, and anatomical defects in tooth morphology (Booij-Vrieling et al., 2010; DeLaurier et al., 2002; Donoghue et al., 1994; Kanzaki et al., 2002; Okuda and Harvey, 1992; Reiter et al., 2005a; Reiter and Mendoza, 2002; Scarlett et al., 1999)

1.8.1 Inflammation

Due to clinical presentation of TR often coinciding with other oral inflammatory diseases (Dupont and Debowes, 2002), inflammation appears to be an important aspect and suspected initiating factor of feline TR. Inflammatory cytokines have been considered to act in the recruitment of osteoclast/odontoclast progenitors. In one study, higher mRNA levels were reported for *IL1β* in teeth with TR lesions than in normal teeth but no such differences were found between pathological and normal gingival samples (DeLaurier et al., 2002). This is supported by observations of these inflammatory cytokines promoting osteoclast differentiation (Amarasekara et al., 2018).

However, it is important to note it has yet to be determined if increased expression of these cytokines is the result of inflammation due to TR or if these are an initiation factor. Additionally, these do not affect the expression of the RANKL and OPG, downstream regulators of osteoclast/odontoclast differentiation. It should also be noted that in this study semi-quantitative RT-PCR was used to measure mRNA of the cytokines, meaning that measurements of this gene expression are questionable (DeLaurier et al., 2002).

In another study looking into the involvement of inflammatory cytokines and the possible role of vitamin D in TR pathophysiology, quantitative PCR analysis was performed (Booij-Vrieling et al., 2010). An increase of stimulatory cytokines such as *IL1β, IL6,* and *TNF* were reported along with nuclear vitamin D receptor (VDR) in tissues with TR lesions when compared to healthy controls. However, cytokines IL-10 and interferon gamma (IFNγ) were also increased in TR affected teeth, which is contradictory as IL-10 is known as an anti-inflammatory cytokine and IFNγ has an inhibitory effect on osteoclastogenesis. The mRNA levels of RANKL and OPG were similar in TR and the control group (Booij-Vrieling et al., 2010). Even though most TR lesions are associated with inflammatory cells, this is not reported in early lesions that are covered with an apparently normal gingiva. Researchers therefore propose that the involvement of inflammatory cells is not a primary event but secondary in TR development.

1.8.2 Diet

Diet is another suggested aetiological factor. In one study, TR was correlated with low calcium or low magnesium intake from homemade food (Mulligan, 1990). This observation is consistent with another cross sectional study in which cats fed a high content of minerals such as calcium, magnesium, phosphorous, and potassium experienced less TR (Lund et al., 1998). However, this study examined homemade foods but most cats are fed commercially prepared foods, which are nutritionally balanced to provide sufficient minerals and therefore mineral deficiencies should not currently be a major issue nor have effect a large proportion of cats (Donoghue et al., 1994). In one study, it was presumed that commercial dry cat food with acidic coatings can lead to TR lesions by altering the pH of the tooth surface However, cats with TR lesions showed a lower pH value of the tooth surface than that in healthy cats and was found not to contribute to TR pathogenesis (Zetner and Steurer, 1992). In another study, indoor cats or city cats which have less chance to hunt prey were found to have a higher risk of TR development however the use of commercial treats showed a reduction of risk by approximately three fold (Scarlett et al., 1999).

Overall, though particular foods in the diet of cats may indicate an increased or lowered risk in developing TR, there appears to be many inconsistencies in if diet contributes to TR initiation. Furthermore, data collection via questionnaires of owners

may be subject to bias or be incorrect due to inconsistent behavioural changes of cats to tooth resorption (e.g. such as expressing pain or selection of wet foods over dry foods). Currently, there are no longitudinal studies to report incidences of feline TR of cats on defined diets with known mineral concentrations. It is therefore undetermined if TR prevalence can be modulated with diet.

1.8.3 Vitamin D and their metabolites

Vitamin D levels can indirectly influence osteoclastic bone resorption via the RANK/RANKL signalling cascade and due to the inability of cats to produce vitamin D in their skin, this is an essential supplement in commercial cat foods (How et al., 1994). Vitamin D and vitamin D metabolites are important regulators of bone turnover and resorption through regulating calcium levels (Bikle, 2014). 25-hydroxyvitamin D is the major circulating form of vitamin D and is commonly measured to determine vitamin D status, however it is not the most active form of vitamin D, therefore measurement of $1,25(OH)_2D_3$ is desirable (Bikle, 2014). Calcium concentrations in serum is maintained in the normal range through the actions of various systemic hormones including parathyroid hormone, fibroblast growth factor 23 and 1,25-dihydroxyvitamin D_3's [$1,25(OH)_2D_3$]. $1,25(OH)_2D_3$ increases intestinal absorption of dietary calcium and recruits haematopoietic stem cells for the production of osteoclasts. $1,25(OH)_2D_3$ does not directly act on osteoclasts however due to their lack of receptors for $1,25(OH)_2D_3$ (Bikle, 2014), but acts on osteoblasts to produce osteoclast stimulating factors such as RANKL. One study reported a link between raised levels of 25-hydroxyvitamin D and odontoclastic tooth resorption (Reiter and Mendoza, 2002), and it was concluded that chronic excess of vitamin D may be a major contributor in TR pathogenesis. However in later studies, raised circulating levels of 25-hydroxyvitamin D in cats with tooth resorption could not be identified and the authors concluded that increased serum 25-hydroxyvitamin D levels as a causative factor could not be supported (Booij-Vrieling et al., 2010; Girard et al., 2010b; Zhang et al., 2006). Though studies have shown systemic levels of vitamin D, including 25-hydroxyvitamin D varies greatly in the serum of TR cats (Booij-Vrieling et al., 2009; Girard et al., 2010a; Reiter et al., 2005b), it's impact on bone and dentition is unclear and still requires further studies to confirm the role of vitamin D in feline TR (Anderson and Atkins, 2008).

1.8.4 Mechanical load

Mechanical load, microfracture of cementum and malocclusion have been suggested as an aetiological factor of TR in cats (Reiter et al., 2005a). Occlusal stress theory, also known as tooth flexure was created to attempt to explain non-carious lesions at the cervical portion of human teeth caused by repeated compressive and occlusal stress during mastication or malocclusion disrupting the bond between the enamel and dentine (Goel et al., 1991). This can also lead to inflammation of the cementum or periodontal ligament leading to the recruitment of odontoclast progenitors to the site. Human PDL cells *in vitro* express RANKL and OPG (Uchiyama et al., 2009). Depending on occlusal stress, RANKL expression is constitutively increased (Choi et al., 2017; Kanzaki et al., 2002; Nakano et al., 2011). A similar process could occur in cats where occlusal stress may induce TR.

Some studies have performed orthodontic treatment in cats (Celebi et al., 2013; Collins and Sinclair, 1988; Davidovitch et al., 1975). After application of mechanical forces to the canines, many resorption lacunae were identified in the apical region of the alveolar bone socket and wide areas of root resorption were clearly observed. Similar histological patterns were observed in mice and humans following orthodontic treatment. This evidence suggests that mechanical load and malocclusion could be contributing factors in the pathogenesis of feline TR.

1.9 Next generation sequencing and applications

For feline TR, there is only one study investigating the possibility of genetic predispositions (Lee et al., 2020b). This is particularly relevant due to a reportedly higher incidence of TR in purebred cats and a widespread presence of TR in siblings within the population, suggesting that there is a potential genetic predisposition for feline TR (Ingham et al., 2001). Therefore, genetic studies into feline tooth resorption may provide insight into the aetiology of feline TR.

Traditional genetic studies involve the use of DNA samples from a defined population where these are genotyped through either PCR, Sanger sequencing, or restriction fragment length polymorphism. The genotype and phenotype are then analysed whilst considering variables. Though this is a valid method for genetic analysis, this process is time consuming and is limited in the number of genes that can be

sequenced. Over the past few decades, sequencing and genetic analysis has rapidly improved in both efficiency and cost, allowing high throughput of samples which can be sequenced in parallel, this is referred to as next generation sequencing (NGS)(Goodwin et al., 2016). This in turn has allowed great progression in genetics and the development of various sequencing techniques including RNA sequencing (RNA-seq).

RNA-seq is a technique that allows the examination of the quantity and sequences of RNA in a sample, allowing investigation of the transcriptome: the total cellular content of RNA such as mRNA, rRNA, and tRNA (Wang et al., 2009). This helps us understand the information of the genome and its functional protein expression. This technique allows the analysis of which genes are expressed in a cell, the level of expression, and the time of expression itself, allowing comparisons of gene expression between different sample groups, treatments or time points. RNA-seq ultimately provides information about the function and transcriptional structure of genes, highlighting features such as post-translational modifications, alternatively spliced transcripts, gene fusions, and sequence variations, such as single nucleotide polymorphisms (SNPs) (Wang et al., 2009). Compared to microarrays, RNA-seq has a greater sensitivity in measuring differential gene expression. One useful aspect of RNA-seq is that unlike hybridisation-based approaches, RNA-seq is not restricted to detecting transcripts corresponding of an existing genomic sequence, making this advantageous in the study of non-model organisms with genomic sequences that are not yet determined or annotated.

SNPs are single nucleotide base variations caused by transitions or transversions, in the same position between individual genomic DNA sequences (Brookes, 1999; Zhao et al., 2019). This is the predominant type of polymorphism in DNA for genetic variation which may be found in various locations, from within genomes, intergenic regions, exons, and introns (Jehan and Lakhanpaul, 2006; Zhao et al., 2019). SNPs in coding regions can be divided into synonymous, where the protein sequence is unaffected, and nonsynonymous, where the protein sequence is affected. Due to the considerable effects of SNPs on protein function and gene expression caused by SNPs, these are therefore of great potential in genetic studies (Mitchell-Olds and Schmitt, 2006). SNPs are found in high density, scalability and distributed throughout

the genome, making them useful in genetic studies in characterising genetic resources and functional gene identification for traits (Seeb et al., 2011). Using RNA-seq data for SNP analysis has quickly become commonplace due to multiple advantages. One advantage is that thousands of SNPs can be discovered and the expression levels of functional genes with sequence variations can be observed simultaneously at a reasonable cost. Another advantage is that locations of SNPs within coding regions associated with biological traits can be identified and translated into phenotype predictions according to the genotype (Yu et al., 2014). Additionally, RNA-seq allows for characterisation of genes, quantification of gene expression, and analysis of post-translational process (Quinn et al., 2013). This has made RNA-seq particularly attractive for genetic polymorphism analysis.

Though RNA-seq can generate massive amounts of data from a single sample, the major challenge comes from the methods of analysing such volumes of data to gain meaningful biological interpretation (Trapnell et al., 2010). Bioinformaticians have contributed to this development with a wide variety of algorithms, analytical software, and analysis pipelines (e.g. Picard, SAMtools, Galaxym Pysam, R, etc.) which has allowed elucidation of biological findings in a wide range of animals. With such a variety and volume of data generated from NGS, this requires to be met by proper analysis to generate a biologically relevant interpretation. In recent years bioinformaticians have contributed to the development of various algorithms, analytical software, and data analysis tools (e.g. Trimmomatic, Picard, R) which have greatly aided in various biological pathways in a broad range of organisms. One example of NGS application is the discovery of approximately 300 novel miRNAs which act as regulators of gene expression in equine osteochondrosis physiopathology and also involved in the cellular response to biomechanical stress in cartilage and bone when comparing healthy and osteochondrosis affected foals (Desjardin et al., 2014).

Using this technique, the results confirmed previous findings of a preliminary proteomics study where equine osteochondrosis was shown to be associated with combined cartilage and bone defects (Desjardin et al., 2014). In one RNA-seq study, transcriptome analysis was performed on ameloblasts during amelogenesis. This provided information on their differential expression and provided a method for

identifying genes and proteins that are critical for dental enamel formation (Simmer et al., 2014). Overall, the large volume of data produced by this method provides invaluable information in elucidating comprehensive pathways along with identifying novel genes involved in both physiological processes and pathological conditions.

1.10 Previous studies

In a recent RNAseq study (Lee, 2019; Lee et al., 2020a), transcriptomic changes were identified when comparing TR affected and unaffected teeth. In this study, a procedure for the isolation of RNA from feline teeth was successfully established along with the generation of feline osteoclasts from primary feline bone marrow *in vitro*. Transcriptomic analysis identified many differentially expressed genes between TR affected and TR unaffected teeth within the same cat. Upregulated genes were known to be associated with osteoclast differentiation and calcium signalling pathways (Lee, 2019). Other upregulated genes identified were involved in muscle and tooth development, suggesting the repair or bone formation in TR affected teeth as a result of tooth resorption. Previous studies into the aetiology of feline TR suggested a possible important role of inflammation and vitamin D (Booij-Vrieling et al., 2010). However, in this study, the expression of inflammatory cytokines, vitamin D receptor, or RANKL showed no statistically significant difference between TR affected and TR unaffected teeth (Lee, 2019). Candidate genes possibly involved in odontoclast dysregulation in TR were identified by RNA-seq data and quantitative PCR. Of these, matrix metalloproteinase 9 was of particular interest due to its potential role in osteoclast biology. In a functional study a MMP9 inhibitor reduced osteoclast formation and resorptive activity *in vitro* (Lee, 2019). Furthermore, whilst feline *MMP9* siRNA inhibited osteoclast differentiation it showed little effect on dentine resorption activity. Overall, the results from this study showed the transcriptome of TR affected teeth was locally different from TR negative teeth and that genes in pathways associated with osteoclast formation were upregulated in TR affected teeth.

1.11 Small interfering RNA molecules (siRNAs) and their applications

Small interfering RNA molecules (siRNA), also called short interfering RNA, are double stranded RNA molecules of 20-25 nucleotides. These occur naturally in the

body and are involved in the downregulation of genes at a post-transcriptional level in RNA interference (RNAi) (Matzke and Birchler, 2005). SiRNAs are produced from 200-500 bp double stranded RNA where an RNA enzyme, Dicer, cleaves the RNA into short fragments of 20-25 bpm, leaving nucleotide overhangs at the 3' hydroxyl termini (Figure 1.6). RNA-induced silencing complex (RISC) attaches to the siRNA. When activated, the anti-sense and sense strands are separated from each other (Agrawal et al., 2003). The exposed anti-sense guides the RISC for downstream RNAi to the complementary mRNA target where endogenous endonucleases cleavage is performed by Argonaute 2 (AGO2). The reduction of mRNA levels then leads to the decrease of encoded proteins of interest.

SiRNAs have been recognised to be a very powerful tool for silencing gene expression *in vitro* and *in vivo* with their sequence specific mechanism in both experimental investigations and therapeutic strategies. A phase 1 clinical trial was conducted in humans involving the systemic administration of siRNA to patients with solid cancers using a targeted, nanoparticle delivery system (Davis et al., 2010). From this study, siRNA was administered systemically to a human showed a reduction in mRNA and protein of a specific gene by an RNAi mechanism. This is an ideal tool for investigating the effect of specific genes on a cellular process and elucidating their role in processes such as osteoclast differentiation.

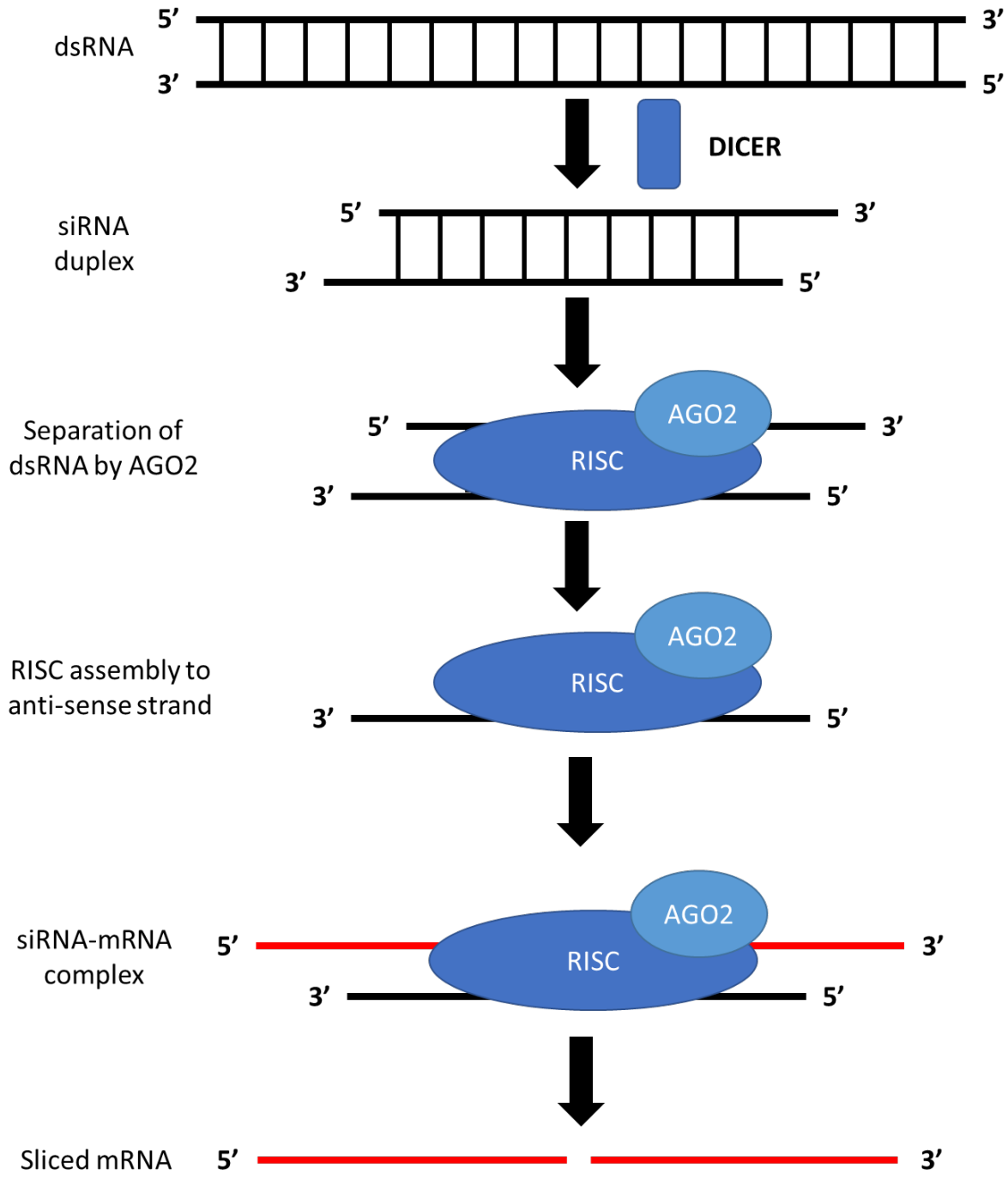

Figure 1.6: Diagram showing siRNA mechanism of action.

1.12 Aims and hypothesis

The aims of this study were to 1) identify SNPs which could provide potential genetic predispositions of TR initiation and progression, 2) investigate the expression of candidate proteins in feline tooth samples, and 3) optimise and investigate candidate gene function in osteoclast differentiation and resorptive activity.

These aims are formed to test the hypothesis that these candidate genes contribute to the development of feline TR by activation of osteoclastogenesis and osteoclast-mediated resorption.

Specifically, I will:

- Analyse RNAseq datasets with an established bioinformatics pipeline according to best practices to identify SNPs and their impacts on gene expression.
- Further analyse RNAseq data for differentially expressed genes and their associated pathways.
- Localise protein expression of candidate genes in histological tooth sections.
- Optimise a method of siRNA transfection via electroporation using a well-established protocol for culturing feline osteoclasts derived from feline bone marrow.
- Test the functional role of three candidate genes (MMP9, CTSK, P2XR4) identified from the RNA-seq data in their ability to influence osteoclast biology and resorption of mineralised tissue. This will be performed using siRNAs targeting the respective feline gene sequences.

2 Materials and methods

2.1 Bioinformatics

2.1.1 RNA sequencing data (RNA-seq data)

RNA-seq was performed in a previous study, investigating odontoclast dysregulation in feline TR by identifying transcriptomic changes between TR+ and TR- teeth (Lee, 2019; Lee et al., 2020b). All raw reads can be accessed from the European Nucleotide Archive (ENA) under the identifier PRJEB24183. Of the total 12 libraries, 9 raw sequencing reads were chosen for re-analysis. This was to assess only TR-ve teeth from TR free cats and TR+ve teeth from TR affected cats. The RNA-seq raw reads are derived from 9 dental samples: 6 TR+ve dental samples from cats with TR and 3 TR-ve samples from cats free from TR (Table 2.1).

Cat ID	Extracted teeth	TR status	TR type	TR stage	Age (Years)	Sex
N14C12	307,308,407,408	-	N/A	N/A	4	F
N28C15	307,407	-	N/A	N/A	9	NF
N29C25	307,407	-	N/A	N/A	10	NF
N08C8	307,407	+	2	2	>5	F
N30C16	308	+	2	2	5	NF
N22C27	404	+	2	2	7	NF
N32C29	108	+	3	4	7	NF
N24C30	307	+	2	2	10	NF
N26C32	407	+	3	4	6	NF

Table 2.1: Sample details and TR phenotyping. Extracted teeth numbers follow modified Triadan system. Triadan system is a three-digit numbering system for numbering teeth across different animal species. The first digit denotes the quadrant: 1-Right upper permanent, 2-Left upper permanent, 3-Right lower permanent, 4-Left lower permanent. The second and third digits denote the tooth position within the quadrant, always starting from the midline. In domestic cats, 01-03: incisors, 04: canine, 06-08: premolars, 09 molars. All cats were mixed breed. N/A: not applicable, F: Female, NF: Neutered female.

2.1.2 Processing raw data and alignment to the feline reference genome

Bioinformatics tools and genome version for best practices were updated to current versions for analysis. All reads were processed using Trimmomatic v0.36 (Bolger et al., 2014) with parameters TRAILING:20 SLIDINGWINDOW:4:20 MINLEN:20. TRAILING:20. These parameters, respectively, remove bases from the 3’ end of a

read if their Phred score is below 20 (Phred scores are the logarithmic of the probability that a base was called incorrectly; a score of 20 is equivalent to 99% accuracy), clip the read if the average Phred score within a 4bp sliding window advanced from the 5' end falls below 20, and require a minimum read length, after trimming, of 20bp. Cleaned reads were aligned against the reference genome, Felis_catus9.0, obtained from Ensembl v98 (Cunningham et al., 2019), using BWA-MEM 0.7.12 (Li and Durbin, 2009) with default parameters. The output files were merged and duplicates marked using Picard Tools v2.5.0 (https://broadinstitute.github.io/picard/, accessed 8th January 2020) to create one BAM file per sample.

2.1.3 Variant calling from aligned reads

Variants were called using GATK v4.1.4.0 with the HaplotypeCaller module (McKenna et al., 2010) with parameter --emit-ref-confidence GVCF, which produces a gVCF which are later merged, in accordance with GATK best practice recommendations (https://gatk.broadinstitute.org/hc/en-us/sections/360007226651-Best-Practices-Workflows, accessed 8th January 2020). Base quality scores were recalibrated using GATK BaseRecalibrator and ApplyBQSR, with Feline SNP data from Ensembl (ftp://ftp.ensembl.org/pub/release 100/fasta/felis_catus/dna/Felis_catus.Felis_catus_9.0.dna.toplevel.fa.gz) as a known source. SNPs from Ensembl were used as a training set and a subset of the highest-confidence calls from the gVCF, generated by merging variant call files (VCFs) GATK CombineGVCFs into a single gVCF, as the truth set. Training sites are used by GATK to recalibrate the scores of variants that overlap with them, whereas truth sites are used to determine where the recalibration model sets a sensitivity cut-off. Training and truth sites were drawn from the same source as there was no independent, and substantive, database of cat SNPs, such as dbSNP (Sherry, 2001), a human only SNP database. The truth subset was obtained using GATK SelectVariants with parameters --select-type-to-include SNP -select "QUAL > 100" -select "DP > 50". Functional effect prediction of each SNP was performed using SnpEff v4.3T.

2.1.4 Prediction of SNP impact on gene expression using SnpEff

SnpEff assesses the putative impact of each SNP on the function of its protein product, classifying them into four categories: High, moderate, low, or modifier (Appendix A). The order is based on the severity on SNP impact on the function of the protein product. For example, a high impact SNP includes frameshift or the gain or loss of a start/stop codon. Moderate impact SNPs include missense variants and splice region variants. Low impact SNPs include synonymous variants and stop retention, the change of codon into another for same amino acid and the mutation of a stop codon into another stop codon respectively. Modifier variants are usually non-coding or affect non-coding genes, which are difficult to predict or have no evidence of impact such as exon and intron variants. This categorisation provides a suitable system in finding significant variants; however, these are predictions and do not exactly predict whether a high or low impact variant produces the phenotype of interest. To increase reliability of observed variants, SNPs with <10 reads to support the variant allele were omitted to provide the following data. Additionally, genes were filtered to restrict analysis to genes with detectable expression in teeth.

2.2 Immunohistochemistry

2.2.1 Tissue processing

Samples were donated to the Edinburgh Memorial Programme (EMP) following full owner's consent presented to the Hospital for Small Animals, The Royal (Dick) School of Veterinary Studies, The University of Edinburgh, UK. Additionally, clinical tooth samples were collected from patients whose owners were willing to participate in the study and have provided full informed and signed consent. The sourcing of all animal tissues for this study was reviewed by the R(D)SVS Veterinary Ethical Research Committee and got approval (VERC reference 160.19).

All samples were initially fixed in 10% neutral buffered formalin and radiographed to assess samples for the presence of resorptive lesions. TR type and staging were confirmed by review of dental radiographs by veterinary dental specialist, S. Thorne (MRCVS, RCVS, American & European Specialist in Veterinary Dentistry, DentalVets, Haddington). Samples were decalcified in 10% ethylenediaminetetraacetic acid (EDTA) at 4°C under gentle agitation for 120 days. To aid the rate of demineralisation, individual teeth were separated.

2.2.2 Paraffin embedding and sectioning

Following demineralisation, samples were wax processed using a Leica ASP300S (Programme protocol recorded in Table 2.2). Though lesions were observed at the enamel-gingival margin, tooth resorption is commonly observed within the bifurcation of teeth in initial stages of the disease. Tooth samples were therefore split across the bifurcation and embedded in paraffin wax. Sections were obtained at 5 μm thickness using a Leica microtome and captured on Superfrost glass slides (Thermoscientific). Samples were left to dry before incubation at 55°C overnight to adhere sections to the slide surface.

Reagent	Duration (hour:min)	Temperature (°C)	Pressure/Vacuum	Drain (sec)
Ethanol 70%	01:00	-	V	80
Ethanol 70%	01:00	-	V	80
Ethanol 90%	01:00	-	V	80
Ethanol 90%	01:00	-	V	80
Ethanol Absolute	01:00	-	V	80
Ethanol Absolute	01:00	-	V	80
Ethanol Absolute	01:00	-	V	140
Xylene	01:00	37	V	80
Xylene	01:00	37	V	80
Xylene	01:00	37	V	140
Paraffin Wax	01:00	62	P/V	140
Paraffin Wax	01:00	62	P/V	140
Paraffin Wax	01:00	62	P/V	140

Table 2.2: Program used for wax processing of sample.

2.2.3 Haematoxylin and Eosin (H&E) staining

To visualise overall structure and state of tooth sections, chemical staining, namely, H&E staining was performed using an automated program in an autostainer machine as detailed in Table 2.3. Cover slips were applied with PERTEX xylene based Mounting Media (CellPath, UK).

Reagent	Duration (minutes:seconds)
Xylene	5:00
Xylene	5:00
Xylene	5:00
100% Ethanol	3:00
100% Ethanol	2:00
95% Ethanol	2:00
Water	5:00
Haematoxylin	3:00
Water	3:00
Water	3:00
Scott's Tap water	2:00
Water	2:00
Eosin	2:00
Water	0:45
70% Ethanol	0:30
95% Ethanol	0:30
95% Ethanol	0:30
100% Ethanol	1:00
100% Ethanol	1:00
Ethanol/xylene	1:00
Xylene	1:00
Xylene	1:00
Xylene	1:00

Table 2.3: Autostainer program for haematoxylin and eosin staining of wax prepared slides.

2.2.4 Tartrate resistant acid phosphatase (TRAcP) reaction on slides

To identify lesions and characterise active osteoclasts and odontoclasts within samples, sample sections were tested for tartrate resistant acid phosphatase (TRAcP). Tartrate resistant acid phosphatase is an osteoclast-specific marker expressed at terminal differentiation and further osteoclastogenesis. TRAcP staining solution was prepared in 0.2M sodium acetate buffer at pH 5.2 with naphthol AS-TR phosphate disodium salt (Sigma-Aldrich), sodium tartrate dihydrate (Sigma-Aldrich),

and fast red TR salt (Sigma-Aldrich). Samples were first dewaxed then incubated in TRAcP reactivity solution overnight at 37°C or until red staining developed. Slides were then washed repeatedly in distilled water until red stain stopped leaching from the sections. Slides were then counter stained in Harris' haematoxylin for 5 minutes. Samples were washed in distilled water and coverslips were mounted with Glycergel mounting media (Dako). Osteoclasts were defined as TRAcP positive cells with more than two nuclei within resorption lesions.

2.2.5 Antibody optimisation and immunohistochemistry

After confirming the presence of odontoclasts, immunohistochemistry was used to co-localise protein expression with TRAcP enzyme activity for the three targets: MMP9, CTSK, and P2XR4.

Antibodies were optimised to ensure specificity and low background staining. To determine the dilution of primary antibody required to provide a maximal reaction with the protein target with minimal background staining, tissue sections were processed using an optimised protocol.

Each optimal antibody dilution is described in Table 2.4 and Table 2.5. Assessment of dilutions of primary and secondary antibodies was determined by bright field microscopy.

Primary Antibody	**Host**	**Manufacturer**	**Stock conc.**	**Dilution**	**Concentration after dilution**
MMP9	Rabbit	Abnova, PAB12714	0.5ug/ul	1:200	2.5ng/ul
CTSK	Mouse	Thermofisher, WH001513M1	0.5ug/ul	1:100	4ng/ul
P2XR4	Rabbit	ProteinTech, 13534-1-AP	0.2ug/ul	1:50	5ng/ul
Isotype control					
Rabbit IgG	Rabbit	Sigma-Aldrich, I5381	6.25ug/ul	1:1250	5ng/ul
Mouse IgG	Mouse	Invitrogen, AB2532938	0.8ug/ul	1:200	4ng/ul

Table 2.4: List of primary antibodies used for immunohistochemistry.

Secondary Antibody	**Host**	**Manufacturer**	**Dilution**
α-rabbit	Goat	Peroxidase-Conjugated Goat Anti-Rabbit Immunoglobulins, Agilent Dako, P0448	1:100
α-mouse	Goat	Peroxidase-Conjugated Goat Anti-Mouse Immunoglobulins, Agilent Dako, P0447	1:100

Table 2.5: List of secondary antibodies used for immunohistochemistry.

Sections were prepared as described in 2.1.1. Sections were first dewaxed before antigen retrieval was performed using 0.1M sodium citrate buffer at pH 6.0 for 90 minutes at 70°C. Samples were then washed before blocking endogenous

peroxidase using 1% hydrogen peroxide in methanol for 30 min at RT. Further blocking was performed using a 1:5 solution of normal goat serum in 5% of Foetal Bovine Serum for 30 min. Primary antibodies were diluted at 1:50 to 1:200 dilution (Table 2.4) in 5% FBS/PBS and applied to the samples to be incubated at 4°C overnight in a humidity chamber. Sections were then washed before application of appropriately diluted horseradish peroxidase labelled secondary antibodies (Agilent Dako UK Ltd.)(Table 2.5) and incubated for 1 h at RT. Sections were washed 3 times with PBS for 5 min. Labelling of samples were developed using ImmPACT™ DAB (Vector Labs Ltd., UK) at RT for 1 min, producing a brown colour in positive sections. All samples were counter-stained with haematoxylin prior to dehydration (Table 2.6), clearing and mounting with PERTEX Xylene-based Mounting Media (CellPath, UK).

Reagent	**Time (minutes:seconds)**
H2O	5:00
Haematoxylin	3:00
H2O	5:00
75%	0:30
95%	0:30
95%	0:30
100%	1:00
100%	1:00
Xylene	1:00
Xylene	1:00
Xylene	1:00

Table 2.6: Protocol for dehydration of slides in Leica Autostainer XL

2.2.6 Microscopy and imaging

Stained slides were imaged using a Nikon Brightfield Compound upright microscope, with Zeiss 105c colour camera & Zen 2 software for image capture. Whole slides were also scanned using a Nanozoomer-XR 9 (Hamamatsu) at 40x magnification.

2.3 Cell culture

2.3.1 Reagents

All cell culture reagents including cell culture media, supplements, and foetal bovine serum (FBS) were obtained from Gibco (Thermo Fisher Scientific, UK) unless otherwise stated. Tissue culture plastics were obtained from various sources, such as cell culture flasks, multiple well plates, microplates, pipette tips, cryogenic vials, and cell strainer (Corning® Sigma-Aldrich., UK or Thermo Fischer Scientific., UK), microcentrifuge tubes (Eppendorf tubes, Axygene, VWR, USA).

2.3.2 Bone marrow isolation and primary cell culture

Osteoclasts are derived from haematopoietic myeloid progenitors by terminal differentiation and currently there are no available immortalised osteoclast cell lines. Therefore, to derive primary feline osteoclasts for culture, bone marrow must first be isolated. The protocol used was modified from published rodent/feline osteoclast culture protocols (Muzylak et al., 2002; Orriss and Arnett, 2012). Femurs, tibiae, and humeri were dissected from cats, washed in 70% ethanol and the proximal and distal ends were cut off. The bone marrow was flushed out using a 25 G needle in α-MEM containing 10% FBS. The bone marrow suspension was passed through a cell strainer and red cells were lysed using 5 ml of Lysis buffer (150 mM NH4Cl, 10 mM NaHCO3, 0.1 mM EDTA) for 5 minutes, on ice.

The cells were washed and resuspended by centrifugation at 400 x g for 5 min in α-MEM containing 10% FBS, 2 mM L glutamine, 100 mg/ml streptomycin, and CSF-1 (mouse recombinant CSF-1, 10 ng/ml, R&D systems) and plated into T75 flasks for 24 h at 37°C/5% CO2 for attachment of stromal cells. On the following day, non-adherent cells were collected and plated on new plastic vessels ($1x10^5/cm^2$) with CSF-1 (at 37°C/5% CO_2)

Cells were initially grown in CSF-1 for 3 days before counting and transfection to allow formation of osteoclast precursor rich population.

2.3.3 Cell counting and viability

Ten microlitres of cell suspension were transferred to a microcentrifuge tube and mixed with 10 µl of trypan blue stain and incubated for 1 min. Ten microlitres of the trypan blue/cell suspension mix were applied to the counting chamber of a

haemocytometer and the cells were counted. Dead cells were distinguished as dark blue stained cells and non-refractile. Cell density was then estimated using the following formula:

$$Cell\ density\ (cells\ per\ ml) = \ average\ cells\ in\ one\ square\ \times\ dilution\ factor\ \times 10^4$$

2.3.4 siRNA design and construction

The siRNA was designed using previously identified genes of interest, MMP9, CTSK and P2XR4. This was achieved by using a pairwise sequence alignment tool (EMBOSS-NEEDLE, The European Bioinformatics Institute; EMBL-EBI) to find homologous regions in the target transcripts with mice. Mice were selected for possible future experiments with mouse osteoclasts. Homologous regions were run through an online design tool, i-Score designer (https://www.med.nagoya-u.ac.jp/neurogenetics/i_Score/i_score.html) and evaluated for GC content and Reynolds score (Reynolds et al., 2004). SiRNA sequences possessing a higher Reynolds score (>8) were chosen. An eight nucleotide T7 Promoter sequence (5' CCTGTCTC 3') was added to the 3' end of both the sense and antisense template strands (Table 2.7).

Gene	MMP9	CTSK	P2XR4
I-Score 5' - 3' sequence	CCAGGAGACUUG CGAACUA	CGUUUAAUAUGG GAAAAAA	GCCUGAACCUGC UUUUUUA
%GC	52.63	26.3	42.1
Reynold's score	8	8	9
Target mRNA	CCAGGAGACTTG CGAACTA	CGTTTAATATGGG AAAAAA	GCCTGAACCTGC TTTTTTA
Antisense template (T7 promoter sequence)	AACCAGGAGACT TGCGAACTA(CCT GTCTC)	AACGTTTAATATG GGAAAAAA(CCTG TCTC)	AAGCCTGAACCT GCTTTTTTA(CCT GTCTC)
Sense template (T7 promoter sequence)	AATAGTTCGCAA GTCTCCTGG(CCT GTCTC)	AATTTTTTCCCAT ATTAAACG(CCTG TCTC)	AATAAAAAAGCAG GTTCAGGC(CCTG TCTC)

Table 2.7: Summary table of target and DNA template sequences used to produce siRNA against feline MMP9, CTSK and P2XR4 with the Silencer siRNA Construction Kit. 8 nt sequence marked in brackets indicates the complementary sequence to the T7 Promoter Primer for the first step of synthesis.

The siRNA oligo templates were transcribed into siRNA using the Silencer® siRNA Construction Kit (Ambion) according to the manufacturer's protocol. In brief, the antisense and sense DNA oligonucleotide templates were resuspended to a concentration of 100 µm and each antisense and sense template aliquot were mixed with the T7 promoter primer in 8 µl of the DNA hybridisation buffer in separate tubes. The reaction was heated to 70°C for 5 minutes and cooled at RT for 5 minutes to allow the eight-nucleotide leader sequence of the DNA oligonucleotide template to anneal to the T7 Promoter primer. Exo-Klenow reaction buffer, dNTPs, nuclease-free water, and Exo-Klenow were added to each reaction and incubated at 37°C for 30 minutes. Two µl of the antisense and sense siRNA templates were transcribed for 2 h at 37°C in separate reactions. These were then mixed with nuclease free water, NTPs, T7 reaction buffer and T7 enzyme mix. The antisense and sense transcriptions were mixed before incubation at 37°C overnight. RNase and DNase were used to digest the double stranded RNA solutions for 2 hours at 37°C. Four hundred microlitres of siRNA binding buffer containing ethanol was added to the

double stranded RNA and incubated for 5 minutes at RT. For each siRNA sample, a filter cartridge was prepared by placing in a 2 ml collection tube and pre-wetting the filter with 100 µl of siRNA wash buffer before addition of each siRNA sample. SiRNA-binding buffer mix was added to the filter cartridge and centrifuged at 80,000 x g for 1 minute. The column was washed twice, with 500 µl of siRNA wash buffer and centrifuged at 80,000 x g for 1 minute in each instance. The filter cartridge was placed into a new collection tube and 100 µl of nuclease-free water pre-heated to 75°C was added before incubation for 2 minutes at RT. These were then centrifuged at 8,000 x g for 2 minutes. The purified siRNAs were quantified through use of a Nanodrop.

2.3.5 Source of mineralised substrates

To evaluate and confirm resorption activity of the osteoclasts, mineralised substrates are required. Corning Osteo Assay Surface multiple well plates were used as a mineralised substrate source. These plates possess a bone-like mineral surface which is coated with proprietary hydroxyapatite to form a mineral surface that is highly uniform and microscopically fine-grained. These plates have been used for both routine resorption assays and high-throughput screening in studying both osteoclast and osteoblast function. Resorption pits can be visualised using reflected light microscopy following TRAP reactivity. Counting and measurements of pit surface area was performed using reflected light microscopy.

2.3.6 RNA interference assays using fresh feline bone marrow

Electroporation was selected as the method of transfection as previous a previous study found electroporation to be significantly more efficient than liposome-mediated transient transfection for feline osteoclast precursors (Lee, 2019). Osteoclast precursors from fresh isolated bone marrow and cultured as detailed in section 2.3.2. On day 3, cells were detached by flushing before counting for electroporation and counted as detailed in section 2.3.3. $2x10^6$ cells were aliquoted for each transfection and spun at 800 x g for 5 minutes (Table 2.8). The cell pellet was resuspended in 100 µl of Mouse Macrophage Nucleofector™ solution with 1.5 µl of siRNA.

Sample	Number of transfections	Number of cells	Nucleofector solution	siRNA added (300 nM)	Number of cells after transfection
Scrambled	2	2.0 x 10^6	100 µl	1.5 µl	2.5 x 10^6
MMP9	2	2.0 x 10^6	100 µl	1.5 µl	1.5 x 10^6
CTSK	2	2.0 x 10^6	100 µl	1.5 µl	1.6 x 10^6
P2XR4	2	2.0 x 10^6	100 µl	1.5 µl	1.9 x 10^6
Untreated	-	2.0 x 10^6	-	-	2.0 x 10^6

Table 2.8: Summary of volumes and number of cells used for each transfection and the number of cells after transfection.

Transfection via electroporation was carried out using the Mouse Macrophage Nucleofector™ (Lonza) electroporation kit. Cells were electroporated in a Nucleofector™ II using program Y-001. Electroporated cells were added to 1 ml of CSF1 media then chilled in ice for 5 minutes. Viable cells were counted using Trypan blue before seeding onto a mineralised plate (Corning) and a coated plastic plate. On osteoplates, cells were seeded at 3 x 10^6 cells/well on a 24-well plate for all conditions with additional wells seeded at 6 x 10^6 cells for untreated cells. On a 6 well coated plastic plate, cells were seeded at 5 x 10^5 cells with an additional well seeded with untreated cells at 8 x 10^5 cells. After 24 hours, cells were supplemented with RANKL (3 ng/ml) to induce osteoclast differentiation.

2.3.7 RNA extraction and RT-qPCR

Cells seeded on coated plastic plates were transfected for 48 hours before RNA extraction. Media was removed from wells and washed with PBS twice. As some cells remained suspended within the media, media and wash suspension were pooled and spun at 800 x g to maximise RNA yield. Remaining cells in wells were lysed directly using 1ml/well QIAzol (QIAGEN) lysis reagent. Lysate was then applied to cell pellets and mixed. Homogenates were left for 5 mins at RT. 0.2 ml chloroform was added to the homogenate and shaken vigorously for 15 s. The homogenate was left for 2-3 mins at room temperature. Homogenates were then centrifuged at 12,000 x g for 15 mins at 4°C. the upper, aqueous phase was carefully transferred to another tube with one volume of 70% ethanol. The mix was then applied to an RNEasy filter column and followed manufacturer's recommended protocol as follows: transferred sample on RNeasy Mini spin column was placed in a 2 ml collection tube and centrifuged for 15 s at ≥ 8,000 x g with flow-through discarded. 350ul of Buffer RW1 was added to the column and centrifuged 15 s at ≥ 8,000 x g, with flow through

discarded. A DNase I incubation mix (10µl of DNase I stock solution + 70 ul Buffer RDD) was applied directly to the RNeasy column membrane and left at RT for 15 mins. 350ul Buffer RW1 was applied to the column and centrifuged 15 s at ≥8000 x *g*, with flow through discarded. 500 ul Buffer RPE was applied to the column and centrifuged 15 s at ≥ 8,000 x *g* to wash the membrane, with flow through discarded. 500 ul Buffer RPE was applied to the column and centrifuged for 2 mins at ≥ 8,000 x g to wash the membrane, with flow through discarded. The RNeasy spin column was centrifuged at full speed for 1 min to dry the membrane. RNA was eluted with 30 ul RNase-free water and applied to the centrifuged for 1 min at ≥8000 x g. Additional step of DNase digestion was also performed. RNA was eluted from the RNAeasy columns using 30ul of RNase free water.

RNA yield was determined based on absorbance at 260 nm (A_{260}) using a Nanodrop™ 1000 Spectrophotometer (Table 2.9). RNA purity was assessed based on the ratios of absorbance at 260 and 280 nm ($A_{260:280}$ ratio) and 260 and 230 nm ($A_{260:230}$ ratio).

Treatment	ng/ul	A260	A280	260/280	260/230	Constant	Cursor Pos.	Cursor abs.	340 raw
Scrambled	24.37	0.609	0.394	1.55	0.18	40	230	3.4	0.308
MMP9	11.74	0.294	0.179	1.64	0.06	40	230	4.627	0.066
CTSK	2.92	0.073	0.049	1.48	0.28	40	230	0.262	0.038
P2XR4	17.04	0.426	0.297	1.43	0.2	40	230	2.173	0.131
Untreated	13.21	0.33	0.223	1.48	0.37	40	230	0.883	0.158

Table 2.9: Summary of measuring RNA purity and quantity using Nanodrop 1000 Spectrophotometer.

2.3.8 First strand complimentary DNA (cDNA) synthesis.

Due to low yield, RNA was not diluted with RNase free water, 10 µl of each condition was used for cDNA synthesis. Aliquots of RNA were denatured at 65°C on a heat block and cooled on ice. A master mix was prepared consisting of 10xRT buffer, 0.5 µM of dNTP mix, 1µl of SuperScript™ II reverse trancriptase (Thermofisher). The cDNA was reverse transcribed at 37°C for 1h in a Thermocycler T-gradient Thermo block (Biometra) and stored at -20°C. cDNA was then used for qPCR to assess knockdown of target transcripts.

2.3.9 Quantitative PCR

A real-time PCR known as quantitative PCR (qPCR) was performed with using high affinity, double stranded DNA-binding dye SYBR Green using a Stratagene MX3000P qPCR system (Agilent Technologies). A commercially available kit was used: 2x SyGreen Blue LoROX mix (qPCR Biosystems). Each qPCR reaction contained 300 nM of gene of interest or reference gene primers (Table 2.10), 2X Mastermix, and 4 µl of nuclease free water in a 96 well plate format. The cDNA template was diluted 1:5 from cDNA and 5 µl was added to the reaction producing a final volume of 25 µl for each reaction. Thermal cycling conditions followed manufacturer's instructions, detailed in Table 2.11. All samples were performed in duplicate or triplicate and cycling threshold (Ct) values for each gene were generated. Two reference genes were used, *GAPDH* and *HPRT*. Relative mRNA expression as fold change was analysed using the calculation of 2-ΔΔCt (Table 2.12). Amplification for MMP9, P2XR4, and CTSK was performed.

Primer sets	Forward/ reverse (F/R)	Sequence (5' – 3')	Amp (bp)	Tm (°C)	NCBI RefSeq Accession
HPRT	F	AACTGGAAAGAATG TCTTGATTGTTG	100	56	EF453697
	R	GACCATCTTTGGAT TATACTGCTTGA			
GAPDH	F	GCCGTGGAATTTG CCGT	82	59	NM_0010093 07
	R	GCCATCAATGACC CCTTCAT			
MMP9	F	TGCCACTTCCCTTT CACCTTC	170	58	XM_0039834 12
	R	TTGCCTTCTCCATT GCCGTC			
CTSK	F	CTACATGACCAATG CCTTCC	372	56.8	XM_0198378 02
	R	TTTCCCCAGTTTTC TCCCC			
P2X4R	F	TCACCCCAGAGAA AGTTCC	93	54.5	XM_0232414 08
	R	CGCCCTACACACA AAACAC			

Table 2.10: List of primer sets used for quantitative PCR

Cycles		**Temperature**	**Time**
Initial denaturation		95°C	2 mins
40 cycles	Denature	95°C	5 secs
	Anneal	60-65°C	20-30 secs
Melt curve analysis		95°C	1 minute
		60°C	30 secs
		95°C	30 secs

Table 2.11: Thermocycling conditions used for qPCR.

ΔCt = Ct for target gene – Ct for reference gene
ΔΔCt= ΔCt of TR positive (+ve) sample – ΔCt of TR negative (-ve) samples
Relative expression = 2-ΔΔCt

Table 2.12: Calculation of relative gene expression based on delta-delta method.

2.3.10 Quantification of cultured tartrate resistant acid phosphatase (TRAcP) positive osteoclasts

Cultured osteoclasts on plastic were washed twice with PBS before fixing in 2.5% glutaraldehyde for 5 minutes. TRAcP reactivity was performed using Acid phosphatase leukocyte kit (Sigma-Aldritch Ltd) according to the manufacturer's protocol with some modification: reduced incubation time of (30 minutes) and without haematoxylin counterstaining. TRAcP positive cells were imaged via light microscopy (Nikon Ni2 brightfield). Osteoclasts were determined to be osteoclast-like when stained positive and possessed greater than two nuclei when visually counted. To count the number of osteoclasts in each well, each well was split into 9 sections and three representative images were taken of each section. The number of TRAP positive cells with at least 2 nuclei were counted from the representative images and calculated as number of cells per area.

2.3.11 Visualising and quantifying resorption activity on mineralised plate

To visualise resorption pits, the Corning Osteo Assay Surface multiple well plates were bleached with contrast enhancements in order to assess surface area of resorption. In short, 10% bleach solution was applied to the wells and incubated for 5 mins at RT. A modified von Kossa staining protocol was utilised to improve the contrast of resorption pits through application of 5% (w/v) aqueous silver nitrate solution to each of the bleached wells and incubated for 30 mins at RT in the dark. The silver nitrate solution was discarded and replaced with distilled water to soak for 5 mins. Upon the mineral surface turning yellow, 5% sodium carbonate (w/v in commercial buffered formalin) was added to the wells and incubated for 4 mins at RT. As the ionic silver (I) reduces to metallic silver, the plate appears with a dark colour. The plates were dried at 50°C for 1 h. Resorption pits were then assessed using light microscopy (Axiocam 105 color). Pictures of osteoplates were taken with a stereomicroscope (Stereolumar Zeiss) and Axioxam MR R3 (0.8 magnification, 6.4x zoom) with Zen system. Osteoplates were inverted to maximise the area captured and to avoid parallax with well walls. Images were converted to TIFF files and analysed with ImageJ software. In ImageJ, images were converted to 8-bit type and a circle was applied to the entire well to capture the measurement only to the area of interest. Contrast was enhanced followed by application of a threshold. Threshold

was kept constant between samples and data collected for further analysis using ImageJ (v1.53g).

2.3.12 Statistical analysis

Due to time constraints, there were no biological replicates and technical replicates of at least two were set up for all experiments. qPCR was performed with three technical replicates.

In vitro experiments and qPCR data were analysed using MxPro (4.10) and GraphPad Prism v9 and all graphs were generated using GraphPad Prism v9 software (GraphPad Prism version 9.0.0 for Windows, GraphPad Software, San Diego, California USA, www.graphpad.com") or Microsoft Office® 2016 (Microsoft Corporation).

Data was analysed using GraphPad Prism and all graphs and diagrams were generated using Microsoft Office© 2008 (Microsoft Corporation) or Graphpad Prism v9 software. P values of <0.05 were considered statistically significant. Data was tested for normal distribution using the D'Agostino-Pearson omnibus K2 normality test. Data following a normal distribution were analysed with parametric tests, however if data was not normally distributed, then non-parametric tests were performed. One-way ANOVA tests were used to compare the differences between more than two groups. Two sample t-tests or Mann Whitney U-tests were used to compare differences between two groups.

3 TR+ve and TR-ve samples possess unique SNPs associated with TR

3.1 Introduction

In the previous RNA-seq analysis more than 1,700 differential expressed genes between TR+ve and TR-ve teeth within the same cats were reported. From these, four main pathways and groups of genes were identified to be likely to drive disease progression such as osteoclast differentiation: vitamin D and calcium signalling, immune signalling, tooth eruption and shedding, and mechanical signalling (Lee, 2019; Lee et al., 2020a). Among these genes MMP9, CTSK, and P2XR4 were found to show significant difference and were validated to be truly differentially expressed by qPCR analysis of TR+ and TR- teeth. However, further investigation may be beneficial as variations in the genes which alter the function of the translated protein without changing gene expression levels may exist. RNA-seq data does not only quantify and identify sequences of expressed genes but can also be used in the identification of SNPs. From this RNA-seq analysis, a subset of 102 candidate genes were selected which were found to be differentially expressed between TR+ and TR- teeth and have been reported in literature to contribute to osteoclast differentiation and their resorptive activity.

The analysis of RNA-seq data requires professional computation skills (bioinformatics), so the RNA-seq data analysis which includes gene sets and pathway analysis was supported by bioinformatician Dr Stephen Bush. As computer programming and developing pipelines for specific analysis are beyond the scope of my study, I performed the initial bioinformatics analysis and the alignment of the annotation was performed by Dr Stephen Bush. However, during data analysis, I was involved in every step of data output and guided on how to use the data. My role in this chapter was to decide how to use the RNA-seq data and summarise the data in such a way to maximise the biologically relevant output from the generated RNA-seq data.

3.1.1 TR+ve samples contain a greater number of SNPs than TR-ve samples

Analysis was filtered to genes with detectable expression in teeth and reliability of observed variants was increased by omitting SNPs with <10 reads supporting the

variant allele. Of the 11,904 genes analysed, 9,543 contained at least one SNP found across all samples (n=9; 6 TR+ve; 3 TR-ve). Of these 9,543 genes, a total of 59,907 SNPs was found across all samples (Table 3.1).

In comparing the number of SNPs found in one or more TR+ve or TR-ve samples, the positive samples show a substantially greater number (42,306 SNPs) than TR-ve samples (17,601 SNPs). Additionally, there is a higher proportion of SNPs found in three or more TR+ve samples than TR-ve samples (8.47% vs 0.72%), where a higher number of SNPs are reproducible. From this analysis, there appears to be a higher association of variation by SNPs in cats with TR than without.

Gene number total	Total no. of SNPs found across all samples	No. of high-impact SNPs found only in TR+ samples	No. of high-impact SNPs found only in TR- samples	No. of SNPs found only in one or more TR+ samples	No. of SNPs found only in one or more TR- samples	No. of SNPs found only in 3 or more TR+ samples	No. of SNPs found only in 3 or more TR- samples
11,904	59,907	51	29	42,306	17,601	3585	128

Table 3.1: Overview of number of SNPs and high impact SNPs in TR+/- samples

3.1.2 TR+ve samples possess a greater number of unique high impact SNPs than TR- samples

Within TR+ve samples, 51 high impact SNPs distributed among 49 genes were identified which are only found in TR+ve samples. Of these SNPs, two different high impact SNPs were each found in genes including myosin heavy chain 13 (MYH13) and keratin 76 (KRT76). SnpEff identified splice acceptor and intron variants, and a stop gain variant within MYH13. KRT76 possessed a loss of start, splice acceptor variant, region variant and intron variant. In the other 47 genes, only one high impact SNP was observed.

In TR-ve samples, a total of 29 high impact SNPs was observed in 28 genes which are found only in TR-ve samples. Of the high impact SNPs, only mitochondrially encoded cytochrome B (MT-CYB) possessed two different high impact SNPs. In each of the 27 other genes, one high impact SNP was found in each. Overall, TR+ve

samples possess a greater number of high impact SNPs than found in TR- samples, suggesting a genetic contribution to feline TR.

3.1.3 SNPs found in only three or more TR+ve and TR-ve samples

TR+ve and TR-ve samples were also compared to view the number of SNPs in genes which are found in three or more samples and their predicted effect. Titin (TTN) contains 28 SNPs, the highest number found in TR+ve samples. Interestingly, Coenzyme Q4 (COQ4) possesses a high impact SNP which can be found in all three TR +samples and the high impact SNP was classified as a stop gain variant. In all three samples, the same variant was observed, where a cytosine is changed to a threonine at position 499/2094, changing the glutamic acid residue to a stop codon. As mentioned in 3.2.2, MYH13 possesses a high impact SNP which can be found in 3 samples. This is classified as a splice acceptor variant and intron variant. KRT76 shows three high impact SNPs but are found in one sample each: a start loss & splice region variant, a splice acceptor variant & intron variant, and a splice acceptor and intron variant. Additional high impact SNPs which are observed in at least 3 other samples are small nuclear RNA activating complex polypeptide 4 (SNAPC4), zinc finger MYM-Type containing 6 (ZMYM6), and MT-CYB.

In TR-ve samples, 108 genes show SNPs in three or more samples. The highest number of SNPs are observed in Family with Sequence Similarity 8 Member A1 (FAM8A1) with four SNPs in three or more TR-ve samples. There are 128 SNPs found in three or more TR-ve samples, however none of these are predicted as high impact SNPs. Based on the associated function of these SNPs in TR+ve samples, there appears to be an association of variants with feline TR in the mitochondrial respiratory chain (Gandhi et al., 2017) and cytoskeletal components (Kim et al., 2020; Maravillas-Montero and Santos-Argumedo, 2012).

3.2 SNPs in candidate genes associated with osteoclast differentiation and/or tooth resorption

To further study the prevalence of SNPs within each TR condition, the gVCF was then filtered to contain only those variants attributed to 102 genes associated with osteoclast differentiation and osteoclast activity, identified by literature review

(Appendix B). From this subset, a total of 477 SNPs was found within 70 genes across all samples (n=9) (Table 3.2). Of these, 281 SNPs were found in TR+ve samples (n=6) in 60 genes, greater than observed in TR-ve samples (n=3) where 196 SNPs were identified in 42 genes (Table 3.2).

In studying the number of SNPs found within this subset of genes of each TR condition (Table 3.2), in TR+ve samples, transforming growth factor beta 1(TGFB1) possessed the greatest number of SNPs (N=19). Following this are interleukin-4 receptor (IL4R) and proto-oncogene tyrosine-protein kinase Src (SRC) which have 13 SNPs and interleukin 12 receptor subunit beta 2 (IL12RB2) and interleukin-10 receptor subunit beta (IL10RB) both possess 11 SNPs. SNPs within these genes were only detectable within TR+ve samples.

Spleen associated tyrosine kinase (SYK) contained 27 SNPs, the highest for all genes in TR-ve samples. Additionally, interleukin-1 receptor type 1 (IL1R1) has 20 SNPs and matrix metallopeptidase 13 (MMP13) contains 16 SNPs in TR-ve samples. SNPs found within these genes are only detectable in TR-ve samples.

In TR+ve samples, it was observed that in 13 genes 18 total SNPs are found in more than three TR+ve samples only. IL12RB2, IL10RB, TNF receptor superfamily member 1A (TNFRSF1A), epidermal growth factor receptor (EGFR), and proto-oncogene c-Fos (FOS) show two SNPs in three or more TR+ samples, with no SNPs observed in three or more TR- samples of the same genes. This is comparatively higher than in TR-ve samples, where only one SNP is observed in BLNK and found in three or more TR-ve samples.

SNPs identified	In any sample	In only TR+ve samples	In only TR-ve samples	More than 3 TR+ve samples	More than 3 TR-ve samples	High-impact SNPs in TR+ve samples	High-impact SNPs in TR-ve samples
Number of genes	70	60	42	13	1	1	1
Total number of SNPs	477	281	196	18	1	1	1

Table 3.2: Summary table of number of genes with SNPs in TR+ve and TR-ve samples.

3.2.1 SNPs in BLNK, NFKB2, TGFB1, and PLAUR within TR+ve samples

In the TR+ve samples, high impact SNPs along with moderate and low impact variants were observed in five genes: B-cell linker protein (BLNK), nuclear factor kappa b subunit 2 (NFKB2), TGFB1, and urokinase plasminogen activator surface receptor (PLAUR) (Table 3.3).

In BLNK, three SNPs including a high impact and two moderate impact variants were observed. These were all found within one TR +ve sample (1146N08_C8_TR+). The high impact variant was classified as a stop gain variant where the cytosine was replaced with a thymine resulting in formation of stop codon in place of the glycine residue. The moderate SNPs were described as missense variants, where a single base change in the codon sequence results in replacement of the amino acid with a different residue. In both observed moderate impact SNPs, isoleucine was replaced with leucine and arginine, respectively. Moderate and low impact SNPs were also observed in genes NFKB2, TGFB1, and PLAUR.

In NKFB2, of a total number of five SNPs, one was predicted as a moderate impact missense variant changing the aspartic acid to a valine residue. This variant is also located in sample 1146N08_C8_TR+ which also possesses SNPs in BLNK.

In TGFB1, four moderate impact missense variants were observed of 35 total SNPs observed, three of which are within the same sample (1146N08_C8_TR+). In respective variants, tryptophan is replaced with glycine, glutamic acid is replaced with glycine, and aspartic acid is replaced with asparagine. A low impact stop retained variant is also observed in this same sample. The remaining moderate variant is observed in a different sample as a missense variant, where a tryptophan is replaced with a glycine.

PLAUR possesses four moderate SNPs and 6 low impact SNPs of a total of ten. Three of these are found in one sample, 1146N24_C30_TR+, one moderate impact and two low impact. The moderate impact is described as a missense variant and splice region variant where an aspartic acid residue is replaced with a glutamic acid. The low impact variants are synonymous variants and a splice region variant and synonymous variant. The one other sample with a moderate variant is a missense

variant and possesses a dbSNP ID rs43929488. This protein activity may then be altered slightly without change in protein expression.

Gene (Chr: Gene start-end)	Number of SNPs in TR+ve samples	Highlighted variant (Position)	Predicted impact	Variant (R->V)	Amino acid change (R-> V)	Effect type	dbSNP ID
BLNK (D2: 57561236-57637324)	3	57569186	High	C->T	Gly->*	Stop gained	None
		57568547	Moderate	C->T	Ile->Leu	Missense variant	None
		57568548	Moderate	A->G	Ile->Arg	Missense variant	None
NFKB2 (D2: 62844226-62880055)	5	62865076	Moderate	G->A	Asp->Val	Missense variant	None
TGFB1 (E2: 13683300-13697684)	35	13685319	Moderate	T->G	Trp->Gly	Missense variant	None
		13685319	Moderate	T->G	Trp->Gly	Missense variant	None
		13692730	Moderate	T->C	Glu->Gly	Missense variant	None
		13695711	Moderate	C->T	Asp->Asn	Missense variant	None
		13689270	Low	C->T	Ter->Ter	Stop retained variant	rs785320607
PLAUR (E2: 12719444-12735105)	10	12719645	Moderate	G->A	Asp->Glu	Missense variant & Splice region variant	None
		12720287	Moderate	G->A	Phe->Tyr	Missense variant	rs43929488
		12719540	Low	C->G	Val->Val	Synonymous variant	None
		12719558	Low	G->A	Lys->Lys	Splice region variant & synonymous variant	None

Table 3.3: Genes of interest in TR+ samples. R->V: Reference->Variant. Amino acid change follows HGVS notation. * - denotes gain of stop codon, no amino acid; Ter denotes a termination/stop codon.

3.2.2 SNPs in MMP14 and SRC in TR-ve samples

Among the TR-ve samples, there are high impact SNPs observed in two genes, MMP14 and SRC (Table 5). MMP14 possesses three total SNPs of high, moderate, and low impact variant. These are found within the same sample, 1146N14_C12_TR-. The high impact is a stop gain variant, located at 75715667 of the gene (75707173-75716116). The moderate impact SNP is described as a missense variant, where a valine is replaced with a glutamic acid residue. Additionally, this possesses a dbSNP ID, rs43840271. Lastly, a low impact synonymous variant is observed for a threonine residue, switching an adenine for a guanine. SRC possesses a total of eleven SNPs in TR-ve samples with one moderate impact SNP. This is a missense variant where an aspartic acid residue is replaced with a glutamic acid residue.

In the three SNPs found in TR-ve samples, one high impact variant was observed in MMP14 along with a moderate and a low impact variant in the same sample, 1146N14_C12_TR-. The high impact is a stop gain variant, moderate impact is a missense variant and the low impact is a synonymous variant. The moderate impact variant has a dbSNP ID rs43840271. This mixture of SNPs indicates that the protein is truncated and severely affected. One moderate impact missense variant is observed in SRC of a total of eleven SNPs found in TR-ve samples which may alter the protein activity. In both the TR+ve and TR-ve samples, the remaining SNPs observed in this dataset are described as modifier impact, mostly consisting of intron variants, upstream gene variants, and downstream gene variants.

Gene (Chr: Gene start-end)	Number of SNPs in TR-ve samples	Highlighted variant (Position)	Effect impact prediction	Variant (R->V)	Amino acid change (R->V)	Effect type	dbSNP IDs
MMP14 (B3: 75707173-75716116)	3	75715667	High	G->A	Glu->*	Stop gained	None
		75715168	Moderate	C->T	Val->Glu	Missense variant	rs43840271
		75715614	Low	A->G	Thr->Thr	Synonymous variant	None
SRC (A3:22426690-22446049)	11	22427660	Moderate	T->C	Asp->Glu	Missense variant	None

Table 3.4: Genes of interest in TR- samples. R->V: Reference->Variant

3.3 SNPs in MMP9, P2XR4, and CTSK

MMP9, P2XR4, and CTSK were also included in this gene subset for study due to their observed association with TR development and osteoclast differentiation and analysed for SNPs which may correlate with altered gene expression observed from previous studies (Table 6). MMP9 possesses 3 SNPs across all samples which are all located in TR+ve samples. These are observed in the same sample, 1146N26_C32_TR+ and are observed as modifier impact. P2XR4 has one SNP found in a TR+ sample, 1146N24_C30_TR+. This is described as a modifier impact intron variant. SNPs in CTSK of both TR+ve and TR-ve samples were unable to be called and analysed due to deprecated Ensembl IDs.

Gene (Chr: Gene start-end)	Number of SNPs in TR+ve samples	Highlighted variant (Position)	Effect impact prediction	Variant (R->V)	Effect type	dbSNP IDs
MMP9 (A3: 15240350-15252577)	3	15243024	MODIFIER	C->T	Upstream gene variant, downstream gene variant, intergenic region	None
		15246921	MODIFIER	T->G	Upstream gene variant, downstream gene variant, intron variant	None
		15247634	MODIFIER	A->G	Upstream gene variant, downstream gene variant, intron variant	None
P2XR4 (D3: 8241568-8259834)	1	8243871	MODIFIER	T->C	Intron variant	None

Table 3.5: Summary of SNPs in candidate genes MMP9 and P2XR4. NB: SNPs are only found in TR+ samples.

3.4 Discussion

In recent years there has been an explosion of next generation sequencing data that has helped us to understand better the underlying genetic causes of disease. This is in part due to the increasing affordability of such analysis and the sheer volume of data which can be reproduced from pre-existing data sets. To allow maximum information to be extracted from such data sets a suite of bioinformatics analysis tools and programmes are now available to the scientific community. SNPs have been of particular interest as their detection may supplement existing gene expression data or provide predictions of gene responses which can be further investigated. One useful tool in SNP analysis is the use of effect impact predictions. These predictions are categorised based on the potential impact of gene mutations on protein function. This can range from loss of function in high impact variants to mostly redundant harmless mutations that have no adverse effect on protein function. However, this is not a precise science as such analysis cannot predict with 100% certainty the impact of such mutations of protein function.

Additionally, modifier impacts are usually noncoding or affect non-coding genes. Though these are in non-coding regions and generally would not have an impact on protein function, they are difficult to predict or have no evidence of impact. Regulatory elements may exist downstream of the gene which may regulate other genes or components, thus not only affecting the gene in which the SNP is found, but also surrounding and associated genes. Regulatory regions include enhancers and silencers that regulate alternative splicing, influence gene expression and can confer susceptibility to disease or modify the genotype-phenotype relationship (Cooper, 2010). Lastly, low impact variants such as synonymous variants may not cause significant changes to protein expression and activity, however optimal codon usage may be hindered. If accumulated in several genes of the same pathway, the efficiency of the system may be affected.

Of the SNPs identified, three genes in particular: COQ4, MT-CYB, and MMP14 show high impact SNPs correlated with osteoclast differentiation and osteoclast activity. Coenzyme Q (CoQ) is a small lipophilic molecule that transports electrons between mitochondrial respiratory chain complexes (complexes I and II to complex III) and

functions as a cofactor for mitochondrial enzymes. COQ4 is an enzyme involved in CoQ biosynthesis (Casarin et al., 2008). In humans, COQ4 transcription initiates at multiple sites. For this, there are two isotypes, where one targets the mitochondria and the other form is unknown in function and lacks a mitochondrial targeting sequence. COQ4 also acts as a cofactor in uncoupling proteins and other mitochondrial dehydrogenases, acts as antioxidant stabilising plasma membrane and regulates extracellular induce ceramide-dependant apoptotic pathway. This is involved in the biosynthesis of COQ10 and mutations in COQ genes are observed to cause primary COQ10 deficiency (Casarin et al., 2008). COQ10 is involved in osteoclast and osteoblast differentiation and is reported to act as an inhibitor of RANKL-induced osteoclast differentiation and as an enhancer of osteoblast differentiation decreasing resorption and enhancing bone formation (Gandhi et al., 2017; Moon et al., 2013; Zheng et al., 2018). In our samples a stop gain variant was observed which may result in a modified COQ4 protein with reduced or no activity, leading to the downregulation of COQ10 and subsequently prevent its inhibition on osteoclast differentiation.

Another gene which shows high impact SNPs within the TR+ve samples is mitochondrially encoded cytochrome b (MT-CYB). This is predicted as a loss of stop codon variant which would lead to the formation of a long protein which may no longer be effective in its function. This is a component of the ubiquinol-cytochrome c reductase complex (by complex III or cytochrome b-c1 complex), which is part of the mitochondrial respiratory chain. This mediates the electron transfer from ubiquinol to cytochrome c and contributes to the generation of a proton gradient across the mitochondrial membrane used for ATP synthesis. Changes in genes relating to the mitochondrial electron transport chain may be important to consider on osteoclastic activity, particularly through intracellular ATP levels. There appears to be an inverse correlation between osteoclast survival and bone resorption, where mature mitochondria-rich osteoclasts have lower levels of intracellular ATP. Severe depletion of ATP leads to increased bone-resorption activity despite accelerated apoptosis (Miyazaki et al., 2012). Additionally, mitochondrial dysfunction has been reported to impair osteogenesis and increases osteoclast activity (Dobson et al., 2020).

MMP enzymes are calcium-dependent zinc-containing endopeptidases part of the metzincin superfamily, a large family of proteases. Collectively, MMP enzymes are known to degrade various extracellular matrix proteins during organogenesis, growth and normal tissue turnover, along with some enzymes processing bioactive molecules. In adult tissues, MMP expression and activity is quite low but is observed to significantly increase in inflammatory disease and have been observed to play a role in tissue destructive oral diseases. For example, the primary role of MMP9 is the degradation and remodelling of the ECM in many tissues including bone and teeth (Christensen and Shastri, 2015). Increased MMP9 activity is implicated in various diseases such as osteoclastoma, Paget's disease, and dental pulp inflammation (Dong et al., 2005; Jain and Bahuguna, 2015). High expression of MMP9 is also reported in early stages of differentiating osteoclasts in cats and appears important in osteoclast formation and resorption (Lee et al., 2020a). Some MMP enzymes appear to contribute to the formation of osteoclasts.

One interesting SNP identified in the TR –ve samples was MMP14, a membrane-associated protease observed to act in control of cell senescence as loss of the gene results in cell senescence and nuclear defects in mice (Gutiérrez-Fernández et al., 2015). MMP14 has been characterised in different pathological conditions such as Winchester Syndrome and Multicentric Osteolysis-Nodulosis-Arthropathy Spectrum in humans. This is due to a peptide substitution of a hydrophobic-region signal-peptide, from a threonine to arginine, preventing interaction of MMP14 with its signal recognition particle and impairing membrane localisation (Evans et al., 2012). In one study, when MMP9 and MMP14 are both knocked out, a highly protected status against either parathyroid hormone or ovariectomy-induced pathological bone loss was reported (Zhu et al., 2020). In our samples, the position of the stop gain is located prior to the last exon of the gene. This may correlate to the transmembrane domain of the protein or the signal peptide (Itoh, 2015). By truncation of either of these two domains, the protein function may be greatly affected. If the signal peptide is lost, the protein will not be properly translocated to the correct location. If the transmembrane domain is lost, the protein will not properly attach to the membrane and may be lost. Overall, this may confer a protective status to the cat and prevent the development of TR.

To be able to properly evaluate the effect of these gene mutations on protein function, these will need to be confirmed experimentally using clinical samples. This may include RNA, DNA, and protein extraction from TR+ve and TR-ve samples. RNA may be used in RNA-seq and qPCR approaches to investigate levels of gene expression and transcript integrity. DNA could be sequenced to check the presence of SNPs within each sample for comparison between disease conditions and with our current predictions. Protein extracts would allow the identification of major changes to protein structure and function as a result of SNPs and provide insight into the contribution to osteoclast differentiation and activity to TR development. This may be done through Western blotting and mass spectrometry. This would be effective in investigating high impact SNPs which are observed in these samples, stop or loss of start mutations, which would significantly alter the molecular weight. However, these methods may not be suitable for easily detecting single amino acid changes in proteins as observed in some moderate impact variants.

Additionally, it would be beneficial to check the interaction of regulatory proteins with DNA through ChIP-Seq as this may not only aid in identifying regulatory regions in coding regions, but possibly the existence of intronic and intergenic regulatory regions. Future studies should investigate genes and proteins according to the data that has been gathered in this project.

3.5 Future steps

The current approach in this study was to use Ensembl (v9.0) to align the raw reads which were previously generated against the Felis Catus genome. Whilst considerable bioinformatics analysis was completed in the limited time available it is recognised, that there are potential issues with the genome alignment due to possible lack and/or quality of gene annotation. Future RNA-seq analysis should exploit Trinity for *de novo* assembly and alignment against the Felis Catus transcriptome (Lee et al., 2020b). This is useful as in the absence of an appropriate reference genome, RNA-seq can be used to construct the transcriptome *de novo* (Hölzer and Marz, 2019). This is especially useful for non-model organisms, such as cats and would overcome the difficulties caused by poor or missing gene

annotations. This would then supplement data gathered about SNPs in the genome with the overall expression of genes.

To aid in the analysis of identified SNPs, it may be beneficial to allow visualisation of genetic variants in pathways. This would allow easier identification of their potential impact on downstream factors and paralogues in pathways. If used with a large dataset, the most commonly affected pathways and components would be highlighted and identify their involvement and degree of importance (Cirillo et al., 2017).

One issue with the bioinformatics approach was the use of a 102 gene subset which was a candidate list of genes related to osteoclast differentiation derived from differentially expressed genes in the RNA-seq analysis. Though an attempt was made to ensure that most genes and pathways relating to osteoclast differentiation and activation was kept in the bioinformatic analysis, it is likely that genes that may be important in osteoclast differentiation and activation may have been omitted. However, this study was intended as a pilot for further studies and can easily be implemented into the bioinformatics pipeline. Additionally, the original subset was obtained by prior comparison to the RNA-seq differential expression study by selecting those genes which show a significant change. A possible inclusion of a gene to look into would be P2XR7. As no difference in expression was reported (Lee et al., 2020b), this was then omitted from this study. However, SNPs in the human orthologue have been observed and functionally characterised. If the SNP in P2XR7 is also present in TR affected cats, then this may indicate similar if not the same effect on TR. Additionally, deficiencies of related genes such as bruton tyrosine kinase (Btk) and tyrosine-protein kinase Tec, in mice have shown to result in an osteopetrotic phenotype because of severe impaired osteoclast differentiation (Shinohara et al., 2008). These genes should be considered in future studies to determine if any difference in their expression is observed in TR+ve cats.

It would also be useful to investigate the expression of high impact variants, such as COQ4, using techniques such as Western blotting and RT-qPCR for their protein and transcript expression. Knockdown experiments and quantification of MMP14 should be investigated in relation to MMP9 due to reported protective status against

osteoclast resorption (Zhu et al., 2020). Functional characterisation of these variants in osteoclast differentiation and activation *in vitro* would be beneficial.

A large portion of information pertaining to the difference in distribution of TR between purebred and mixed populations of cats is often anecdotal. To test the incidence of TR between purebred and mixed populations, this could be performed through a survey of dental radiographs. A high number of purebred cats would be required however as purebred cats only make up a small proportion of the general population. To investigate for the presence of SNPs associated with TR and compare the incidence between purebred and mixed cats, DNA screening could be performed, where sample DNA can be obtained through oral swabs, other tissue samples or blood from animals with known TR status. This would overcome the complications and limitations encountered in this project where tooth sample are difficult to obtain as unaffected teeth in TR-ve cats and cats at a younger age do not require extraction. The samples that were obtained for this project were from cats that were on average 7 years old. There is much evidence of age-related risks. However, in this study the correlation of age and TR presence was not investigated due to small sample number and lack of statistical power.

To confirm age-related risk of TR and to investigate the extent and severity of TR between age groups and their initial formation then a larger sample set is required. To mitigate this, further investigation could be carried out by comparison with other SNP data which have been generated from cats. One example is where 63k SNPs were identified using a DNA array with a dataset of over 2,000 feline samples with representations of 41 breeds, a random bred population and four wild felid species (Gandolfi et al., 2018). As this is an extensive study, this would allow comparison of conclusions from this project and previously identified SNPs (Lee, 2019). However, as the TR status of these cats are unknown, the differences between breeds is reliant on candidate SNPs which are shown as markers of TR. If the candidate SNPs are reliable, these would then inform whether there is a predisposition and if this is more frequent in purebred cats.

4 MMP9, P2XR4 and CTSK protein expression can be located to odontoclasts in teeth affected by feline tooth resorption

4.1 Introduction

In previous studies (Lee, 2019; Lee et al., 2020a), analysis of RNA-seq data highlighted several genes correlated to osteoclast differentiation which were differentially expressed in TR+ve teeth when compared to TR-ve teeth. MMP9, P2XR4, and CTSK were selected as candidate genes for investigation as they were differentially expressed in TR+ve teeth compared to TR-ve teeth and are involved in osteoclast differentiation. However, in this study RNA was extracted from the entire tooth which does not show if this differential expression is evenly distributed throughout the entire tooth, or in distinct locations, for example to specific cells in the dental microenvironment. To localise the expression of these proteins, immunohistochemistry was performed on histological sections of feline dental samples. Additionally, siRNA transfection was previously performed to examine the effect of MMP9 in osteoclast formation and activity (Lee, 2019; Lee et al., 2020a). Further siRNA transfection of MMP9, P2XR4 and CTSK was performed to investigate and compare their effect on osteoclast differentiation and their resorptive activity.

4.2 MMP9, P2XR4 and CTSK expression by immunohistochemistry

In this study, the teeth from six feline mandibles were analysed. Of these samples, five samples were TR +ve and one was TR -ve. Mandibles were radiographed (Figure 4.1) and tooth TR type and staging were confirmed by review of dental radiographs by veterinary dental specialist, S. Thorne (MRCVS, RCVS, American & European Specialist in Veterinary Dentistry, DentalVets, Haddington)(Table 4.1). Of the six samples, a range of TR stages were observed and varied in number of affected teeth. Cat 3 reports the greatest number of TR affected teeth with all teeth affected and the premolars of both mandibles are in stage 5 or missing. Similarly cat 4 shows most teeth affected by TR aside from 309 but shows the most teeth at late stages of TR with teeth 408 and 409. In contrast, cats 1 and 5 have the least of overall TR stages among their dentition with only 304, 404, and 407 affected. Cat 2 has the least number of TR affected teeth of all cats other than TR-ve cat 6, however this is in tooth 407 which has reached late stages of resorption (staged as 3-4).

For antibody optimisation, primary antibodies were optimised using primary isotype control antibodies. These lack specificity to the target but match the class and type of the primary antibody used. When primary antibodies were substituted with primary isotype controls, background labelling was found to be virtually absent. This observation indicated that the protocols were highly specific in detecting MMP9, CTSK, and P2XR4 in feline teeth. However, weak immunostaining was observed on dentine. This moderate cross-reactivity in specific locations did not interfere with the interpretation of results as corresponding structures were clearly distinguishable from the regions and tissues of interest.

MMP9 antibody was optimised in the previous study (Lee, 2019). CTSK and P2XR4 antibodies were optimised using positive control feline tissues such as epithelial cells and liver cells and osteoclast rich tissues from mice, i.e. 2-day old mouse tibiae. Stains were visualised by microscopy and assessed for specific protein expression. Specific protein expression was confirmed by cross-comparison with serial sections using respective isotype control antibodies. Background staining of positive control tissue using primary isotype control antibodies remained minimal and CTSK and P2XR4 staining were distinguishable from isotype controls. All antibodies were successfully optimised. P2XR4 and CTSK were successfully localised in feline dental tissues.

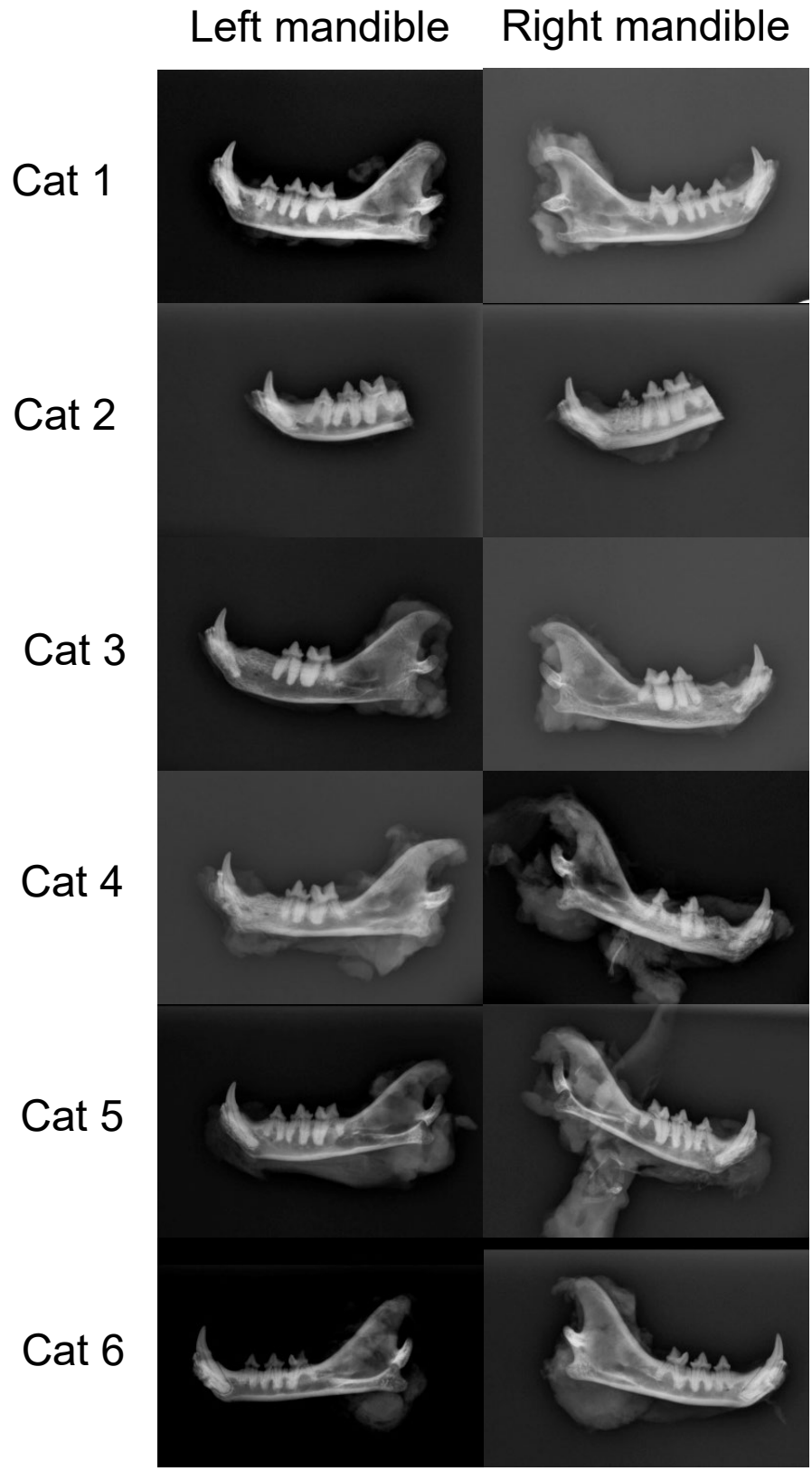

Figure 4.1: Radiographs of feline mandible samples, each hemimandible radiographed separately. Cats 1-5 were diagnosed as TR+; Cat 6 was diagnosed as TR-.

Name or ref number/Cat	L Mandible	TR	R Mandible	TR
2019-1/Cat 1	304	TR +	404	TR +
	307	TR -	407	TR +
	308	TR -	408	TR -
	309	TR -	409	TR -
2019-2/Cat 2	304	TR -	404	TR -
	307	TR -	407	TR + S3-4
	308	TR -	408	TR -
	309	TR -	409	TR -
2019-3/Cat 3	304	TR +	404	TR +
	307	missing or S5	407	missing or S5
	308	TR +	408	TR +
	309	TR +	409	TR +
2019-4/Cat 4	304	TR +	404	TR +
	307	missing or S5	407	missing or S5
	308	TR +	408	TR + S3
	309	TR -	409	TR + S3-4
2019-5/Cat 5	304	TR +	404	TR +
	307	TR -	407	TR +
	308	TR -	408	TR -
	309	TR -	409	TR -
2019-6/Cat 6	304	TR -	404	TR -
	307	TR -	407	TR -
	308	TR -	408	TR -
	309	TR -	409	TR -
Clinical sample 1	-	-	409	TR+

Table 4.1: Sample information and TR status. TR type and staging were confirmed by review of dental radiographs by veterinary dental specialist, S. Thorne (MRCVS, RCVS, American & European Specialist in Veterinary Dentistry, DentalVets, Haddington). S= Stage of TR

4.2.1 MMP9, P2XR4, and CTSK was expressed in feline tooth sections

In order to distinguish true resorbing cells, a consensus was reached where only multinucleated cells within an obvious resorption pit of dental tissues were considered to be odontoclasts. To aid in identification of osteoclasts and odontoclasts, samples were assessed for TRAcP activity (Figure 4.2). Within TR+ve samples, TRAcP activity was observed on dental hard tissues such as cementum and dentine, where multinucleated cells could be observed within resorption pits. In TR-ve samples, TRAcP activity was also observed, however all positive TRAcP multinucleated cells were confined to the alveolar bone and were not observed in any dental hard tissue. Of the six samples checked for TRAcP activity, only three samples showed resorptive lesions with odontoclasts.

It was observed in the majority of TR+ve teeth that there was loss of periodontal ligament fibres, narrowed or complete loss of periodontal ligament space and replacement with bone-like tissue, demonstrating a degree of ankylosis. At the cementoenamel junction (Figure 4.3 A1), the cementum in TR-ve teeth forms a thin and regular layer along the dentine which gradually increases as it approaches the root of the tooth. In TR+ve teeth, the cementum layer becomes irregular and thickens due to attempts to repair damage made to the cementum layer such as resorption (Figure 4.3 B1). Upon damage and repair of tooth resorption, osteoblasts are introduced to the sites of damage and replaces the dental mineralised tissue with bone in ankylosis, fusing the alveolar bone with the tooth, losing the PDL layer in the process. This can be observed in Figure 4.3 B2 from a TR +ve tooth, where there is little to no PDL remaining and is instead a mixture of cementum and alveolar bone. This contrasts the continuous even layer of PDL cells observed in the TR-ve tooth in Figure 4.3 A2. From these observations, many samples showed late stages of resorption.

After confirming the presence of active odontoclasts, immunohistochemistry was performed using serial sections of regions where positive TRAcP activity was observed. In both TR+ve and TR-ve samples, antibody labelling for MMP9, CTSK, and P2XR4 co-localised with TRAcP activity. In TR+ve samples, MMP9 protein showed strong expression in multinucleated cells (odontoclasts) which resorbed cementum and dentine (Figure 4.4). MMP9 was also expressed in multinucleated

cells (osteoclasts) resorbing alveolar bone in TR-ve samples, however this expression appears weaker. In both TR+ve and TR-ve samples, CTSK was strongly expressed by osteoclasts and odontoclasts. P2XR4 was also expressed though somewhat weakly. The expression of P2XR4 appears stronger in TR+ve odontoclasts resorbing cementum and dentine than osteoclasts in TR-ve resorbing alveolar bone. These observations are also seen in other stained TR+ samples showing co-localisation of MMP9, CTSK, and P2XR4 expression with multinucleated TRAcP positive cells (Figure 4.5).

In all TR+ve samples, there was an apparent lack of PDL and cementum where late stages of TR are observed with only bone and dentine observed. In the TR-ve samples, there is little cementum present, but there is still PDL/fibrous tissue and granular tissue present in Figure 4.5A. In areas of extensive resorption through cementum into the underlying dentine, this was often populated with granular tissue instead of PDL, suggesting an involvement of inflammation. Additionally, TRAcP activity was observed within the dentine which appears to have begun from the root canal/dental pulp within the tooth (Figure 4.5B). This may be internal resorption of the tooth, but it may be caused by extensive external resorption deeper into the dentine by the pulp. This is difficult to determine as the tissue below the lesion is not present. Additionally, bone was observed by this area of resorption, suggesting ankylosis in response to resorption. Overall, from these observations, multinucleated odontoclasts and osteoclasts express MMP9, CTSK, and P2XR4 within dental tissues, suggesting an involvement in feline TR.

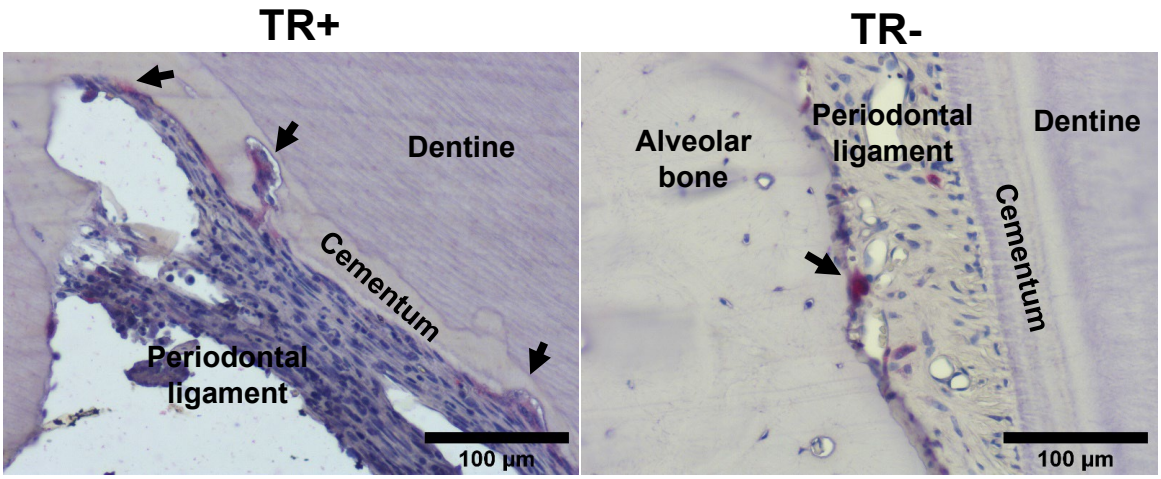

Figure 4.2: Representative images of TRAcP activity on TR +ve sample (left) and TR -ve sample (right). Odontoclasts (left) and osteoclasts (right) stain positively as red and indicated by arrows. Scale bar: 100 µm

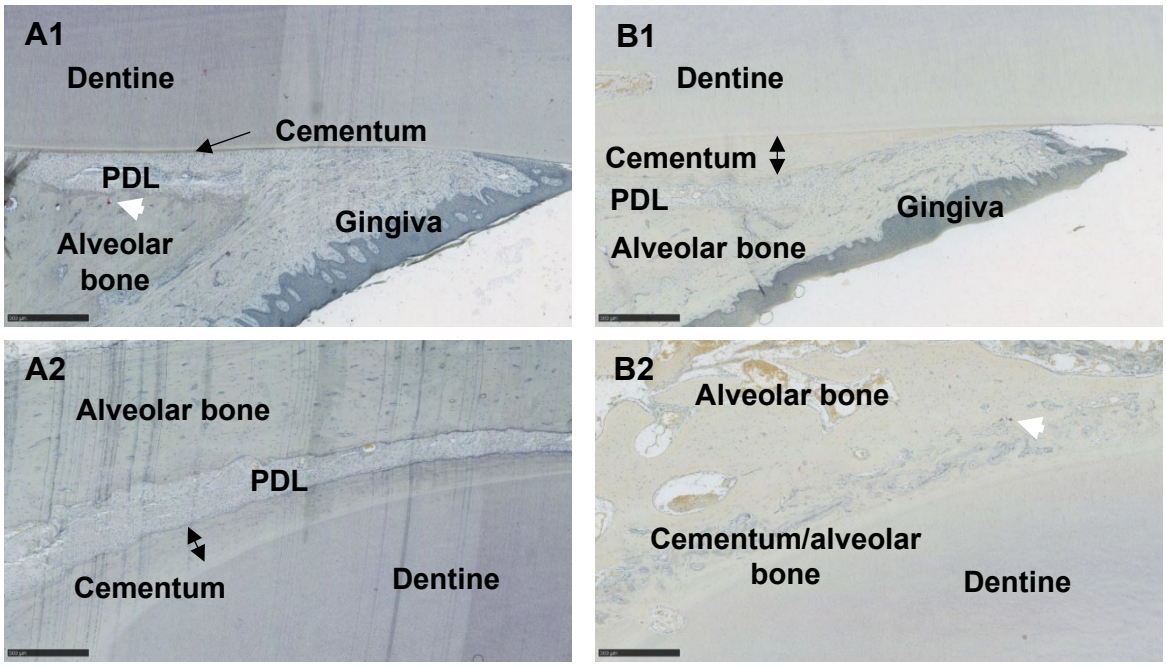

Figure 4.3: TRAP activity of teeth 404 from TR- cat A) and TR+ cat B); 1) Neck of tooth 2) Root of tooth. TRAP activity indicated by white arrows. Scale bar: 500 µm.

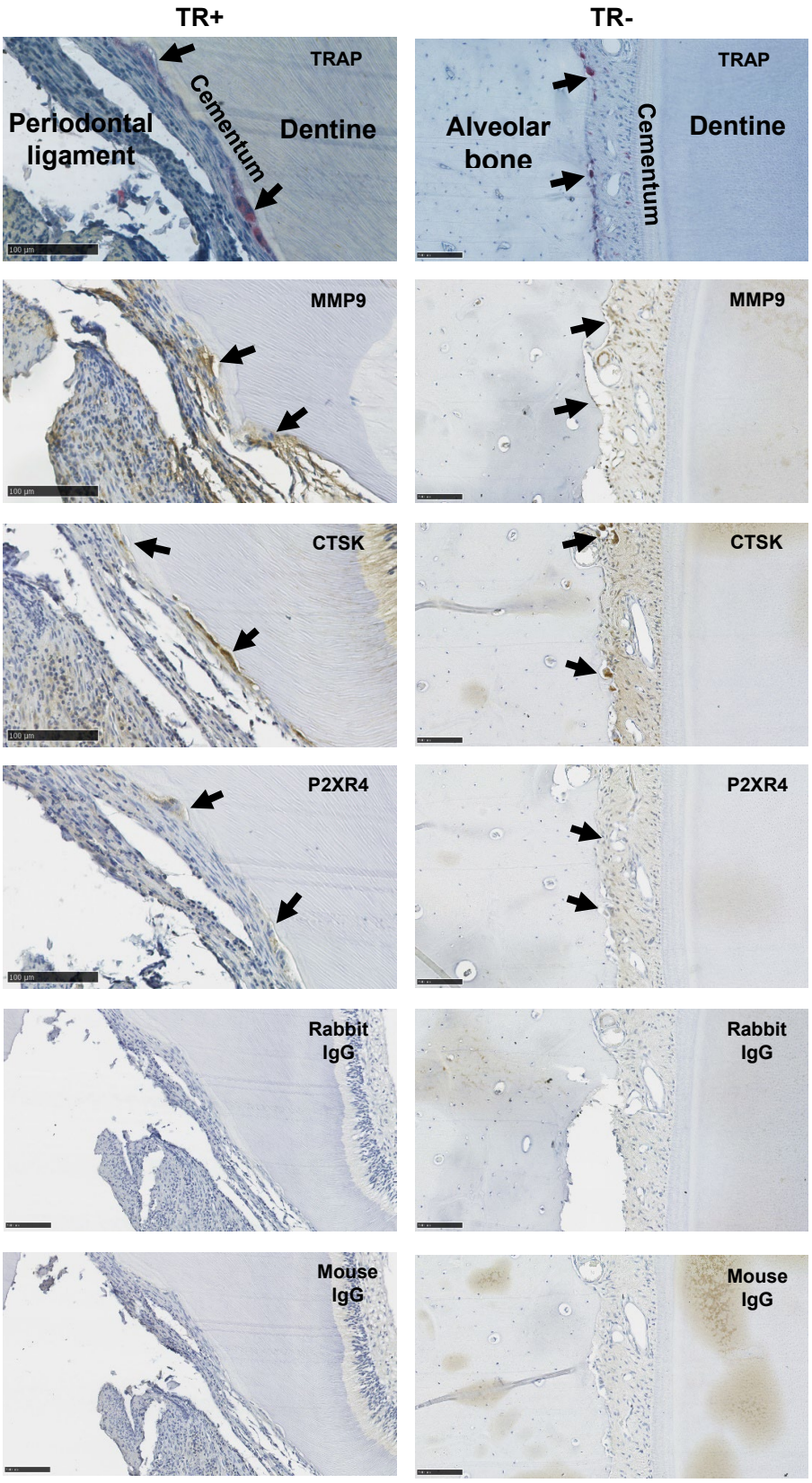

Figure 4.4: TRAcP activity and immunohistochemical staining of serial sections. Cat 2 for TR+ sample; Cat 6 for TR- sample. Osteoclasts in TR- cats focused on bone as indicated by arrows; Odontoclasts in TR+ cats focused on mineralised dental tissue. Scale bar: 100µm

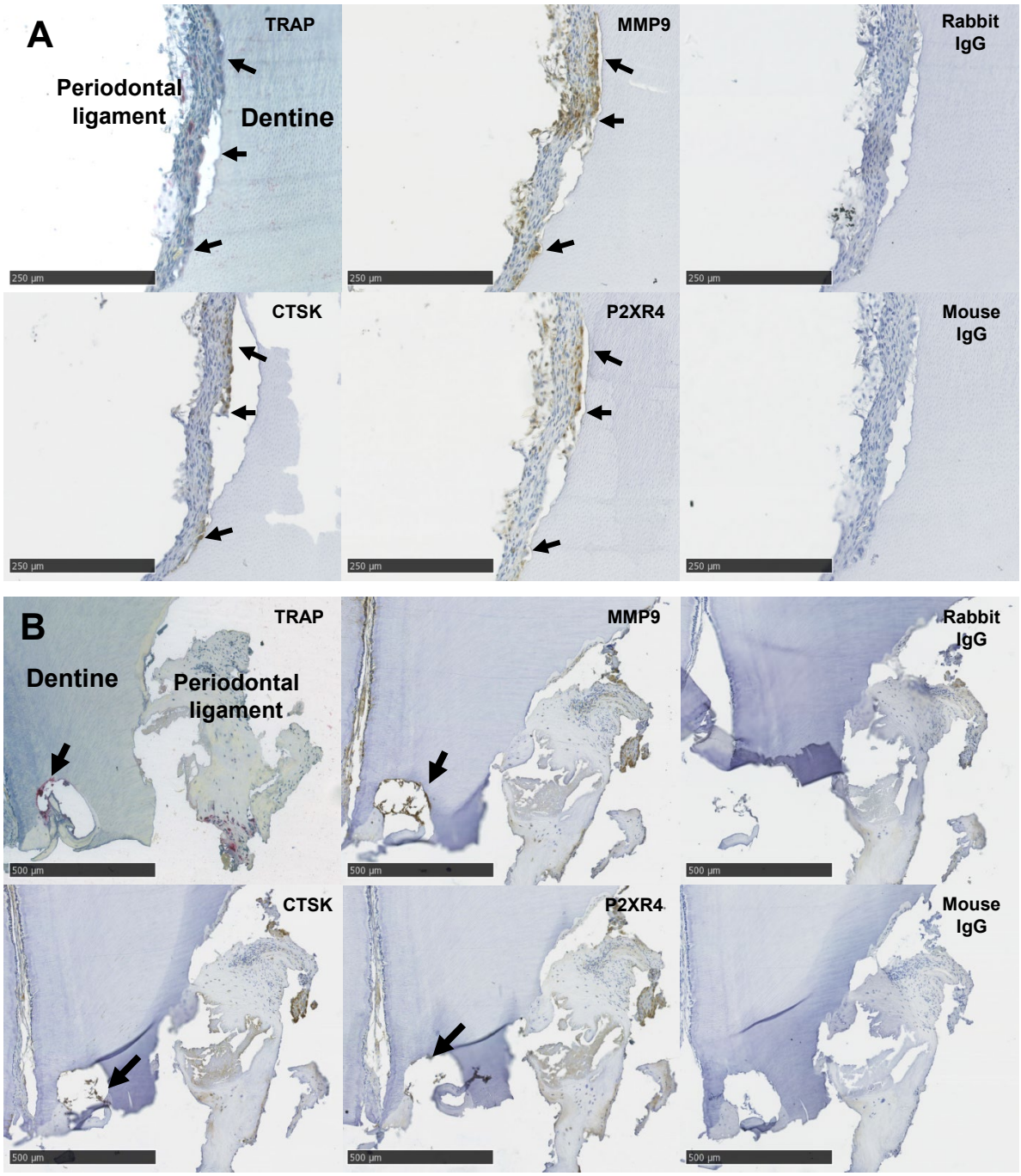

Figure 4.5: Immunohistochemical staining of serial sections from different TR+ cats with horse-radish peroxidase antibodies. A) cat 4; B) Clinical sample. Arrows indicate common areas of multinucleated TRAcP positive cells in resorptive pits. Scale bar: A) 250µm; B) 500 µm

4.3 Functional studies of feline osteoclasts *in vitro*

4.3.1 Differentiation of feline osteoclasts post-transfection of feline specific siRNAs targeting MMP, P2XR4 and CTSK

Following siRNA transfections, cells were observed and imaged under dark field microscopy over the course of 16 days at instances where changes were observed. Electroporation is known to induce high cell death and its effects on cell characteristics. This was observed in the ability of osteoclasts to grow and differentiate in early osteoclast development during cell culture. In the untreated controls, osteoclast precursors were noticeably larger than non-targeting sequence siRNA treated control cells during early RANKL treatment (Figure 4.6). At day 6, untreated controls showed small numbers of cell fusion, forming small multinucleated cells. In comparison, negative siRNA control (scrambled), at day 6 showed little growth and no fusion. Upon day 8, a greater degree of cell fusion was observed in untreated control cells, leading to the formation of large multinucleated cells which continued to form to day 11. For scrambled siRNA treated cells, multinucleated cells continued to form at day 11 which were similar in number and size to early fusion observed at day 3 of untreated controls. This delay in cell fusion was also observed in all other siRNA treatments, MMP9, CTSK, and P2XR4.

On day 16, untreated cells saw a reduction in the number of large multinucleated cells compared to day 13, which may be due to apoptosis after terminal differentiation by RANKL. For Scrambled treated cells at day 16, multinucleation had reached sizes comparable to untreated cells of day 8. For other siRNA treatments cell fusion was also delayed and varied. Cells transfected with CTSK siRNA followed similar growth and fusion as scrambled cells, with multinucleated cells of comparable size but fewer than observed in scrambled. MMP9 and P2XR4 in contrast showed little to no fusion even at day 16. Osteoclasts appeared to be fusing and resorbing after transfecting for Scrambled and CTSK treated cells as observed in Figure 4.7 by clear areas of the overall mineralised well surface. Overall, from observations of cell growth and fusion, transfection causes delays to the growth and fusion of feline osteoclast precursors. MMP9 and P2XR4 transfection appear to greatly reduce osteoclast fusion while CTSK showed little reduction in multinucleation when compared to negative control scrambled siRNA treated cells.

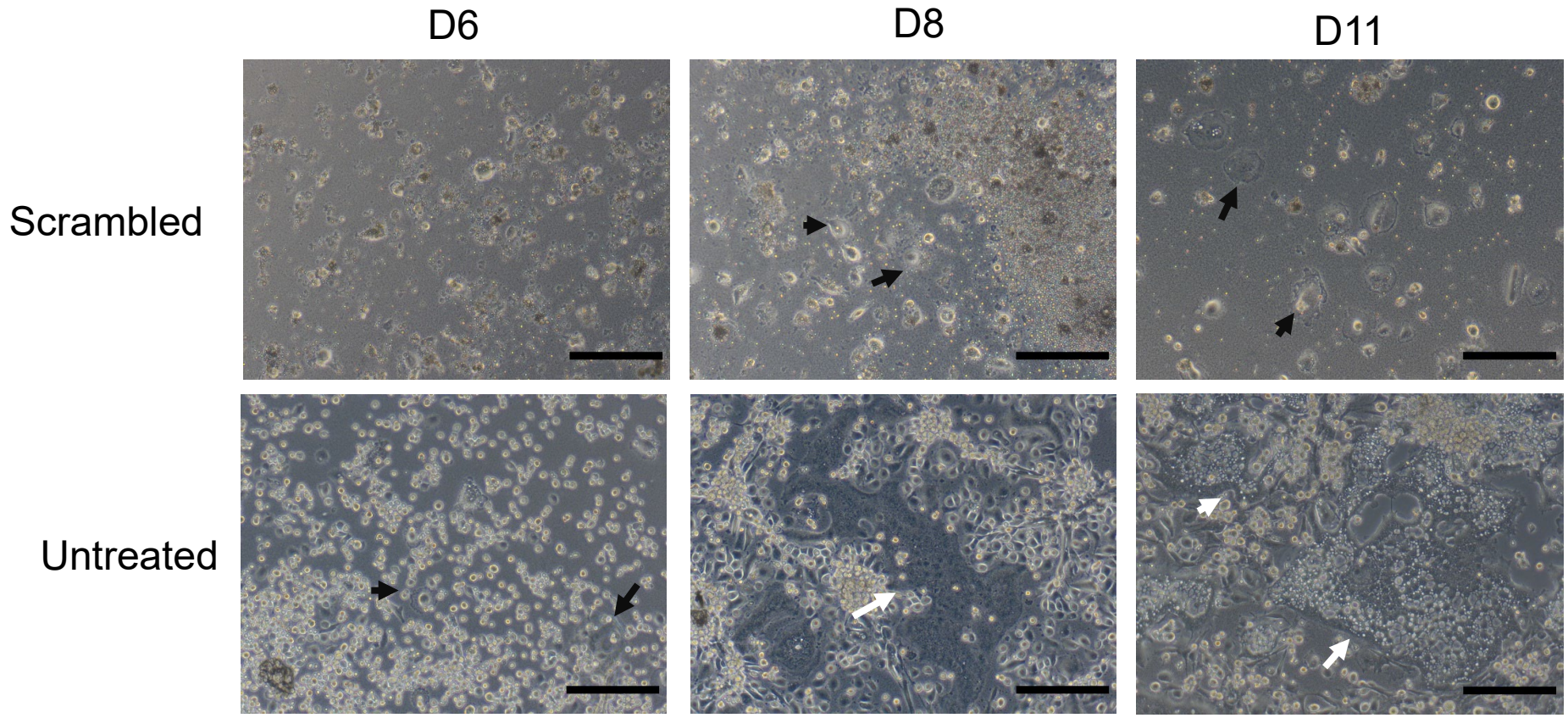

Figure 4.6: Fusion of osteoclast precursors into multinucleated cells on mineralised plates. At day 6, untreated cells show small levels of multinucleation. On day 8, scrambled cells show small levels of multinucleation via cell fusion, while untreated cells show high levels of multinucleation, generating large multinucleated cells. Multinucleated cells indicated by black arrows; large multinucleated cells indicated by white arrows Scale bar: 200 μm.

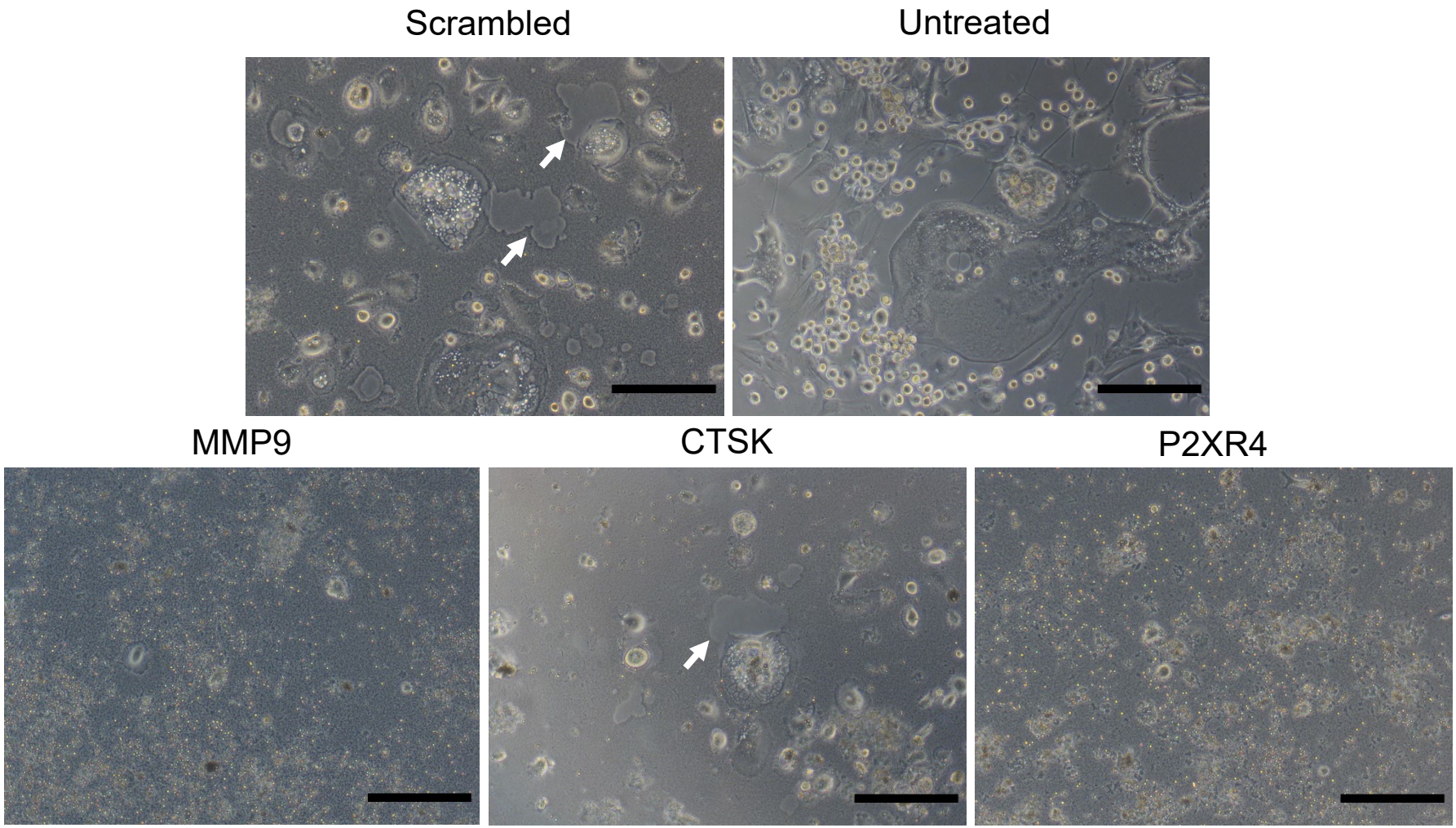

Figure 4.7: Images of cell culture on day 16 days of RANKL treatment post-transfection on mineralised plates. Resorptive activity may be observed in Scrambled and CTSK images where clear zones are indicated by arrows. Note, untreated well appears completely clear with no mineralisation observed. Scale bar: 200 μm

4.3.2 Reduction of MMP9, P2XR4, and CTSK mRNA expression post-transfection was not statistically supported

To assess the efficiency in gene silencing of the individual targets caused by siRNA transfection, qPCR was performed and amplified for MMP9, P2XR4, CTSK, scrambled, and normalised with two housekeeping genes, GAPDH and HPRT. Cells were transfected for 48 hours before cell lysis and RNA extraction was performed for assessment of mRNA levels (Table 4.2). However, it should be noted that due to time restrictions, there was not sufficient time to optimise and test a range of siRNAs for each of our targets, therefore a previously validated MMP9 siRNA and untested siRNA against CTSK and P2XR4 were used. Subsequently, primer efficiency and optimisation of qPCR could not be achieved with reduced time for experiments. This was reflected in the melt curves of qPCR where GAPDH, MMP9 and P2XR4 show two separate peaks where only a single peak should be reported (Figure 4.8).

Following electroporation, untreated and scrambled mRNA levels should remain similar however there is variation observed in all siRNA treatments. For MMP9 mRNA, untreated was 5.5-fold higher than scrambled, but this was not found to be statistically significant (P=0.2). This observed difference, however, may be due to some cell death in the scrambled controls during electroporation.

In MMP9 silencing, a reduction of 26% of MMP9 mRNA was observed when compared to scrambled treated cells however this reduction is not significant (P=0.7).

For CTSK treatment, CTSK mRNA was reduced by 13% compared to scrambled negative control cells, however this reduction wass not significant (P=0.1). When comparing untreated and scrambled, untreated shows 74% less CTSK mRNA than scrambled treated cells however this difference is not significant (P=0.2)

P2XR4 silencing saw an increase in P2XR4 mRNA by approximately 4.5-fold when compared to scrambled treated cells but was also not deemed significantly different (P=0.7). Untreated cells show 57% less P2XR4 mRNA when compared to scrambled treatment but was not deemed statistically significant (P=0.2). From these results, only MMP9 showed a marginal reduction in mRNA levels and with CTSK and P2XR4 no reduction was observed. In conclusion, I was unable to confirm that the siRNA was able to knockdown their intended targets.

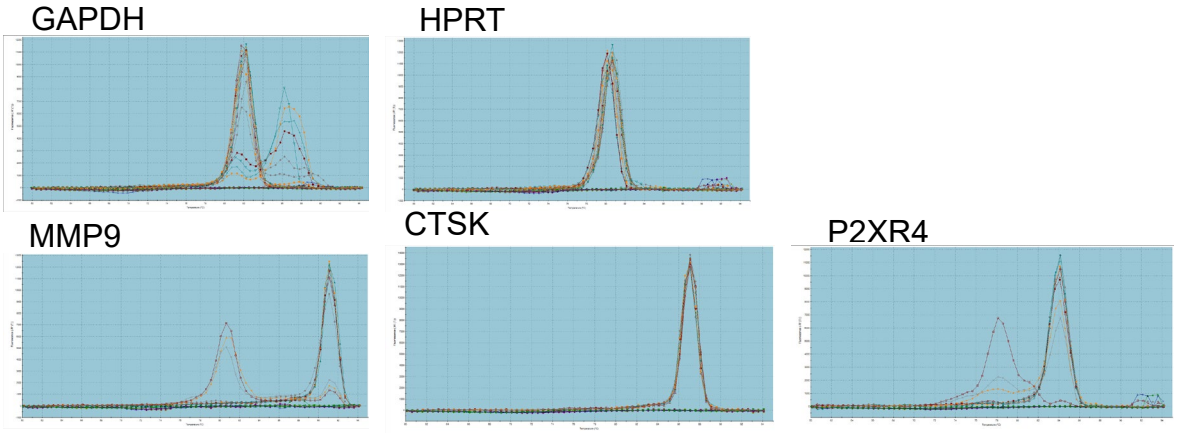

Figure 4.8: Melt curves from qPCR of various genes. MMP9 and P2XR4 show two peaks, GAPDH also shows peaks after the main peak.

Primer	Treatment	Mean ($2^{\delta\delta Ct}$)	Standard error of mean	Standard deviation
MMP9	Untreated	5.559655	0.7343	1.038
	Scrambled	1	0.61	1.056
	MMP9	0.740428	0.1673	0.2898
CTSK	Untreated	0.260917	0.03994	0.05649
	Scrambled	1	0.01054	0.01826
	CTSK	0.8693	0.02092	0.03623
P2XR4	Untreated	0.435274	0.004526	0.006400
	Scrambled	1	1.911	3.310
	P2XR4	4.53647	0.6492	1.124

Table 4.2: Summary of qPCR data and statistical analysis. n=3 for each treatment

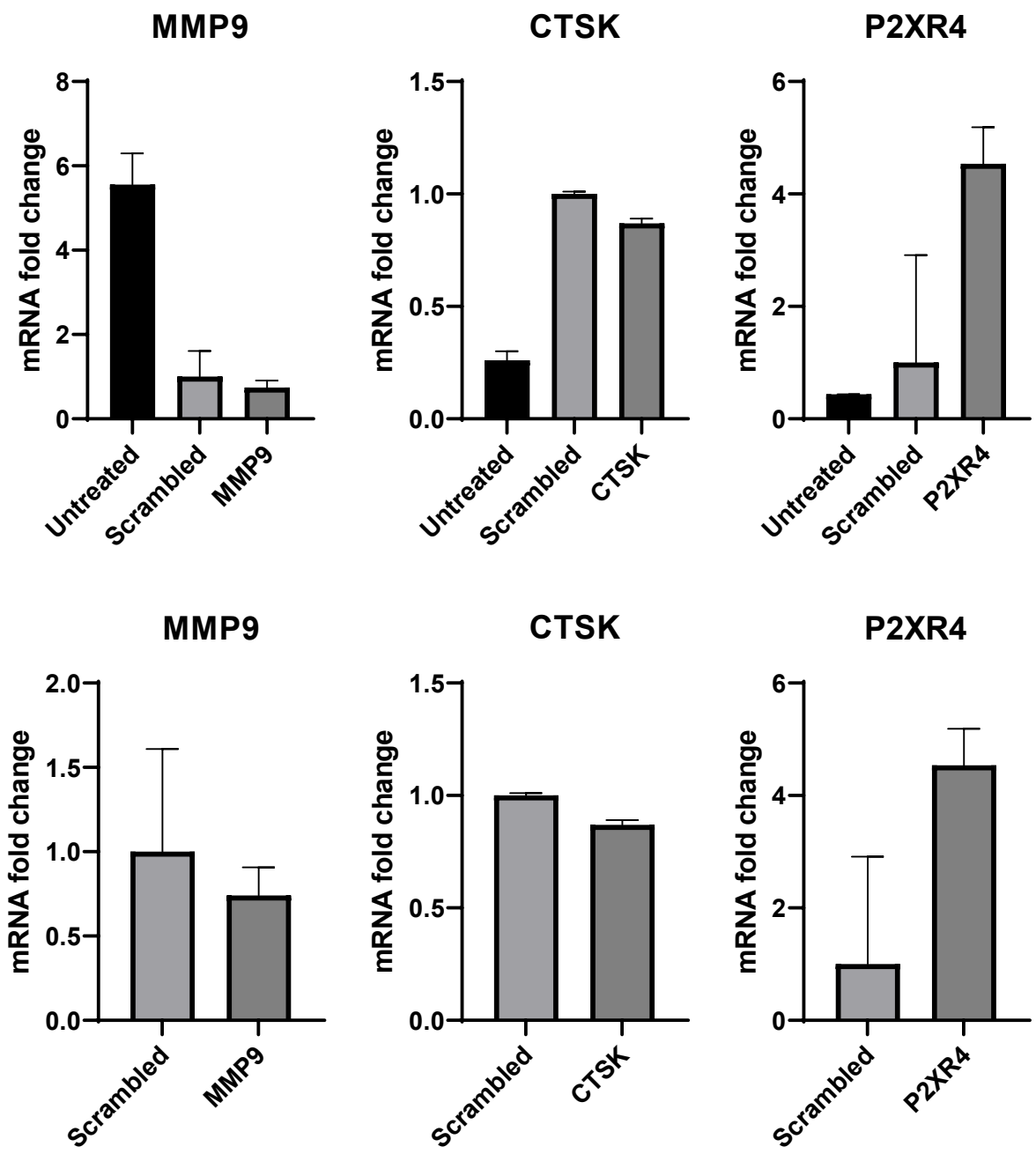

Figure 4.9: MMP9 mRNA expression levels show reduction (48 hours post-transfection) by MMP9 siRNA electroporation of feline osteoclast precursors. Graph represents relative expression as fold changes + SEM bars.

4.3.3 MMP9, P2XR4, and CTSK silencing reduces osteoclast density

To quantify the reduction in osteoclast formation, cells were assessed for TRAcP activity. Osteoclasts were defined as TRAcP positive cells with at least two nuclei and were counted from representative images and calculated as number of cells per area (Figure 4.2; Table 4.3). A significant reduction was observed between untreated cells and scrambled treated cells, dropping from 2044 cells/cm^2 to 1375 cells/cm^2 (P=0.0003) and untreated cells were significantly greater in number of positive TRAcP cells/cm^2 than treated cells (P<0.0001 for MMP9, CTSK, P2XR4) (Figure 4.11). CTSK showed an average of 586 positive TRAcP cells/cm2 which was significantly less than scrambled treated cells (P=0.0040) but was significantly greater than both MMP9 and P2XR4 (P<0.0001 in both). MMP9 and P2XR4 showed significantly less positive TRAcP cells/cm^2 than scrambled treated cells (P<0.0001 in both). MMP9 had 37 positive TRAcP cells/cm^2, greater than P2XR4, 80 positive TRAcP cells/cm^2, however there was no statistically significant difference (P=0.3547). Overall, siRNA treatment with MMP9, CTSK, and P2XR4 significantly reduced the formation of multinucleated osteoclasts. This confirms previous observations where MMP9 and P2XR4 show a large reduction of osteoclast formation and resorptive activity and CTSK shows a slight reduction compared to scrambled control.

Treatment	**Mean (cells/cm^2)**	**Standard error of mean**	**Standard deviation**
Untreated	2044	90.86	667.7
Scrambled	1375	222.2	1155
MMP9	36.96	22.35	116.1
CTSK	585.5	76.12	395.5
P2XR4	80.07	39.09	203.1

Table 4.3: Summary table of statistical analysis. n = 27 for each treatment

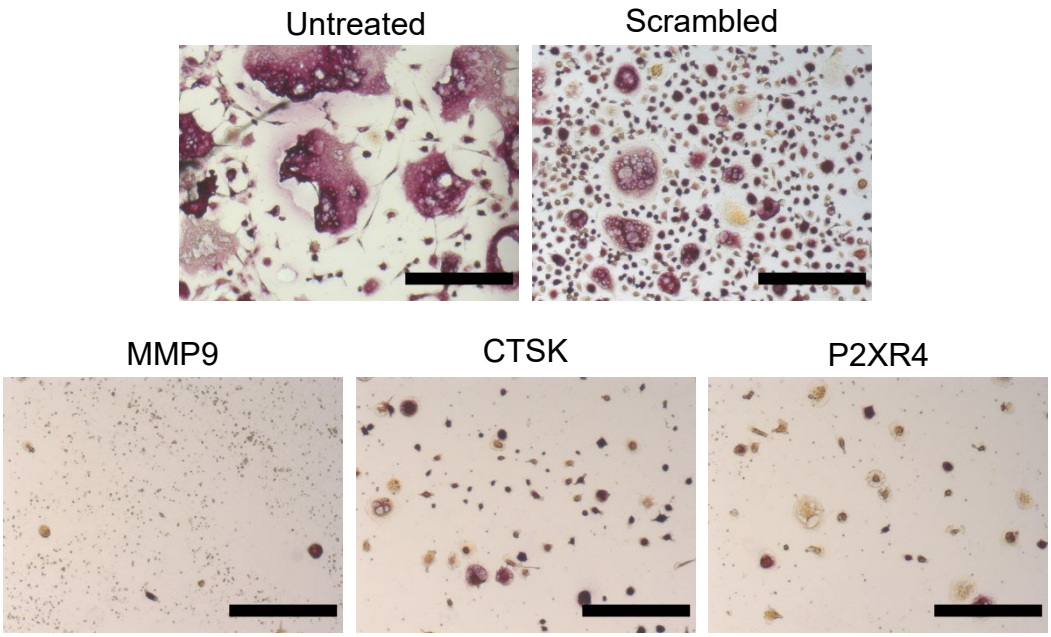

Figure 4.10: Representative images of TRAcP activity of cells on day 16. Untreated cells show a much larger number of osteoclasts and a higher degree of multinucleation than treated cells. Under transfection, there are many TRAcP positive cells, but many are not multinucleated. Scale bar: 100 μm

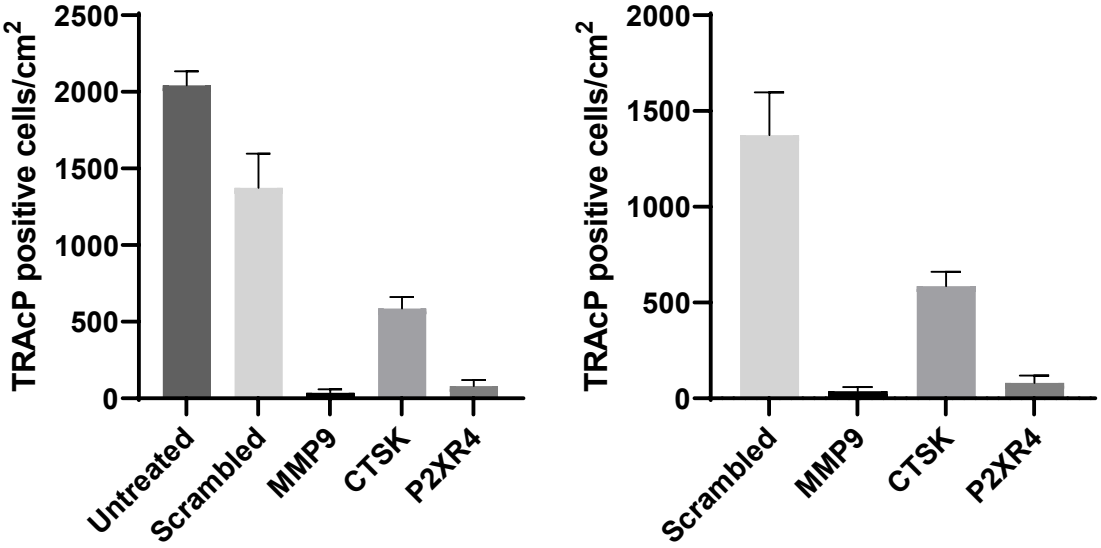

Figure 4.11: Silencing of MMP9, CTSK, and P2XR4 reduce the number of multinucleated TRAcP positive cells/cm2. Graphs represent TRAcP positive cells/cm2 for each condition with SEM bars.

4.3.4 MMP9, P2XR4, and CTSK silenced cells show a reduction in resorptive activity

In order to assess the resorptive activity of transfected cells, van Kossa staining was performed on wells at day 16 following bleaching of cells. This allows high contrast visualisation of osteoclast resorptive activity on mineralised surfaces where mineralised surfaces appear dark in colour by staining and the ability to quantify mineralisation in cell culture (Figure 4.12).

Treated cells shows much lower proportions of resorption compared to the untreated cells (Figure 4.13). Untreated cells showed resorption of 26.18%, whereas transfected cells showed less than 1% of the overall area (Figure 4.13). Among treated cells, MMP9 showed the overall greatest reduction in resorption of 0.04%. P2XR4 showed a reduction with 0.14% resorption and CTSK showed 0.24% resorption. Scrambled also showed little resorption with 0.33%.

Two technical replicates were set up however this was not sufficient for statistical analysis. Though these results are not statistically significant, the observed trend of reduction by siRNA correlates with observations of cell culture where electroporation both delays and affects the ability of osteoclast to differentiate. However, the trend of MMP9 observed in this transfection is correlating of results observed in cell culture images, van Kossa staining, and positive TRAcP cell count.

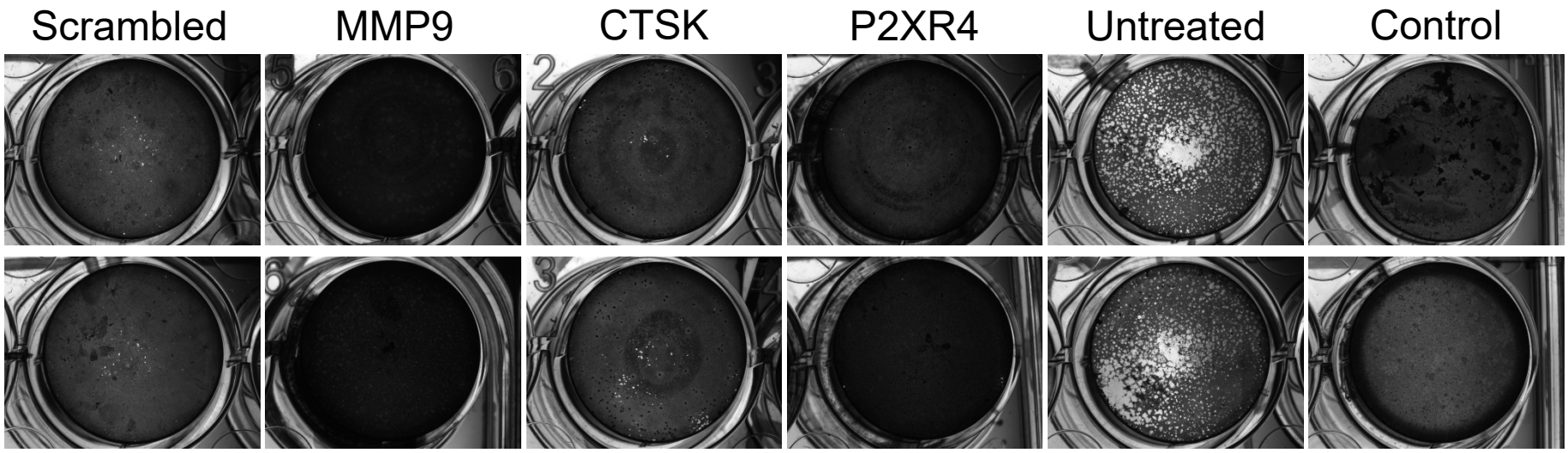

Figure 4.12: Whole well images of van Kossa staining using stereolumar lens. Control well contained media and no cells. Diameter of well: 1.5554 cm (Area = 1.9 cm2)

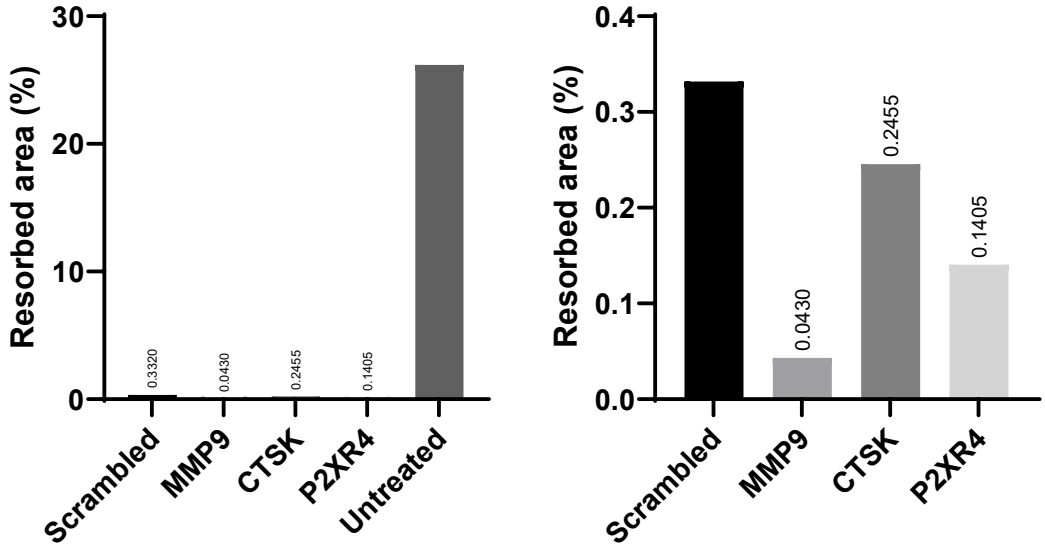

Figure 4.13: Percentage resorbed area of mineralised surface quantified from van Kossa staining. Resorbed area in the well was measured using ImageJ with threshold function.

4.4 IHC and cell culture discussion

4.4.1 IHC

One difficulty encountered during this project was the duration required for all samples to be sufficiently decalcified to allow sectioning for histological analysis. Even after 120 days, some samples did not show sufficient decalcification for sectioning. Optional methods may include acid decalcification; however, this method may greatly affect target proteins within the tissue, i.e. TRAP enzyme activity may be rendered inert, removing the ability to verify odontoclasts within the tissue. Ten percent EDTA was selected as a gentler alternative. Modifications to this solution may allow faster decalcification without altering antigen stability.

In previous studies, attempts were made to optimise antibodies to detect products of genes such as P2XR4 and CTSK which were found to be upregulated in TR+ve teeth by qPCR. This was to confirm the altered gene expression at a protein level and to identify which cells express these proteins in dental tissue. MMP9 was the only antibody successfully optimised and the other antibodies failed to label their target specifically when compared to isotype controls. However, in this project, P2XR4 and CTSK antibodies were successfully optimised and found to label osteoclasts and odontoclasts within dental tissue. Due to time restrictions, optimisation of IHC was restricted to these three targets and quantitative results were lacking, however optimisation of previous targets such as RANK, RANKL, OPG, and SPI.1 protein should also be attempted in future studies. This may provide insight into the localisation and interaction between key proteins of osteoclast differentiation within the dental microenvironment.

It was found in this study that every tooth section did not contain a TR lesion even though each section was collected from a TR+ve tooth. This lack of odontoclasts is also reported in other studies (Reiter et al., 2005a; Reiter and Mendoza, 2002) and though odontoclasts rapidly resorb, their lifespan are limited which makes obtaining histological sections of each stage difficult (Booij-Vrieling et al., 2010; Okuda and Harvey, 1992; Reiter et al., 2005a). Fluorescent immunohistochemistry may be a technique which could be used to allow visualisation of multiple protein targets within the same tissue and their potential co-localisation. Multiple antibody staining would

then reduce the issues where limited serial sections can be acquired of a TR lesion. This could be attempted in future studies however individual staining with HRP conjugated antibodies would be sufficient for initial antibody optimisation. Furthermore, IHC could be improved through the semi-quantification of protein expression and TRAcP positive cells in TR lesions.

It is important to note that the availability of feline specific antibodies is quite limited and previously documented antibodies which have been reported to work in feline tissues are no longer commercially available (Senn et al., 2010). For example, antibodies for RANK, RANKL, and OPG which were previously documented to work in feline tissues were originally polyclonal but have now been replaced with monoclonal antibodies. Therefore, further antibody optimisation is required to expand investigations into other genes.

4.4.2 Cell culture

The functional analysis of candidate genes was performed by knockdown using siRNA. Confirmation of knockdown was performed by qPCR, and effect of knockdowns were assessed by measuring TRAcP activity of multinucleated cells, and van Kossa staining to assess resorption on mineralised plates. The osteoclasts were differentiated from feline bone marrow cells collected at post-mortem. Of the siRNA treatments, MMP9 showed the most promising trend where MMP9 mRNA levels were decreased 48 hours after transfection when compared to scrambled control. Though this result and all other siRNA treatments were not found to be statistically significantly, the trend observed for MMP9 was concurrent with results observed in the previous study (Lee, 2019). For CTSK and P2XR4, the variation of CTSK and P2XR4 mRNA in untreated cells when compared to scrambled and CTSK/P2XR4 conditions is highly unusual. This may be due to failure to amplify the target genes and/or optimisation of siRNA primers and/or qPCR primers. Overall, in this transfection, MMP9, CTSK, and P2XR4 siRNA failed to show statistically significant reduction in mRNA of target genes.

Untreated and scrambled cells should in theory not show any difference however large variation is reported in all siRNA treatments. One issue is the siRNA transfection is being performed on cells while they are differentiating.

In previous studies, it was reported that MMP9 was highly expressed in early stages of osteoclast precursors and its high expression is maintained throughout osteoclast differentiation (Lee, 2019). As the expression of the other two targets have not been investigated, the knockdown effect of two other target genes in early stages of osteoclast differentiation may not be effective or very different. Future studies would then need to confirm the expression levels of CTSK and P2XR4 during osteoclast differentiation and determine which stage of osteoclast differentiation might be beneficial for siRNA transfection.

One complication to account for may be off target effects. In some cases, siRNA may not act to cleave/degrade target mRNA sequences but instead act as miRNA, blocking translation of mRNA as proteins or by off targeting effects increase gene expression (Scacheri et al., 2004). Due to decrease of the protein expression, a feedback loop may be triggered to increase transcription of the intended target gene thus producing an unexpectedly higher mRNA expression.

The failure to optimise these silencing approaches may be due to issues of the siRNA, the qPCR primers or both. It should also be noted that primer efficiency was not considered for these two genes, therefore the quantification of these genes is limited. Primer efficiency of MMP9 was performed in the previous study (Lee, 2019). This was reflected in the melting curve analysis where two separate peaks are observed for CTSK and P2XR4. This indicates that the primers have dimerisation problems and may not be correctly amplifying DNA during qPCR. Another potential source is pipetting errors during qPCR as the standard error of the mean (SEM) of some values are quite large, such as scrambled MMP9 mRNA which shows 0.61 and P2XR4 mRNA reporting 1.9 in scrambled cells suggesting large variation between technical replicates. Additionally, one factor may be the RNA itself which is reported as both low quality and quantity which would negatively impact amplification with the primers and the validity of the results.

Testing for primer efficiency should be performed prior to future studies to ensure the quality and effectiveness of these primers. To ensure the correct size of PCR products are produced by the primers, these may be run on a gel to determine if the primers are amplifying their target specifically by checking for single bands of the

correct size. Additionally, in the optimisation of siRNA transfection, multiple siRNAs should be generated for a single target and compared in their efficiency of RNA interference. Only one siRNA was designed for each target gene in this study due to time constraints. Therefore, in future studies, further optimisation of siRNAs and transfection via electroporation is required

In the assessment of siRNA effects on multinucleated TRAcP cells, a significant reduction in cell number and size is observed in all siRNA treatments when compared to controls. This suggests that the siRNA transfection has had some effect and indicates the relative importance of these genes in osteoclast formation and activity. This correlates with the growth and fusion observed in the images obtained at each timepoint. Additionally, the trends observed in quantification of van Kossa appears to follow these observations. This is then promising to suggest the importance of MMP9, CTSK, and P2XR4 in osteoclast differentiation and activity. However, in all cases, further biological and technical repeats are required in further investigation to ensure results are statistically significant. It should be noted, I only had the opportunity to perform this experiment and these techniques once and so was not able to remove technical error from these results.

For van Kossa staining, whole well imaging was performed to quantify the proportion of area resorbed by osteoclasts. However, one limitation of this technique is the algorithm used for setting a threshold in accepting values of the images. This was performed in a semi-automatic manner, where threshold values were slightly adjusted to each sample as the automated function incorrectly areas of no resorption as areas with resorption. One method to mitigate this may be the use of multiple representative images of each of the wells as performed with the TRAcP cell counting. This would allow quantification at a higher magnification which would remove the difficulties associated with whole well images. In addition, the inclusion of more biological and technical replicates is required.

One difficulty observed during cell culture and electroporation was the lack of even distribution of cells across the well. This may be due to swirling of cell media causing osteoclasts or disruption of cells during addition/changing of media. Additionally, osteoclast precursors were initially floating and only later became adherent.

Furthermore, due to osteoclast fusion, cells may cluster in areas of the well, leading to large areas without cells. This may affect the ability to accurately count TRAcP cells in culture without the use of whole well imaging. A possible solution which may improve fusion of cells may be the use of the small well surface area of a 48-well format instead of 24-well format.

Electroporation in this study affected the ability of osteoclasts to grow and differentiate. Optimisation of cell number used in electroporation is required along with measurement of cell viability both before and after transfection. An additional consideration of the growth of osteoclasts is the use of RANKL, which is known to induce apoptosis of osteoclasts after a duration of time. This is particularly seen in the untreated controls where a large area of resorption is observed in the centre of the well, however upon inspection by dark field microscopy and TRAP activity, cells are dead or floating at the centre of the well. This is not observed in the treated conditions which may be due to the delay of osteoclast differentiation caused by electroporation.

Another consideration is the source of feline primary cells for cell culture. Currently, there are no immortalised osteoclast cell lines which means that primary feline myeloid precursors for culture must be isolated from bone marrow. During this study, multiple attempts were made in culturing feline osteoclast from frozen bone marrow and electroporating them, however cells were not growing properly or fusing even for untreated cells. In the last attempt, the cell culture was performed using osteoclasts derived from fresh feline bone marrow acquired after the Covid lockdown. This proved significantly better as cells were visibly growing and fusing both after siRNA transfection as well in the untreated controls. It is highly recommended in future studies that fresh feline bone marrow should be used in place of frozen bone marrow and if frozen bone marrow must be used, cells should be first assessed to grow under normal conditions before proceeding. Overall, from these results MMP9, CTSK, and P2XR4 do indicate their importance in osteoclast function and involvement in feline TR development. Further optimisation of siRNAs, qPCR primers and conditions as well as multiple biological and technical replicates will be required to validate these results.

4.4.3 Future steps

The data obtained from these experiments indicate that MMP9, CTSK, and P2XR4 are involved in osteoclast differentiation and resorptive activity and thus possible involvement with TR development. Though the RNAi effects on gene expression can be investigated by qPCR, end product knockdown should be prioritised as the initial test of evaluating RNAi effectiveness. Western blotting would be the most effective method as this would allow not only detection but also quantification of protein knockdown. As antibodies have been optimised and shown to target specific proteins within feline tissue, these same antibodies could be optimised for use in Western blotting. Due to time constraints and lack of fresh bone marrow samples, the cell culture and siRNA transfection could not be optimised. Under normal optimisation, a control would be set up in order to evaluate the normal expression levels of target genes. This would aid in measuring the differential expression and possible temporal expression of genes therefore providing information of optimal time points for transfection. This is important as transfection in this study assumed expression of these genes would be from the beginning of RANKL treatment, however this may not necessarily be true, where genes may remain expressed at low levels until later stages. In the siRNA design, siRNA sequences were blasted for homologous regions in the target transcripts of mice. This would allow functional studies in mouse osteoclast cells. If suitably similar in regulation of osteoclast formation, this would aid in with the lack and difficulty of obtaining feline samples. Additional further steps for RNAi would include optimisation of cell density and cell viability for transfection via electroporation.

For cell culture experiments, though the mineralised plate does replicate the mineralised surface of teeth to a degree, they do not account for the organic components of bone and teeth found *in vivo* and so by-products from the degradation of such tissue may not be accounted for using these *in vitro* approaches. The use of dentine or bone from biological sources may be useful as the substrate would be more replicative of the true dental environment. Additionally, the use of a pure osteoclast culture and a mineralised surface may indicate which genes are involved in their pathway, however further additions to replicate the feline dental microenvironment could be employed. Osteoclasts are known to communicate with

various other cells within the dental microenvironment including periodontal ligament cells and osteoblasts which have been observed to express RANKL (De Araujo et al., 2007; Hasegawa et al., 2002; Oshiro et al., 2001; Sasaki, 2003b).

Future osteoclast functional studies should include *in vitro* assays to mimic the *in vivo* dental microenvironment as the formation of osteoclasts and their activation is tightly regulated through other cells in their local vicinity. Different combinations of cell types may allow insight into the degree of influence of certain cells on osteoclast activity. The replication of the entire tooth development would be an arduous task; however, some aspects may be replicated. For example, using the growth of an osteoclast monolayer on a mineralised surface with an overlying monolayer of PDL and gingival cells may allow a suitable co-culture and *in vivo* replication of the layered environment on the mineralised surface of the tooth. Cells could be grouped into sections of the mineralised tissue with or without PDL cells to investigate endogenous interactions between PDL cells and osteoclasts.

Reference list

Agrawal, N., Dasaradhi, P.V.N., Mohmmed, A., Malhotra, P., Bhatnagar, R.K., Mukherjee, S.K., 2003. RNA Interference: Biology, Mechanism, and Applications. Microbiol. Mol. Biol. Rev. 67, 657–685. https://doi.org/10.1128/mmbr.67.4.657-685.2003

Amarasekara, D.S., Yun, H., Kim, S., Lee, N., Kim, H., Rho, J., 2018. Regulation of osteoclast differentiation by cytokine networks. Immune Netw. https://doi.org/10.4110/in.2018.18.e8

Anderson, P.H., Atkins, G.J., 2008. The skeleton as an intracrine organ for vitamin D metabolism. Mol. Aspects Med. https://doi.org/10.1016/j.mam.2008.05.003

Andreasen, J.O., 1985. External root resorption: its implication in dental traumatology, paedodontics, periodontics, orthodontics and endodontics. Int. Endod. J. 18, 109–118. https://doi.org/10.1111/j.1365-2591.1985.tb00427.x

AVDC Nomenclature | AVDC.org [WWW Document], n.d. URL https://avdc.org/avdc-nomenclature/ (accessed 1.20.21).

Barba-Recreo, P., Del Castillo Pardo De Vera, J.L., García-Arranz, M., Yébenes, L., Burgueño, M., 2014. Zoledronic acid - Related osteonecrosis of the jaws. Experimental model with dental extractions in rats. J. Cranio-Maxillofacial Surg. 42, 744–750. https://doi.org/10.1016/j.jcms.2013.11.005

Bartlett, J.D., 2013. Dental Enamel Development: Proteinases and Their Enamel Matrix Substrates. ISRN Dent. 2013, 1–24. https://doi.org/10.1155/2013/684607

Bei, M., 2009. Molecular genetics of tooth development. Curr. Opin. Genet. Dev. https://doi.org/10.1016/j.gde.2009.09.002

Bellows, J., 1993. Radiographic signs and diagnosis of dental disease. Semin. Vet. Med. Surg. (Small Anim). 8, 138–145.

Berger, M., Stich, H., Hüster, H., Roux, P., Schawalder, P., 2004. Feline dental resorptive lesions in the 13th to 14th centuries. J. Vet. Dent. 21, 206–213. https://doi.org/10.1177/089875640402100401

Bikle, D.D., 2014. Vitamin D metabolism, mechanism of action, and clinical applications. Chem. Biol. https://doi.org/10.1016/j.chembiol.2013.12.016

Boissy, P., Saltel, F., Bouniol, C., Jurdic, P., Machuca-Gayet, I., 2002. Transcriptional Activity of Nuclei in Multinucleated Osteoclasts and Its Modulation by Calcitonin. Endocrinology 143, 1913–1921. https://doi.org/10.1210/endo.143.5.8813

Bolger, A.M., Lohse, M., Usadel, B., 2014. Trimmomatic: A flexible trimmer for Illumina sequence data. Bioinformatics 30, 2114–2120. https://doi.org/10.1093/bioinformatics/btu170

Booij-Vrieling, H.E., Ferbus, D., Tryfonidou, M.A., Riemers, F.M., Penning, L.C., Berdal, A., Everts, V., Hazewinkel, H.A.W., 2010. Increased vitamin D-driven signalling and expression of the vitamin D receptor, MSX2, and RANKL in tooth resorption in cats. Eur. J. Oral Sci. 118, 39–46. https://doi.org/10.1111/j.1600-0722.2009.00707.x

Booij-Vrieling, H.E., Tryfonidou, M.A., Riemers, F.M., Penning, L.C., Hazewinkel, H.A.W., 2009. Inflammatory cytokines and the nuclear vitamin D receptor are implicated in the pathophysiology of dental resorptive lesions in cats. Vet. Immunol. Immunopathol. 132,

160–166. https://doi.org/10.1016/j.vetimm.2009.05.015

Boyle, W.J., Simonet, W.S., Lacey, D.L., 2003. Osteoclast differentiation and activation. Nature. https://doi.org/10.1038/nature01658

Brookes, A.J., 1999. The essence of SNPs. Gene. https://doi.org/10.1016/S0378-1119(99)00219-X

Burgess, T.L., Qian, Y.X., Kaufman, S., Ring, B.D., Van, G., Capparelli, C., Kelley, M., Hsu, H., Boyle, W.J., Dunstan, C.R., Hu, S., Lacey, D.L., 1999. The ligand for osteoprotegerin (OPGL) directly activates mature osteoclasts. J. Cell Biol. 145, 527–538. https://doi.org/10.1083/jcb.145.3.527

Cahill, D.R., Marks, S.C., 1980. Tooth eruption: evidence for the central role of the dental follicle. J. Oral Pathol. Med. 9, 189–200. https://doi.org/10.1111/j.1600-0714.1980.tb00377.x

Casarin, A., Jimenez-Ortega, J.C., Trevisson, E., Pertegato, V., Doimo, M., Ferrero-Gomez, M.L., Abbadi, S., Artuch, R., Quinzii, C., Hirano, M., Basso, G., Ocaña, C.S., Navas, P., Salviati, L., 2008. Functional characterization of human COQ4, a gene required for Coenzyme Q10 biosynthesis. Biochem. Biophys. Res. Commun. 372, 35–39. https://doi.org/10.1016/j.bbrc.2008.04.172

Celebi, A.A., Demirer, S., Catalbas, B., Arikan, S., 2013. Effect of ovarian activity on orthodontic tooth movement and gingival crevicular fluid levels of interleukin-1β and prostaglandin E2 in cats. Angle Orthod. 83, 70–75. https://doi.org/10.2319/012912-78.1

Choi, E.K., Lee, J.H., Baek, S.H., Kim, S.J., 2017. Gene expression profile altered by orthodontic tooth movement during healing of surgical alveolar defect. Am. J. Orthod. Dentofac. Orthop. 151, 1107–1115. https://doi.org/10.1016/j.ajodo.2016.10.039

Choi, H.-D., Noh, W.-C., Park, J.-W., Lee, J., Suh, J.-Y., 2011. Analysis of gene expression during mineralization of cultured human periodontal ligament cells. J. Periodontal Implant Sci. 41, 30. https://doi.org/10.5051/jpis.2011.41.1.30

Christensen, J., Shastri, V.P., 2015. Matrix-metalloproteinase-9 is cleaved and activated by Cathepsin K. BMC Res. Notes 8, 322. https://doi.org/10.1186/s13104-015-1284-8

Cirillo, E., Parnell, L.D., Evelo, C.T., 2017. A Review of Pathway-Based Analysis Tools That Visualize Genetic Variants. Front. Genet. 8, 174. https://doi.org/10.3389/fgene.2017.00174

Coles, S., 1990. The Prevalence of Buccal Cervical Root Resorptions in Australian Cats. J. Vet. Dent. 7, 14–16. https://doi.org/10.1177/089875649000700401

Collins, M.K., Sinclair, P.M., 1988. The local use of vitamin D to increase the rate of orthodontic tooth movement. Am. J. Orthod. Dentofac. Orthop. 94, 278–284. https://doi.org/10.1016/0889-5406(88)90052-2

Cunningham, F., Achuthan, P., Akanni, W., Allen, J., M, Armean, I.M., Bennett, R., Bhai, J., Billis, K., Boddu, S., Cummins, C., Davidson, C., Dodiya, K.J., Gall, A., Girón, C.G., Gil, L., Grego, T., Haggerty, L., Haskell, E., Hourlier, T., Izuogu, O.G., Janacek, S.H., Juettemann, T., Kay, M., Laird, M.R., Lavidas, I., Liu, Z., Jane, Marugán, J.C., Maurel, T., Mcmahon, A.C., Moore, B., Morales, J., Mudge, J.M., Nuhn, M., Ogeh, D., Parker, A., Parton, A., Patricio, M., Imran, A., Schmitt, B.M., Schuilenburg, H., Sheppard, D., Sparrow, H., Stapleton, E., Szuba, M., Taylor, K., Threadgold, G., Thormann, A., Vullo, A., Walts, B., Winterbottom, A., Zadissa, A., Chakiachvili, M., Frankish, A., Hunt, S.E.,

Kostadima, M., Langridge, N., Martin, F.J., Muffato, M., Perry, E., Ruffier, M., Staines, D.M., Trevanion, S.J., Aken, B.L., Yates, A.D., Zerbino, D.R., Flicek, P., 2019. Ensembl 2019. Nucleic Acids Res. 47, D745–D751. https://doi.org/10.1093/nar/gky1113

Darcey, J., Qualtrough, A., 2013. Resorption: Part 1. Pathology, classification and aetiology. Br. Dent. J. 214, 439–451. https://doi.org/10.1038/sj.bdj.2013.431

Davidovitch, Z., Montgomery, P.C., Eckerdal, O., Gustafson, G.T., 1975. Cellular localization of cyclic AMP in periodontal tissues during experimental tooth movement in cats. Calcif. Tissue Res. 19, 317–329. https://doi.org/10.1007/BF02564014

Davis, M.E., Zuckerman, J.E., Choi, C.H.J., Seligson, D., Tolcher, A., Alabi, C.A., Yen, Y., Heidel, J.D., Ribas, A., 2010. Evidence of RNAi in humans from systemically administered siRNA via targeted nanoparticles. Nature 464, 1067–1070. https://doi.org/10.1038/nature08956

De Araujo, R.M.S., Oba, Y., Moriyama, K., 2007. Identification of genes related to mechanical stress in human periodontal ligament cells using microarray analysis. J. Periodontal Res. 42, 15–22. https://doi.org/10.1111/j.1600-0765.2006.00906.x

Delaissé, J.M., Eeckhout, Y., Neff, L., François-Gillet, C., Henriet, P., Su, Y., Vaes, G., Baron, R., 1993. (Pro)collagenase (matrix metalloproteinase-1) is present in rodent osteoclasts and in the underlying bone-resorbing compartment. J. Cell Sci. 106 (Pt 4, 1071–1082.

DeLaurier, A., Allen, S., Flandre, C., Horton, M.A., Price, J.S., 2002. Cytokine expression in feline osteoclastic resorptive lesions. J. Comp. Pathol. 127, 169–177. https://doi.org/10.1053/jcpa.2002.0577

Desjardin, C., Vaiman, A., Mata, X., Legendre, R., Laubier, J., Kennedy, S.P., Laloe, D., Barrey, E., Jacques, C., Cribiu, E.P., Schibler, L., 2014. Next-generation sequencing identifies equine cartilage and subchondral bone miRNAs and suggests their involvement in osteochondrosis physiopathology. BMC Genomics 15, 798. https://doi.org/10.1186/1471-2164-15-798

Dobson, P.F., Dennis, E.P., Hipps, D., Reeve, A., Laude, A., Bradshaw, C., Stamp, C., Smith, A., Deehan, D.J., Turnbull, D.M., Greaves, L.C., 2020. Mitochondrial dysfunction impairs osteogenesis, increases osteoclast activity, and accelerates age related bone loss. Sci. Rep. 10, 11643. https://doi.org/10.1038/s41598-020-68566-2

Dong, Z., Bonfil, R.D., Chinni, S., Deng, X., Trindade Filho, J.C., Bernardo, M., Vaishampayan, U., Che, M., Sloane, B.F., Sheng, S., Fridman, R., Cher, M.L., 2005. Matrix metalloproteinase activity and osteoclasts in experimental prostate cancer bone metastasis tissue. Am. J. Pathol. 166, 1173–1186. https://doi.org/10.1016/S0002-9440(10)62337-1

Donoghue, S., Scarlett, J.M., Williams, C.A., Saidla, J., 1994. Diet as a Risk Factor for Feline External Odontoclastic Resorption. J. Nutr. 124, 2693S-2694S. https://doi.org/10.1093/jn/124.suppl_12.2693S

Drake, M.T., Clarke, B.L., Khosla, S., 2008. Bisphosphonates: Mechanism of action and role in clinical practice. Mayo Clin. Proc. https://doi.org/10.4065/83.9.1032

Dupont, G.A., Debowes, L.J., 2002. Comparison of Periodontitis and Root Replacement in Cat Teeth with Resorptive Lesions. J. Vet. Dent. 19, 71–75. https://doi.org/10.1177/089875640201900202

Ek-Rylander, B., Barkhem, T., Ljusberg, J., Öhman, L., Andersson, K.K., Andersson, G., 1997. Comparative studies of rat recombinant purple acid phosphatase and bone tartrate-resistant acid phosphatase. Biochem. J. 321, 305–311. https://doi.org/10.1042/bj3210305

Evans, B.R., Mosig, R.A., Lobl, M., Martignetti, C.R., Camacho, C., Grum-Tokars, V., Glucksman, M.J., Martignetti, J.A., 2012. Mutation of membrane type-1 metalloproteinase, MT1-MMP, causes the multicentric osteolysis and arthritis disease winchester syndrome. Am. J. Hum. Genet. 91, 572–576. https://doi.org/10.1016/j.ajhg.2012.07.022

Farcas, N., Lommer, M.J., Kass, P.H., Verstraete, F.J.M., 2014. Dental radiographic findings in cats with chronic gingivostomatitis (2002-2012). J. Am. Vet. Med. Assoc. 244, 339–345. https://doi.org/10.2460/javma.244.3.339

Floyd, M.R., 1991. The modified Triadan system: nomenclature for veterinary dentistry. J. Vet. Dent. 8, 18–19.

Fukushima, H., Kajiya, H., Takada, K., Okamoto, F., Okabe, K., 2003. Expression and role of RANKL in periodontal ligament cells during physiological root-resorption in human deciduous teeth. Eur. J. Oral Sci. 111, 346–352. https://doi.org/10.1034/j.1600-0722.2003.00051.x

Gandhi, S.S., Muraresku, C., McCormick, E.M., Falk, M.J., McCormack, S.E., 2017. Risk factors for poor bone health in primary mitochondrial disease. J. Inherit. Metab. Dis. 40, 673–683. https://doi.org/10.1007/s10545-017-0046-2

Gandolfi, B., Alhaddad, H., Abdi, M., Bach, L.H., Creighton, E.K., Davis, B.W., Decker, J.E., Dodman, N.H., Grahn, J.C., Grahn, R.A., Haase, B., Haggstrom, J., Hamilton, M.J., Helps, C.R., Kurushima, J.D., Lohi, H., Longeri, M., Malik, R., Meurs, K.M., Montague, M.J., Mullikin, J.C., Murphy, W.J., Nilson, S.M., Pedersen, N.C., Peterson, C.B., Rusbridge, C., Saif, R., Shelton, D.G., Warren, W.C., Wasim, M., Lyons, L.A., 2018. Applications and efficiencies of the first cat 63K DNA array. Sci. Rep. 8, 1–15. https://doi.org/10.1038/s41598-018-25438-0

Girard, N., Servet, E., Biourge, V., Hennet, P., 2008. Feline tooth resorption in a colony of 109 cats. J. Vet. Dent. 25, 166–174. https://doi.org/10.1177/089875640802500302

Girard, N., Servet, E., Hennet, P., Biourge, V., 2010a. Tooth resorption and vitamin D3 status in cats fed premium dry diets. J. Vet. Dent. 27, 142–147. https://doi.org/10.1177/089875641002700301

Girard, N., Servet, E., Ing, F., Hennet, P., Biourge, V., 2010b. Tooth Resorption and Vitamin D 3 Status in Cats Fed Premium Dry Diets, J VET DENT.

Goel, V.K., Khera, S.C., Ralston, J.L., Chang, K.H., 1991. Stresses at the dentinoenamel junction of human teeth-A finite element investigation. J. Prosthet. Dent. 66, 451–459. https://doi.org/10.1016/0022-3913(91)90504-P

Goldberg, M., Kulkarni, A.B., Young, M., Boskey, A., 2011. Dentin: Structure, composition and mineralization. Front. Biosci. - Elit. 3 E, 711–735. https://doi.org/10.2741/e281

Goodwin, S., McPherson, J.D., McCombie, W.R., 2016. Coming of age: Ten years of next-generation sequencing technologies. Nat. Rev. Genet. https://doi.org/10.1038/nrg.2016.49

Gorrel, C., 2015. Tooth resorption in cats: Pathophysiology and treatment options. J. Feline

Med. Surg. 17, 37–43. https://doi.org/10.1177/1098612X14560098

Gorrel, C., Larsson, A., 2002. Feline odontoclastic resorptive lesions: unveiling the early lesion. J. Small Anim. Pract. 43, 482–488. https://doi.org/10.1111/j.1748-5827.2002.tb00018.x

Goto, T., Tanaka, T., Kiyoshima, T., Moroi, R., Tsukuba, T., Yamamoto, K., Nishimura, Y., Himeno, M., 1994. Localization of cathepsins B, D, and L in the rat osteoclast by immuno-light and -electron microscopy. Histochemistry 101, 33–40. https://doi.org/10.1007/BF00315829

Grier IV, R.L., Wise, G.E., 1998. Inhibition of tooth eruption in the rat by a bisphosphonate. J. Dent. Res. 77, 8–15. https://doi.org/10.1177/00220345980770011201

Gutiérrez-Fernández, A., Soria-Valles, C., Osorio, F.G., Gutiérrez-Abril, J., Garabaya, C., Aguirre, A., Fueyo, A., Fernández-García, M.S., Puente, X.S., López-Otín, C., 2015. Loss of MT 1- MMP causes cell senescence and nuclear defects which can be reversed by retinoic acid . EMBO J. 34, 1875–1888. https://doi.org/10.15252/embj.201490594

Hammarström, L., Lindskog, S., 1985. General morphological aspects of resorption of teeth and alveolar bone. Int. Endod. J. 18, 93–108. https://doi.org/10.1111/j.1365-2591.1985.tb00426.x

Harokopakis-Hajishengallis, E., 2007. Physiologic root resorption in primary teeth: molecular and histological events. J. Oral Sci. 49, 1–12. https://doi.org/10.2334/josnusd.49.1

Harvey, C.E., Orsini, P., McLahan, C., Schuster, C., 2004. Mapping of the radiographic central point of feline dental resorptive lesions. J. Vet. Dent. 21, 15–21. https://doi.org/10.1177/089875640402100102

Hasegawa, T., Kikuiri, T., Takeyama, S., Yoshimura, Y., Mitome, M., Oguchi, H., Shirakawa, T., 2002. Human periodontal ligament cells derived from deciduous teeth induce osteoclastogenesis in vitro. Tissue Cell 34, 44–51. https://doi.org/10.1054/tice.2002.0223

Heaton, M., Wilkinson, J., Gorrel, C., Butterwick, R., 2004. A rapid screening technique for feline odontoclastic resorptive lesions. J. Small Anim. Pract. 45, 596–601. https://doi.org/10.1111/j.1748-5827.2004.tb00181.x

Hölzer, M., Marz, M., 2019. De novo transcriptome assembly: A comprehensive cross-species comparison of short-read RNA-Seq assemblers. Gigascience 8, 1–16. https://doi.org/10.1093/gigascience/giz039

How, K.L., Hazewinkel, H.A.W., Mol, J.A., 1994. Dietary vitamin D dependence of cat and dog due to inadequate cutaneous synthesis of vitamin D. Gen. Comp. Endocrinol. 96, 12–18. https://doi.org/10.1006/gcen.1994.1154

Hsu, H., Lacey, D.L., Dunstan, C.R., Solovyev, I., Colombero, A., Timms, E., Tan, H.L., Elliott, G., Kelley, M.J., Sarosi, I., Wang, L., Xia, X.Z., Elliott, R., Chiu, L., Black, T., Scully, S., Capparelli, C., Morony, S., Shimamoto, G., Bass, M.B., Boyle, W.J., 1999. Tumor necrosis factor receptor family member RANK mediates osteoclast differentiation and activation induced by osteoprotegerin ligand. Proc. Natl. Acad. Sci. U. S. A. 96, 3540–3545. https://doi.org/10.1073/pnas.96.7.3540

Huang, X., Bringas, P., Slavkin, H.C., Chai, Y., 2009. Fate of HERS during tooth root development. Dev. Biol. 334, 22–30. https://doi.org/10.1016/j.ydbio.2009.06.034

Ingham, K.E., Gorrel, C., Blackburn, J., Farnsworth, W., 2001. Prevalence of odontoclastic

resorptive lesions in a population of clinically healthy cats. J. Small Anim. Pract. 42, 439–443. https://doi.org/10.1111/j.1748-5827.2001.tb02497.x

Itoh, Y., 2015. Membrane-type matrix metalloproteinases: Their functions and regulations. Matrix Biol. https://doi.org/10.1016/j.matbio.2015.03.004

Jain, A., Bahuguna, R., 2015. Role of matrix metalloproteinases in dental caries, pulp and periapical inflammation: An overview. J. Oral Biol. Craniofacial Res. https://doi.org/10.1016/j.jobcr.2015.06.015

Jehan, T., Lakhanpaul, S., 2006. Single nucleotide polymorphism (SNP)–Methods and applications in plant genetics: A review. Indian J. Biotechnol. 5.

Jiang, N., Guo, W., Chen, M., Zheng, Y., Zhou, J., Kim, S.G., Embree, M.C., Songhee Song, K., Marao, H.F., Mao, J.J., 2015. Periodontal Ligament and Alveolar Bone in Health and Adaptation: Tooth Movement. Front. Oral Biol. 18, 1–8. https://doi.org/10.1159/000351894

Kamat, M., Puranik, R., Vanaki, S., Kamat, S., 2013. An insight into the regulatory mechanisms of cells involved in resorption of dental hard tissues. J. Oral Maxillofac. Pathol. 17, 228. https://doi.org/10.4103/0973-029X.119736

Kanzaki, H., Chiba, M., Shimizu, Y., Mitani, H., 2002. Periodontal Ligament Cells Under Mechanical Stress Induce Osteoclastogenesis by Receptor Activator of Nuclear Factor κB Ligand Up-Regulation via Prostaglandin E2 Synthesis. J. Bone Miner. Res. 17, 210–220. https://doi.org/10.1359/jbmr.2002.17.2.210

Kim, M., Franke, V., Brandt, B., Lowenstein, E.D., Schöwel, V., Spuler, S., Akalin, A., Birchmeier, C., 2020. Single-nucleus transcriptomics reveals functional compartmentalization in syncytial skeletal muscle cells. Nat. Commun. 11, 1–14. https://doi.org/10.1038/s41467-020-20064-9

Kong, Y.Y., Yoshida, H., Sarosi, I., Tan, H.L., Timms, E., Capparelli, C., Morony, S., Oliveira-dos-Santos, A.J., Van, G., Itie, A., Khoo, W., Wakeham, A., Dunstan, C.R., Lacey, D.L., Mak, T.W., Boyle, W.J., Penninger, J.M., 1999. OPGL is a key regulator of osteoclastogenesis, lymphocyte development and lymph-node organogenesis. Nature 397, 315–323. https://doi.org/10.1038/16852

Lacey, D.L., Timms, E., Tan, H.L., Kelley, M.J., Dunstan, C.R., Burgess, T., Elliott, R., Colombero, A., Elliott, G., Scully, S., Hsu, H., Sullivan, J., Hawkins, N., Davy, E., Capparelli, C., Eli, A., Qian, Y.X., Kaufman, S., Sarosi, I., Shalhoub, V., Senaldi, G., Guo, J., Delaney, J., Boyle, W.J., 1998. Osteoprotegerin ligand is a cytokine that regulates osteoclast differentiation and activation. Cell 93, 165–176. https://doi.org/10.1016/S0092-8674(00)81569-X

Lee, S., 2019. A study of odontoclast dysregulation in feline tooth resorption. The University of Edinburgh.

Lee, S., Bush, S.J., Thorne, S., Mawson, N., Farquharson, C., Bergkvist, G.T., 2020a. Transcriptomic profiling of feline teeth highlights the role of matrix metalloproteinase 9 (MMP9) in tooth resorption. Sci. Rep. 10, 18958. https://doi.org/10.1038/s41598-020-75998-3

Lee, S., Bush, S.J., Thorne, S., Mawson, N., Farquharson, C., Bergkvist, G.T., 2020b. Transcriptomic profiling of feline teeth highlights the role of matrix metalloproteinase 9 (MMP9) in tooth resorption. Sci. Rep. 10, 18958. https://doi.org/10.1038/s41598-020-75998-3

Lekic, P., Mcculloch, C.A.G., 1996. Periodontal ligament cell populations: The central role of fibroblasts in creating a unique tissue. Anat. Rec. 245, 327–341. https://doi.org/10.1002/(SICI)1097-0185(199606)245:2<327::AID-AR15>3.0.CO;2-R

Li, H., Durbin, R., 2009. Fast and accurate short read alignment with Burrows-Wheeler transform. Bioinformatics 25, 1754–1760. https://doi.org/10.1093/bioinformatics/btp324

Liu, D., Wise, G.E., 2008. Expression of endothelial monocyte-activating polypeptide II in the rat dental follicle and its potential role in tooth eruption. Eur. J. Oral Sci. 116, 334–340. https://doi.org/10.1111/j.1600-0722.2008.00547.x

Liu, D., Yao, S., Pan, F., Wise, G.E., 2005. Chronology and regulation of gene expression of RANKL in the rat dental follicle. Eur. J. Oral Sci. 113, 404–409. https://doi.org/10.1111/j.1600-0722.2005.00245.x

Lommer, M.J., Verstraete, F.J.M., 2000. Prevalence of odontoclastic resorption lesions and periapical radiographic lucencies in cats: 265 cases (1995–1998). J. Am. Vet. Med. Assoc. 217, 1866–1869. https://doi.org/10.2460/javma.2000.217.1866

Lumsden, A.G., 1988. Spatial organization of the epithelium and the role of neural crest cells in the initiation of the mammalian tooth germ. Development 103 Suppl, 155–169.

Lund, E.M., Bohacek, L.K., Dahlke, J.L., King, V.L., Kramek, B.A., Logan, E.I., 1998. Prevalence and risk factors for odontoclastic resorptive lesions in cats. J. Am. Vet. Med. Assoc. 212, 392–395.

Maravillas-Montero, J.L., Santos-Argumedo, L., 2012. The myosin family: unconventional roles of actin-dependent molecular motors in immune cells. J. Leukoc. Biol. 91, 35–46. https://doi.org/10.1189/jlb.0711335

Marks, S.C., Schroeder, H.E., 1996. Tooth eruption: Theories and facts. Anat. Rec. 245, 374–393. https://doi.org/10.1002/(SICI)1097-0185(199606)245:2<374::AID-AR18>3.0.CO;2-M

Matzke, M.A., Birchler, J.A., 2005. RNAi-mediated pathways in the nucleus. Nat. Rev. Genet. https://doi.org/10.1038/nrg1500

Mestrinho, L.A., Runhau, J., Bragança, M., Niza, M.M.R.E., 2013. Risk assessment of feline tooth resorption: a Portuguese clinical case control study. J. Vet. Dent. 30, 78–83. https://doi.org/10.1177/089875641303000202

Mitchell-Olds, T., Schmitt, J., 2006. Genetic mechanisms and evolutionary significance of natural variation in Arabidopsis. Nature. https://doi.org/10.1038/nature04878

Miyazaki, T., Iwasawa, M., Nakashima, T., Mori, S., Shigemoto, K., Nakamura, H., Katagiri, H., Takayanagi, H., Tanaka, S., 2012. Intracellular and extracellular ATP coordinately regulate the inverse correlation between osteoclast survival and bone resorption. J. Biol. Chem. 287, 37808–23. https://doi.org/10.1074/jbc.M112.385369

Mohn, K.L., Jacks, T.M., Schleim, K.D., Harvey, C.E., Miller, B., Halley, B., Feeney, W.P., Hill, S.L., Hickey, G., 2009. Alendronate binds to tooth root surfaces and inhibits progression of feline tooth resorption: A pilot proof-of-concept study. J. Vet. Dent. 26, 74–81. https://doi.org/10.1177/089875640902600201

Moon, H.-J., Ko, W.-K., Jung, M.-S., Kim, J.H., Lee, W.-J., Park, K.-S., Heo, J.-K., Bang, J.B., Kwon, I.K., 2013. Coenzyme Q10 Regulates Osteoclast and Osteoblast Differentiation. J. Food Sci. 78, H785–H791. https://doi.org/10.1111/1750-3841.12116

Mulligan, T.W., 1990. Feline cervical line lesions. Vet Med Rep. 2, 343–9.

Muzylak, M., Flanagan, A.M., Ingham, K., Gunn, N., Price, J., Horton, M.A., 2002. A feline assay using osteoclasts generated in vitro from peripheral blood for screening anti-resorptive agents. Res. Vet. Sci. 73, 283–290. https://doi.org/10.1016/s0034-5288(02)00109-1

Nakano, Y., Yamaguchi, M., Fujita, S., Asano, M., Saito, K., Kasai, K., 2011. Expressions of RANKL/RANK and M-CSF/c-fms in root resorption lacunae in rat molar by heavy orthodontic force. Eur. J. Orthod. 33, 335–343. https://doi.org/10.1093/ejo/cjq068

Nanci, A., TenCate, A.R., 2017. Ten Cate's oral histology, 9th ed. Elsevier.

O'Brien, C.A., 2010. Control of RANKL gene expression. Bone. https://doi.org/10.1016/j.bone.2009.08.050

Okuda, A., Harvey, C.E., 1992. Etiopathogenesis of feline dental resorptive lesions. Vet. Clin. North Am. Small Anim. Pract. https://doi.org/10.1016/S0195-5616(92)50133-4

Orriss, I.R., Arnett, T.R., 2012. Rodent osteoclast cultures. Methods Mol. Biol. 816, 103–117. https://doi.org/10.1007/978-1-61779-415-5_8

Oshiro, T., Shibasaki, Y., John Martin, T., Sasaki, T., 2001. Immunolocalization of vacuolar-type H+-ATPase, cathepsin K, matrix metalloproteinase-9, and receptor activator of NFkB ligand in odontoclasts during physiological root resorption of human deciduous teeth. Anat. Rec. 264, 305–311. https://doi.org/10.1002/ar.1127

Park, J.H., Lee, N.K., Lee, S.Y., 2017. Current understanding of RANK signaling in osteoclast differentiation and maturation. Mol. Cells. https://doi.org/10.14348/molcells.2017.0225

Piper, K., Boyde, A., Jones, S.J., 1992. The relationship between the number of nuclei of an osteoclast and its resorptive capability in vitro. Anat. Embryol. (Berl). 186, 291–299. https://doi.org/10.1007/BF00185977

Que, B.G., Wise, G.E., 1997. Colony-stimulating factor-1 and monocyte chemotactic protein-1 chemotaxis for monocytes in the rat dental follicle. Arch. Oral Biol. 42, 855–860. https://doi.org/10.1016/S0003-9969(97)00072-1

Quinn, E.M., Cormican, P., Kenny, E.M., Hill, M., Anney, R., Gill, M., Corvin, A.P., Morris, D.W., 2013. Development of Strategies for SNP Detection in RNA-Seq Data: Application to Lymphoblastoid Cell Lines and Evaluation Using 1000 Genomes Data. PLoS One 8, e58815. https://doi.org/10.1371/journal.pone.0058815

Reiter, A.M., Lewis, J.R., Okuda, A., 2005a. Update on the etiology of tooth resorption in domestic cats. Vet. Clin. North Am. - Small Anim. Pract. https://doi.org/10.1016/j.cvsm.2005.03.006

Reiter, A.M., Lyon, K.F., Nachreiner, R.F., Shofer, F.S., 2005b. Evaluation of calciotropic hormones in cats with odontoclastic resorptive lesions. Am. J. Vet. Res. 66, 1446–1452. https://doi.org/10.2460/ajvr.2005.66.1446

Reiter, A.M., Mendoza, K.A., 2002. Feline odontoclastic resorptive lesions: An unsolved enigma in veterinary dentistry. Vet. Clin. North Am. Small Anim. Pract. 32, 791–837. https://doi.org/https://doi.org/10.1016/S0195-5616(02)00027-X

Reynolds, A., Leake, D., Boese, Q., Scaringe, S., Marshall, W.S., Khvorova, A., 2004. Rational siRNA design for RNA interference. Nat. Biotechnol. 22, 326–330.

https://doi.org/10.1038/nbt936

Roux, P., Berger, M., Stoffel, M., Stich, H., Doherr, M.G., Bosshard, D., Schawalder, P., 2005. Observations of the periodontal ligament and cementum in cats with dental resorptive lesions. J. Vet. Dent. 22, 74–85. https://doi.org/10.1177/089875640502200201

Saltman, L.H., Javed, A., Ribadeneyra, J., Hussain, S., Young, D.W., Osdoby, P., Amcheslavsky, A., van Wijnen, A.J., Stein, J.L., Stein, G.S., Lian, J.B., Bar-Shavit, Z., 2005. Organization of transcriptional regulatory machinery in osteoclast nuclei: Compartmentalization of Runx1. J. Cell. Physiol. 204, 871–880. https://doi.org/10.1002/jcp.20329

Sasaki, T., 2003a. Differentiation and functions of osteoclasts and odontoclasts in mineralized tissue resorption. Microsc. Res. Tech. 61, 483–495. https://doi.org/10.1002/jemt.10370

Sasaki, T., 2003b. Differentiation and functions of osteoclasts and odontoclasts in mineralized tissue resorption. Microsc. Res. Tech. 61, 483–495. https://doi.org/10.1002/jemt.10370

Sasaki, T., Ueno-Matsuda, E., 1992. Immunocytochemical localization of cathepsins B and G in odontoclasts of human deciduous teeth. J. Dent. Res. 71, 1881–1884. https://doi.org/10.1177/00220345920710120501

Scacheri, P.C., Rozenblatt-Rosen, O., Caplen, N.J., Wolfsberg, T.G., Umayam, L., Lee, J.C., Hughes, C.M., Shanmugam, K.S., Bhattacharjee, A., Meyerson, M., Collins, F.S., 2004. Short interfering RNAs can induce unexpected and divergent changes in the levels of untargeted proteins in mammalian cells. Proc. Natl. Acad. Sci. U. S. A. 101, 1892–1897. https://doi.org/10.1073/pnas.0308698100

Scarlett, J.M., Saidla, J., Hess, J., 1999. Risk Factors for Odontoclastic Resorptive Lesions in Cats. J. Am. Anim. Hosp. Assoc. 35, 188–192. https://doi.org/10.5326/15473317-35-3-188

Seeb, J.E., Carvalho, G., Hauser, L., Naish, K., Roberts, S., Seeb, L.W., 2011. Single-nucleotide polymorphism (SNP) discovery and applications of SNP genotyping in nonmodel organisms. Mol. Ecol. Resour. https://doi.org/10.1111/j.1755-0998.2010.02979.x

Seibel, M.J., Robins, S.P., Bilezikian, J.P., 2006. Dynamics of Bone and Cartilage Metabolism, Dynamics of Bone and Cartilage Metabolism. Elsevier. https://doi.org/10.1016/B978-0-12-088562-6.X5000-6

Senn, D., Schwalder, P., Roux, P., Bosshardt, D.D., Stoffel, M.H., 2010. Immunohistochemical Localization of Osteoclastogenic Cell Mediators in Feline Tooth Resorption and Healthy Teeth. J. Vet. Dent. 27, 75–83. https://doi.org/10.1177/089875641002700201

Sherry, S.T., 2001. dbSNP: the NCBI database of genetic variation. Nucleic Acids Res. 29, 308–311. https://doi.org/10.1093/nar/29.1.308

Shinohara, M., Koga, T., Okamoto, K., Sakaguchi, S., Arai, K., Yasuda, H., Takai, T., Kodama, T., Morio, T., Geha, R.S., Kitamura, D., Kurosaki, T., Ellmeier, W., Takayanagi, H., 2008. Tyrosine Kinases Btk and Tec Regulate Osteoclast Differentiation by Linking RANK and ITAM Signals. Cell 132, 794–806. https://doi.org/10.1016/j.cell.2007.12.037

Simmer, J.P., Richardson, A.S., Wang, S.K., Reid, B.M., Bai, Y., Hu, Y., Hu, J.C.C., 2014. Ameloblast transcriptome changes from secretory to maturation stages, in: Connective Tissue Research. Informa Healthcare, pp. 29–32. https://doi.org/10.3109/03008207.2014.923862

Thesleff, I., 2015. Molecular Genetics of Tooth Development. Princ. Dev. Genet. Second Ed. 19, 393–405. https://doi.org/10.1016/B978-0-12-405945-0.00022-3

Thesleff, I., 2003. Epithelial-mesenchymal signalling regulating tooth morphogenesis. J. Cell Sci. 116, 1647–1648. https://doi.org/10.1242/jcs.00410

Toyosawa, S., Ogawa, Y., Chang, C.K., Hong, S.S., Yagi, T., Kuwahara, H., Wakasa, K. ichi, Sakurai, M., 1991. Histochemistry of tartrate-resistant acid phosphatase and carbonic anhydrase isoenzyme II in osteoclast-like giant cells in bone tumours. Virchows Arch. A Pathol. Anat. Histopathol. 418, 255–261. https://doi.org/10.1007/BF01606064

Trapnell, C., Williams, B.A., Pertea, G., Mortazavi, A., Kwan, G., Van Baren, M.J., Salzberg, S.L., Wold, B.J., Pachter, L., 2010. Transcript assembly and quantification by RNA-Seq reveals unannotated transcripts and isoform switching during cell differentiation. Nat. Biotechnol. 28, 511–515. https://doi.org/10.1038/nbt.1621

Uchiyama, M., Nakamichi, Y., Nakamura, M., Kinugawa, S., Yamada, H., Udagawa, N., Miyazawa, H., 2009. Dental pulp and periodontal ligament cells support osteoclastic differentiation. J. Dent. Res. 88, 609–614. https://doi.org/10.1177/0022034509340008

Väänänen, H.K., Horton, M., 1995. The osteoclast clear zone is a specialized cell-extracellular matrix adhesion structure. J. Cell Sci. 108 (Pt 8, 2729–2732.

van Wessum, R., Harvey, C.E., Hennet, P., 1992. Feline dental resorptive lesions. Prevalence patterns. Vet. Clin. North Am. Small Anim. Pract. 22, 1405–1416. https://doi.org/10.1016/S0195-5616(92)50134-6

Wang, Z., Gerstein, M., Snyder, M., 2009. RNA-Seq: A revolutionary tool for transcriptomics. Nat. Rev. Genet. https://doi.org/10.1038/nrg2484

Wang, Z., McCauley, L., 2011. Osteoclasts and odontoclasts: signaling pathways to development and disease. Oral Dis. 17, 129–142. https://doi.org/10.1111/j.1601-0825.2010.01718.x

Wise, G.E., Frazier-Bowers, S., D'Souza, R.N., 2002. Cellular, Molecular, and Genetic Determinants of Tooth Eruption. Crit. Rev. Oral Biol. Med. 13, 323–335. https://doi.org/10.1177/154411130201300403

Wise, G.E., King, G.J., 2008. Mechanisms of tooth eruption and orthodontic tooth movement. J. Dent. Res. https://doi.org/10.1177/154405910808700509

Wise, G.E., Lumpkin, S.J., Huang, H., Zhang, Q., 2000. Osteoprotegerin and osteoclast differentiation factor in tooth eruption. J. Dent. Res. 79, 1937–1942. https://doi.org/10.1177/00220345000790120301

Wise, G.E., Yao, S., 2006. Regional differences of expression of bone morphogenetic protein-2 and RANKL in the rat dental follicle. Eur. J. Oral Sci. 114, 512–516. https://doi.org/10.1111/j.1600-0722.2006.00406.x

Yamamoto, Tsuneyuki, Hasegawa, T., Yamamoto, Tomomaya, Hongo, H., Amizuka, N., 2016. Histology of human cementum: Its structure, function, and development. Jpn. Dent. Sci. Rev. https://doi.org/10.1016/j.jdsr.2016.04.002

Yu, C., Abbott, P., 2007. An overview of the dental pulp: its functions and responses to injury. Aust. Dent. J. 52, S4–S6. https://doi.org/10.1111/j.1834-7819.2007.tb00525.x

Yu, Y., Wei, J., Zhang, X., Liu, J., Liu, C., Li, F., Xiang, J., 2014. SNP Discovery in the Transcriptome of White Pacific Shrimp Litopenaeus vannamei by Next Generation Sequencing. PLoS One 9, e87218. https://doi.org/10.1371/journal.pone.0087218

Zeichner-David, M., Oishi, K., Su, Z., Zakartchenko, V., Chen, L.S., Arzate, H., Bringas, P., 2003. Role of Hertwig's Epithelial Root Sheath Cells in Tooth Root Development. Dev. Dyn. 228, 651–663. https://doi.org/10.1002/dvdy.10404

Zetner, K., Steurer, I., 1992. The influence of dry food on the development of feline neck lesions. J. Vet. Dent. 9, 4–6.

Zhang, P., Cupp, C., Kerr, W., 2006. Vitamin D status in cats with and without feline odontoclastic resorptive lesions 28.

Zhao, Y., Wang, K., Wang, W.L., Yin, T.T., Dong, W.Q., Xu, C.J., 2019. A high-throughput SNP discovery strategy for RNA-seq data. BMC Genomics 20, 160. https://doi.org/10.1186/s12864-019-5533-4

Zheng, D., Cui, C., Yu, M., Li, X., Wang, L., Chen, X., Lin, Y., 2018. Coenzyme Q10 promotes osteoblast proliferation and differentiation and protects against ovariectomy-induced osteoporosis. Mol. Med. Rep. 17, 400–407. https://doi.org/10.3892/mmr.2017.7907

Zhu, L., Tang, Y., Li, X.Y., Keller, E.T., Yang, J., Cho, J.S., Feinberg, T.Y., Weiss, S.J., 2020. Osteoclast-mediated bone resorption is controlled by a compensatory network of secreted and membrane-tethered metalloproteinases. Sci. Transl. Med. 12. https://doi.org/10.1126/scitranslmed.aaw6143

Appendix A: SnpEff prediction details

Adapted from http://snpeff.sourceforge.net/SnpEff_manual.html#effNc

Effect Seq. Ontology	Effect Classic	Description and example of effect	Impact
stop_gained	STOP_GAINED	Variant causes a STOP codon e.g.: Cag/Tag, Q/*	HIGH
missense_variant	NON_SYNONYMOUS_CODING	Variant causes a codon that produces a different amino acid e.g.: Tgg/Cgg, W/R	MODERATE
splice_region_variant	SPLICE_SITE_BRANCH_U12	A variant affective putative (Lariat) branch point from U12 splicing machinery, located in the intron.	MODERATE
splice_region_variant	SPLICE_SITE_REGION	A sequence variant in which a change has occurred within the region of the splice site, either within 1-3 bases of the exon or 3-8 bases of the intron.	LOW
splice_region_variant	SPLICE_SITE_BRANCH	A variant affective putative	LOW

		(Lariat) branch point, located in the intron.	
synonymous_variant	SYNONYMOUS_CODING	Variant causes a codon that produces the same amino acid e.g.: Ttg/Ctg, L/L	LOW
stop_retained_variant	SYNONYMOUS_STOP	Variant causes stop codon to be mutated into another stop codon. e.g.: taA/taG, */*	LOW
downstream_gene_variant	DOWNSTREAM	Downstream of a gene (default length: 5K bases)	MODIFIER
intergenic_region	INTERGENIC	The variant is in an intergenic region	MODIFIER
intron_variant	INTRON	Variant hits and intron. Technically, hits no exon in the transcript.	MODIFIER
upstream_gene_variant	UPSTREAM	Upstream of a gene (default length: 5K bases)	MODIFIER
5_prime_UTR_variant	UTR_5_PRIME	Variant hits 5'UTR region	MODIFIER

Appendix B: List of candidate genes used for variant calling

ENSEMBL gene name	Gene location	Description
ENSFCAG00000002531	D1: 101,344,581-101,360,735	Spi-1 proto-oncogene
ENSFCAG00000003633	A1: 199,084,913-199,126,561	colony stimulating factor 1 receptor
ENSFCAG00000024132	D3: 82,412,401-82,467,834	TNF receptor superfamily member 11a
ENSFCAG00000005912	A1: 28,177,897-28,209,736	TNF superfamily member 11
ENSFCAG00000010245	A3: 14,751,502-14,756,639	osteoclast stimulatory transmembrane protein
ENSFCAG00000042335	A2: 8,744,820-8,746,541	acid phosphatase 5, tartrate resistant
ENSFCAG00000014014	A3: 15,240,350-15,252,577	matrix metallopeptidase 9
ENSFCAG00000007443	A2: 98,473,589-98,629,883	calcitonin receptor
ENSFCAG00000003643	C1: 105,944,163-105,952,068	cathepsin K (ENSFCAG00000003643, This identifier is not in the current EnsEMBL database, Chromosome C1: 105,944,163-105,952,068)
ENSFCAG00000002774	B2: 42,227,009-42,236,717	triggering receptor expressed on myeloid cells 2
ENSFCAG00000006617	E2: 17,734,990-17,738,668	TYRO protein tyrosine kinase binding protein
ENSFCAG00000006655	E2: 62,849,973-62,859,079	cytochrome b-245 alpha chain
ENSFCAG00000003145	X: 33,290,937-33,420,228	cytochrome b-245 beta chain
ENSFCAG00000001880	F2: 65,039,472-65,068,414	TNF receptor superfamily member 11b
ENSFCAG00000005436	E2: 13,683,300-13,697,684	transforming growth factor beta 1
ENSFCAG00000036217	F1: 57,903,509-57,983,526	transforming growth factor beta 2
ENSFCAG00000002495	D3: 626,526-629,413	purinergic receptor P2X 2
ENSFCAG00000012452	D3: 8,241,568-8,259,834	purinergic receptor P2X 4
ENSFCAG00000040501	D3: 29,610,166-29,620,235	purinergic receptor P2X 6
ENSFCAG00000005949	A3: 35,391,663-35,677,323	phospholipase C beta 4

ENSFCAG00000002495	D3: 626,526-629,413	purinergic receptor P2X 7
ENSFCAG00000005899	A3: 105,049,334-105,056,407	interleukin 1 beta
ENSFCAG00000012152	A3: 60,432,973-60,509,005	Interleukin 1 receptor type 1
ENSFCAG00000012150	A3: 60,558,218-60,626,908	IL1 receptor type 2
ENSFCAG00000018587	C2: 79,661,275-79,708,179	interleukin 1 receptor accessory protein
ENSFCAG00000043150	X: 24,699,000-25,844,198	interleukin 1 receptor accessory protein like 1
ENSFCAG00000044125	X: 87,143,667-88,283,541	interleukin 1 receptor accessory protein like 2
ENSFCAG00000007557	B1: 121,815,943-121,909,534	Nuclear factor κ B subunit 1
ENSFCAG00000001242	D2: 62,844,226-62,880,055	Nuclear factor κ B subunit 2
ENSFCAG00000006868	B4: 41,441,023-41,453,334	TNF receptor superfamily member 1A
ENSFCAG00000003778	C1: 8,949,584-8,980,450	TNF receptor superfamily member 1B
ENSFCAG00000043839	E2: 44,903,313-44,905,335	TNFRSF1A associated via death domain
ENSFCAG00000000884	D3: 96,134,961-96,241,617	Nuclear factor of activated T cells 1
ENSFCAG00000025370	B3: 122,573,803-122,577,110	Fos proto-oncogene, AP-1 transcription factor subunit
ENSFCAG00000024972	C1: 48,184,940-48,185,944	Jun proto-oncogene, AP-1 transcription factor subunit
ENSFCAG00000024419	A2: 37,078,196-37,185,869	melanocyte inducing transcription factor
ENSFCAG00000041539	F2: 72,293,023-72,295,834	MYC proto-oncogene, bHLH transcription factor
ENSFCAG00000006991	A3: 22,426,690-22,446,049	SRC proto-oncogene, non-receptor tyrosine kinase.
ENSFCAG00000000389	D4: 95,522,134-95,536,107	TNF receptor associated factor 2
ENSFCAG00000036371	D1: 92,085,833-92,100,810	TNF receptor associated factor 6
ENSFCAG00000007459	D1: 55,903,609-56,091,566	GRB2 associated binding protein 2
ENSFCAG00000015647	B3: 108,576,890-108,606,457	JNK1/MAPK8 associated membrane protein
ENSFCAG00000011912	B4: 144,035,018-144,040,404	mitogen-activated protein kinase 11
ENSFCAG00000014214	D4: 3,867,611-3,927,566	spleen associated tyrosine kinase

ENSFCAG00000009032	A3: 19,249,415-19,288,184	Phospholipase C gamma 1
ENSFCAG00000004987	A3: 19,249,415-19,288,184	Phospholipase C gamma 2
ENSFCAG00000008409	D1: 67,396,933-67,554,104	Suppressor of tumorigenicity 5
ENSFCAG00000024594	B4: 76,746,763-76,801,995	Vitamin D receptor
ENSFCAG00000001551	A1: 173,152,341-173,616,172	Calcium/calmodulin-dependent protein kinase IV
ENSFCAG00000007140	D2: 57,561,236-57,637,324	B cell linker
ENSFCAG00000011383	D1: 72,977,211-72,996,288	cytochrome P450 family 2 subfamily R member 1
ENSFCAG00000007063	C1: 203,815,043-203,846,732	cytochrome P450 family 27 subfamily A member 1
ENSFCAG00000004851	B1: 149,797,032-149,829,578	GC vitamin D binding protein
ENSFCAG00000014701	B4: 86,178,390-86,182,260	cytochrome P450 family 27 subfamily B member 1
ENSFCAG00000002452	A3: 8,530,133-8,547,391	cytochrome P450 family 24 subfamily A member 1
ENSFCAG00000008095	A3: 105,113,193-105,121,209	interleukin 1 alpha
ENSFCAG00000009165	A2: 116,633,403-116,637,410	interleukin 6
ENSFCAG00000010859	A1: 126,565,845-126,597,331	interleukin 6 signal transducer
ENSFCAG00000026747	F1: 70,922,039-70,964,740	interleukin 6 receptor
ENSFCAG00000039518	F1: 66,012,454-66,016,966	Fc fragment of IgE receptor Ig
ENSFCAG00000012690	D4: 88,695,387-88,700,964	Prostoglandin E synthase 2
ENSFCAG00000014204	B3: 123,201,056-123,223,052	transforming growth factor beta 3
ENSFCAG00000002490	A1: 111,778,712-111,787,546	Interleukin 4
ENSFCAG00000023022	E3: 22,898,365-22,919,205	interleukin 4 receptor
ENSFCAG00000033485	B2: 52,598,405-52,602,387	interleukin 17A.
ENSFCAG00000031349	B4: 35,248,036-35,269,988	Interleukin 17 receptor A
ENSFCAG00000009014	B4: 95,329,479-95,334,070	interferon gamma.

ENSFCAG00000030336	B2: 126,545,404-126,567,117	interferon gamma receptor 1
ENSFCAG00000026593	C2: 11,922,074-11,941,177	interferon gamma receptor 2
ENSFCAG00000012214	C2: 12,071,470-12,099,315	interleukin 10 receptor subunit beta
ENSFCAG00000007522	A2: 13,331,773-13,350,303	interleukin 12 receptor subunit beta 1
ENSFCAG00000001940	C1: 56,033,911-56,113,169	interleukin 12 receptor subunit beta 2
ENSFCAG00000007750	A3: 60,214,630-60,250,273	interleukin 18 receptor 1
ENSFCAG00000019058	A3: 60,172,927-60,206,518	interleukin 18 receptor accessory protein
ENSFCAG00000040011	D1: 61,729,133-61,730,954	interleukin 18 binding protein
ENSFCAG00000033844	E2: 4,028,214-4,035,55	osteoclast associated Ig-like receptor.
ENSFCAG00000041932	B2: 45,989,373-46,319,813	Corebinding factor a (RUNX family transcription factor 2)
ENSFCAG00000000506	B1: 115,392,681-115,489,868	Epidermal growth factor
ENSFCAG00000008121	A3: 89,816,476-89,943,682	Transforming growth factor A
ENSFCAG00000015468	A2: 70,929,863-71,137,727	epidermal growth factor receptor
ENSFCAG00000008323	B4: 63,235,582-63,247,292	parathyroid hormone like hormone
ENSFCAG00000023081	F1: 23,931,093-23,937,628	Cyclooxygenase-2.
ENSFCAG00000003517	B1: 42,798,585-42,823,240	plasminogen activator, tissue type
ENSFCAG00000015567	D2: 36,474,690-36,480,459	plasminogen activator, urokinase
ENSFCAG00000005230	E2: 12,719,444-12,735,105	plasminogen activator, urokinase receptor
ENSFCAG00000023975	B2: 147,295,707-147,339,275	plasminogen
ENSFCAG00000005795	E3: 8,113,271-8,118,367	serpin family E member 1
ENSFCAG00000015791	D1: 1,401,792-1,409,178	matrix metallopeptidase 1
ENSFCAG00000005935	E2: 35,009,403-35,033,495	matrix metallopeptidase 1
ENSFCAG00000008190	X: 42,009,392-42,013,438	TIMP metallopeptidase inhibitor 1

ENSFCAG00000046765	E1: 59,984,594-60,030,711	TIMP metallopeptidase inhibitor 2
ENSFCAG00000034191	B4: 129,932,264-129,990,895	TIMP metallopeptidase inhibitor 3
ENSFCAG00000028966	A2: 53,158,432-53,164,180	TIMP metallopeptidase inhibitor 4
ENSFCAG00000006626	B3: 75,707,173-75,716,116	matrix metallopeptidase 14
ENSFCAG00000015790	D1: 1,332,173-1,344,105	matrix metallopeptidase 8
ENSFCAG00000000118	D1: 1,510,418-1,522,314	matrix metallopeptidase 13
ENSFCAG00000007792	C2: 59,012,182-59,036,422	CD200 molecule
ENSFCAG00000015041	B1: 55,061,788-55,081,968	Cathepsin B
ENSFCAG00000042335	A2: 8,744,820-8,746,541	acid phosphatase 5, tartrate resistant
ENSFCAG00000008982	F2: 52,017,317-52,025,001	dendrocyte expressed seven transmembrane protein
ENSFCAG00000033649	B1: 43,620,167-43,685,346	secreted frizzled related protein 1.
ENSFCAG00000026462	B2: 44,507,114-44,521,541	vascular endothelial growth factor A.